BERICHTE
aus dem Fachbereich Geowissenschaften
der Universität Bremen

Nr. 133

Felis, T.

CLIMATE AND OCEAN VARIABILITY RECONSTRUCTED FROM STABLE ISOTOPE RECORDS OF MODERN SUBTROPICAL CORALS (NORTHERN RED SEA)

Berichte, Fachbereich Geowissenschaften, Universität Bremen, Nr. 133,
111 Seiten, Bremen 1999

ISSN 0931-0800

Die "Berichte aus dem Fachbereich Geowissenschaften" werden in unregelmäßigen Abständen vom Fachbereich 5, Universität Bremen, herausgegeben.

Sie dienen der Veröffentlichung von Forschungsarbeiten, Doktorarbeiten und wissenschaftlichen Beiträgen, die im Fachbereich angefertigt wurden.

Die Berichte können bei:

Frau Gisela Boelen

Sonderforschungsbereich 261

Universität Bremen

Postfach 330 440

D 28334 BREMEN

Telefon: (49) 421 218-4124

Fax: (49) 421 218-3116

angefordert werden.

Zitat:

Felis, T.

Climate and ocean variability reconstructed from stable isotope records of modern subtropical corals (Northern Red Sea).

Berichte, Fachbereich Geowissenschaften, Universität Bremen, Nr. 133, 111 Seiten, Bremen, 1999.

ISSN 0931-0800

CLIMATE AND OCEAN VARIABILITY RECONSTRUCTED FROM STABLE ISOTOPE RECORDS OF MODERN SUBTROPICAL CORALS (NORTHERN RED SEA)

Dissertation

zur Erlangung des Grades
Doktor der Naturwissenschaften
(Dr. rer. nat.)

am
Fachbereich Geowissenschaften
der
Universität Bremen

vorgelegt von

Thomas Felis

Bremen, 1999

Tag des Kolloquiums:

18. Februar 1999

Gutachter:

Professor Dr. Gerold Wefer

Professor Dr. Rüdiger Henrich

Prüfer:

Professor Dr. Horst D. Schulz

Privatdozent Dr. André Freiwald

Abstract

Climate and ocean variability reconstructed from stable isotope records of modern subtropical corals (northern Red Sea)

Widespread instrumental climate data are available for only about one century and therefore cannot resolve the full range of interannual-, decadal-, and multidecadal-scale climate variability. Stable isotope records derived from the skeletons of annually banded, massive corals from the tropical and subtropical reefs can be used to reconstruct the climate variability of the past several hundred years and therefore provide a better understanding of the interaction between the different modes of the global climate system.

A 245-year (1750-1995) coral oxygen isotope record ($\delta^{18}O$) from Ras Umm Sidd (Egypt) near the southern tip of the Sinai Peninsula (Ras Mohammed National Park) in the northern Red Sea provides a bimonthly-resolution time series from this subtropical location (~28°N) at the northern rim of the African-Asian desert belt. The coral $\delta^{18}O$-based sea surface temperatures suggest that mean annual sea surface temperatures between 1751 and 1900 were ~0.3°C lower than the 20th century average. The coral record, supported by instrumental and proxy records of climate, reveals that during colder periods on the interannual to interdecadal/multidecadal timescale the northern Red Sea region is more arid (higher evaporation) whereas the eastern Mediterranean region in the north is wetter. During warmer periods the northern Red Sea region is less arid (lower evaporation) whereas the eastern Mediterranean region is drier. This pattern is explained by variations in the latitudinal position of the subtropical westerly jet stream, the associated subtropical high-pressure belt, and therefore the descending branch of the northern Hadley cell with its subsiding air, as well as of the moisture bringing North Atlantic westerlies which are located in the north of this system. The northern Red Sea is probably the only site in the world oceans where deep water formation occurs and reef corals grow. The winter $\delta^{18}O$ values of the coral record can be used to detect episodic events of deep water formation of the Red Sea thermohaline circulation during anomalously arid and cold winters. Spectral analysis of the coral time series reveals that both the North Atlantic Oscillation and the El Niño-Southern Oscillation phenomenon of tropical Pacific origin contributed significantly to the climate variability of the Middle East during the past 245 years on interannual to multidecadal timescales. The results suggest that interaction between extratropical and tropical modes of the global climate system has an important control on subtropical climate variability via atmospheric teleconnections, and that a prominent cooling interval in the first half of the 19th century evident in several Northern Hemisphere temperature reconstructions can be related to a 70-year climate oscillation of most probably North Atlantic origin, at least for the Middle East region. The Ras Umm Sidd coral oxygen isotope record ($\delta^{18}O$) therefore provides a valuable source of information on Middle East climate and Red Sea ocean history.

The environmental interpretation of the stable carbon isotopic variations ($\delta^{13}C$) in the skeletons of massive corals is still a matter of debate. A 19-year stable carbon isotope record (1974-1993) in bimonthly resolution derived from a coral from Eilat (Israel) at the northern end of the Gulf of Aqaba (northern Red Sea) documents interannual events of extraordinarily large plankton blooms, indicated by anomalous ^{13}C depletions in the coral skeleton. These blooms are caused by deep vertical water mass mixing, convectively driven in colder winters, which results in increased supplies of nutrients to the surface waters. The deep vertical mixings can sometimes be driven by the cooling occuring throughout the Middle East after large tropical volcanic eruptions. There is evidence in the coral record for an indirect volcanic signal of the eruptions of El Chichón (Mexico, 1982) and Mount Pinatubo (Philippines, 1991). Deep mixing induced isotopic variations of the dissolved inorganic carbon in the surface waters can be neglected at this location. It is therefore suggested that the ^{13}C skeletal depletions can be best explained by changes in the coral's autotrophy-heterotrophy diet, through increased heterotrophic feeding on zooplankton during the blooms. If these conclusions are substantiated by further work, seasonal stable carbon isotope records ($\delta^{13}C$) of corals which change from autotrophy under normal conditions to increased heterotrophy during bloom events may be used as indicators of ocean paleoproductivity at interannual resolution, available from no other source.

Zusammenfassung

Climate and ocean variability reconstructed from stable isotope records of modern subtropical corals

Rekonstruktion der Variabilität von Klima und Ozean anhand von Chronologien stabiler Isotope aus rezenten subtropischen Korallen (nördliches Rotes Meer)

Instrumentelle Klimaaufzeichnungen reichen meist nicht weiter als ein Jahrhundert in die Vergangenheit zurück. Daher können sie auch nicht das gesamte Spektrum der zwischenjährlichen, dekadischen sowie der multidekadischen Klimavariabilität auflösen. Chronologien stabiler Isotope, gewonnen aus jährlich gebänderten massiven Korallen der tropischen und subtropischen Riffe, bieten die Möglichkeit die Klimavariabilität der letzten mehreren hundert Jahre zu rekonstruieren. Sie steuern damit zu einem umfassenderen Verständnis des Zusammenwirkens der verschiedenen Phänomene des globalen Klimasystems bei.

Eine 245jährige (1750-1995) Sauerstoffisotopenchronologie ($\delta^{18}O$) einer Koralle aus Ras Umm Sidd (Ägypten) nahe der südlichen Spitze der Sinaihalbinsel (Ras Mohammed Nationalpark) im nördlichen Roten Meer wurde erstellt. Diese subtropische Lokation (~28°N) liegt am nördlichen Rand des afrikanisch-asiatischen Wüstengürtels. Die Chronologie hat eine zweimonatliche Auflösung. Die vom $\delta^{18}O$ der Koralle abgeleiteten Oberflächenwassertemperaturen lassen vermuten, daß die mittleren jährlichen Oberflächenwassertemperaturen zwischen 1751 und 1900 um etwa 0.3°C geringer waren als der Durchschnittswert des 20. Jahrhunderts. Die Korallenchronologie, unterstützt von instrumentellen und paläoklimatischen Aufzeichnungen zeigt an, daß während kälterer Perioden die Region des nördlichen Rote Meeres arider (höhere Evaporation) und die weiter nördlich gelegenere Region des östlichen Mittelmeeres feuchter ist. Während wärmerer Perioden dagegen ist es im nördlichen Roten Meer weniger arid (geringere Evaporation) und im östlichen Mittelmeer trockener. Dieses Muster, das sich auf zwischenjährliche sowie interdekadische/multidekadische Zeiträume bezieht, wird mit Veränderungen in der geographischen Breite des subtropischen westlichen Jetstreams erklärt. Eine wichtige Rolle spielt dabei der mit dem Subtropenjet assoziierte subtropische Hochdruckgürtel und somit der abwärts gerichtete Zweig der nördlichen Hadley-Zelle mit seinen absinkenden Luftmassen sowie die nördlich dieses Systems gelegenen feuchtigkeitbringenden nordatlantischen Westwinde. Das nördliche Rote Meer ist höchstwahrscheinlich die einzige Lokation in den Weltozeanen an der Korallen wachsen und Tiefenwasserbildung stattfindet. Die Winter-$\delta^{18}O$-Werte der Korallenchronologie lassen sich dazu benutzen, episodische Ereignisse von Tiefenwasserbildung der thermohalinen Zirkulation des Roten Meeres zu rekonstruieren. Diese finden in besonders ariden und kalten Wintern statt. Spektralanalysen der Korallenzeitreihe zeigen, daß die

Nordatlantische Oszillation als auch das Klimaphänomen der El Niño-Südlichen Oszillation, das seinen Ursprung im tropischen Pazifik hat, signifikant zur zwischenjährlichen bis multidekadischen Klimavariabilität im Nahen Osten während der letzten 245 Jahre beisteuerten. Die Ergebnisse zeigen, daß ein Zusammenwirken von außertropischen und tropischen Phänomenen des globalen Klimasystems über atmosphärische Fernwirkungen eine wichtige Rolle in der Kontrolle der Klimavariabilität der Subtropen spielt. Weiterhin kann eine ausgeprägte Kälteperiode, die in mehreren Temperaturrekonstruktionen der Nordhemisphäre für die erste Hälfte des 19. Jahrhunderts angezeigt wird, zumindest für die Region des Nahen Ostens auf eine Klimaoszillation von 70 Jahren zurückgeführt werden. Diese Klimaoszillation hat ihren Ursprung höchstwahrscheinlich im Nordatlantik. Die Korallen-Sauerstoffisotopenchronologie ($\delta^{18}O$) von Ras Umm Sidd liefert somit wertvolle Informationen zur Klimageschichte des Nahen Ostens als auch zur ozeanographischen Geschichte des Roten Meeres.

Die Interpretation des stabilen Kohlenstoffisotopensignals ($\delta^{13}C$) im Skelett massiver Korallen als Umweltindikator wird noch immer viel diskutiert. Eine 19jährige Chronologie stabiler Kohlenstoffisotope (1974-1993) einer Koralle aus Eilat (Israel) am nördlichen Ende des Golfs von Aqaba (nördliches Rotes Meer) mit zweimonatlicher Auflösung dokumentiert zwischenjährliche Ereignisse außerordentlich starker Planktonblüten. Diese Ereignisse werden im Korallenskelett durch anomale ^{13}C-Abreicherungen angezeigt. Die Planktonblüten werden durch eine besonders tiefe konvektive Durchmischung der Wassersäule in kälteren Wintern verursacht, da diese zu einer verstärkten Zufuhr von Nährstoffen in das Oberflächenwasser führt. Diese besonders tiefen Durchmischungsereignisse können manchmal durch eine im Nahen Osten nach starken tropischen Vulkanausbrüchen auftretende Abkühlung verursacht werden. In der Korallenchronologie ist ein indirektes Signal der Vulkanausbrüche des El Chichón (Mexiko, 1982) and des Mount Pinatubo (Philippinen, 1991) erkennbar. Änderungen in der isotopischen Zusammensetzung des gelösten anorganischen Kohlenstoffs im Oberflächenwasser durch die besonders tiefe Wassermassendurchmischung können an dieser Lokation vernachlässigt werden. Es wird daher vorgeschlagen, die ^{13}C-Abreicherungen im Skelett mit Änderungen im Autotrophie-Heterotrophie Verhältnis der Nahrungsaufnahme der Koralle zu erklären. Es wird von einer verstärkten heterotrophen Nahrungsaufnahme von Zooplankton durch die Koralle während der Blüten ausgegangen. Wenn diese Schlußfolgerungen durch weitere Arbeiten bestätigt werden, könnten saisonale Chronologien stabiler Kohlenstoffisotope ($\delta^{13}C$) von Korallen, die von Autotrophie unter normalen Bedingungen zu verstärkter Heterotrophie während Planktonblütenereignissen wechseln, als Indikatoren der Ozeanpaläoproduktivität in zwischenjährlicher Auflösung verwendet werden.

Acknowledgments

I like to thank Professor Gerold Wefer, my primary advisor, for the opportunity to pursue this thesis and his multifarious support of my studies. I wish to thank Jürgen Pätzold, my co-advisor, for encouragement, criticism, and fruitful discussions during this work. Professor Rüdiger Henrich is gratefully acknowledged for being a referee to this thesis.

This work benefitted much from the scientific and logistic support of Professor Yossi Loya and Maoz Fine from Tel Aviv University. Drilling the RUS-95 core would not have been possible without the permission of the Egyptian Environmental Affairs Agency (EEAA) and other authorities in Egypt. I gratefully acknowledge the permission for sampling in the Ras Mohammed National Park.

I wish to thank Tom Crowley, Amatzia Genin, and Boaz Lazar for constructive comments, and Ted McConnaughey for thoughtful and extensive discussions. I wish to thank Mike Evans, Colin Price, Ahuva Almogi-Labin, Gidon Eshel, and Dan Schrag for informations or discussions; Judith Lean, Terry Quinn, Xiahong Feng, Georg Heiss, and Christof Appenzeller for providing data; and Mike Mann for providing data prior to publication.

I thank my fellow Ph.D. candidates, Henning Kuhnert, Helge Arz, and Chris Moos for constructive scientific input as well as for the good atmosphere at the Geosciences Department of Bremen University. Frank Lamy, Georg Kirst, Nils Andersen, Sylke Draschba, Birger Schlünz, Yaser A. Moustafa, and many others also contributed to this. I like to thank Monika Segl for effectively running the mass spec lab, and Birgit Meyer-Schack for running all the samples. I thank Chris Moos for water isotopic analysis, and Cécile Gervais for giving a length scale to the RUS-95 sampling profile and for the nitrogen tests. Many thanks to Gerrit Meinecke and Götz Ruhland for keeping the computers and the network running, and to Volker Ratmeyer for printing the several posters.

This work is part of the multidisciplinary Egyptian, Israeli, Palestinian (since 1999 also Jordanian) and German "Red Sea Program on Marine Sciences", funded by the BMBF (German Federal Ministry for Education, Science, Research, and Technology) through grant 03F0151A.

I wish to thank the "Graduiertenkolleg Stoff-Flüsse in marinen Geosystemen" at Bremen University for funding my participation in the "AGU Fall Meeting 1997" (San Francisco) and in the "IGBP PAGES Open Science Meeting 1998" (London). I thank the European Commission for funding my participation in the "European Union Advanced Study Course on Holocene Climate Reconstruction" at the Environmental Change Research Centre, University College London, 1998.

I am most grateful to Judith for support and tolerating my working style during the past years.

Table of contents

1. Introduction

1.1. Reconstructing the climatic variability of the past several hundred years

Widespread instrumental climate data are available for only about one century, a period arguably modified by anthropogenic activities [e.g., *Mann et al.*, 1998]. These short instrumental records cannot resolve the full range of decadal-, multidecadal-, and centennial-scale natural climate variability. Therefore, proxy climate indicators in at least annual resolution must be used for the reconstruction of the climate variability during the past millennium. These indicators are based on varied proxy sources (tree rings, ice cores, banded corals, varved sediments). The resulting paleoclimatic records based on these proxy sources are a central issue for the assessment of pertubations to the natural climate variability by anthropogenic forcing, and, consequently, for climate predictability. Furthermore, centuries-long continuous proxy records of climate variability are essential for a better understanding of the interaction between the different modes of the global climate system, e.g., the El Niño-Southern Oscillation phenomenon, the Asian monsoon, or the North Atlantic Oscillation. The variability of these modes and their interaction has important socio-economic effects owing to their worldwide modulation of droughts, floods, storms, snowfall, or fish stocks.

In most areas of the tropics and subtropics continuous instrumental observations of climate rarely span more than the past 30-40 years. Coral records from the tropical/subtropical reefs provide a tool for reconstructing the climate variability of the past several hundred years, thereby extending the instrumental datasets of these regions. The mean annual temperature reconstruction of *Mann et al.* [1998] for the past six centuries, which is based on tree ring, ice core, coral, and long historical and instrumental records, in the tropics and subtropics is mainly based on coral records (Figure 1.1). This

is due to the fact that most trees fail to produce well-defined annual rings in these latitudes, and other proxy sources are rare. The reconstruction for the Northern Hemisphere is shown in Figure 1.2. However, to reconstruct mean global temperatures back over the entire millennium there is the need for more reconstructions from high-quality annual-resolution proxy climate indicators in the diverse regions of the globe.

The possible importance of the low latitudes, especially the tropical Pacific, in producing both orbital-scale (forced) and millennial-scale (internal) climate cycles was recently pointed out [*Cane*, 1998]. The idea is that unstable ocean-atmosphere interactions in the tropical Pacific change regional sea surface temperature (SST) distributions. These SST variations are linked to extratropical climate changes via so-called "teleconnection" patterns. There is some evidence for El Niño-like states to favor interglacial conditions and La Niña-like states to favor glacial conditions [*Cane*, 1998]. The role of the low latitudes and the tropics in millennial-scale climatic changes, which are acompanied by shifts as abrupt as decades, is still unclear [*Stocker*, 1998]. High-resolution paleoclimatic archives like annually banded corals are therefore required to understand the decadal- to multidecadal-scale climate variability of the low latitudes and will hopefully also provide implications for the understanding of past climatic changes on much larger timescales.

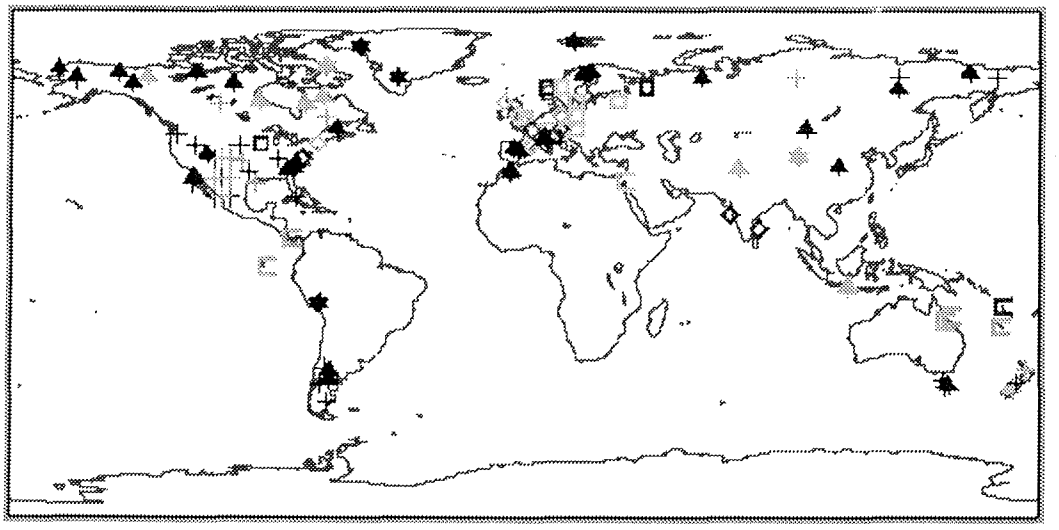

Figure 1.1. Distribution of high-resolution proxy climate indicators used in a global reconstruction of annual temperature patterns over the past six centuries [*Mann et al.*, 1998]. Dendroclimatic reconstructions are indicated by 'tree' symbols, ice core/ice melt proxies by 'star' symbols and coral records by 'C' symbols. Long historical and instrumental records are shown by squares (temperature) or diamonds (precipitation). Groups of '+' symbols indicate principal components of dense tree-ring sub-networks, with the number of such symbols indicating the number of retained principal components. For further discussion see *Mann et al.* [1998].

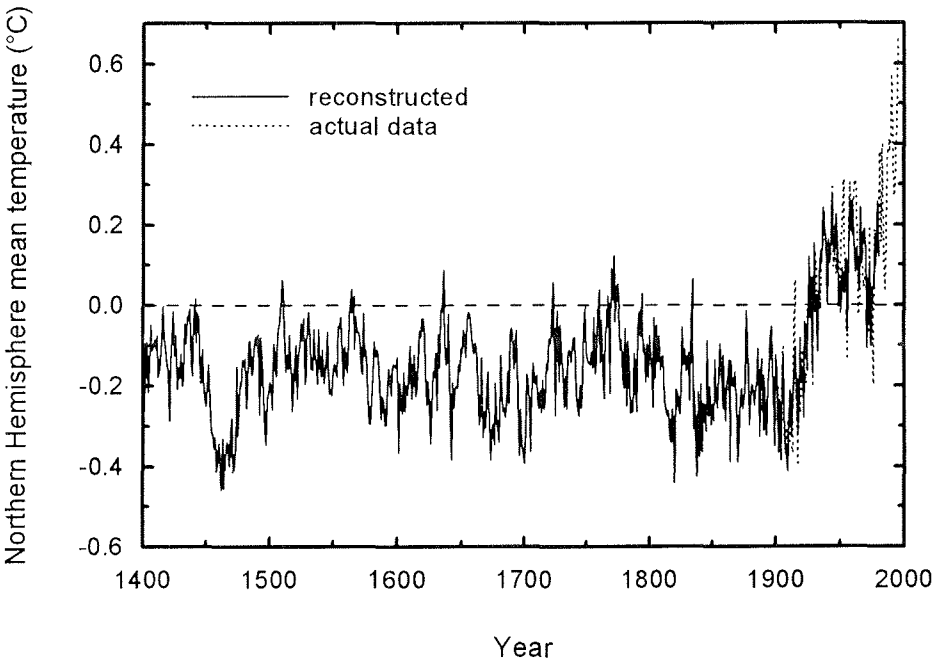

Figure 1.2. Northern Hemisphere mean annual temperature reconstruction based on the multivariate calibration of widely distributed high-resolution proxy climate indicators (see Figure 1.1) [*Mann et al.*, 1998]. The zero line corresponds to the 1902-1980 calibration mean of the quantity. Actual data are shown up to 1995. Northern Hemisphere mean annual temperatures for 1990, 1995, and 1997 were warmer than any other year since 1400. For further discussion see *Mann et al.* [1998].

1.2. Coral stable isotope records of paleoclimate

1.2.1. Introduction

The stable isotopic composition of marine calcareous organisms has been widely used for paleoenvironmental reconstructions [e.g., *Wefer and Berger*, 1991]. The use of scleractinian reef corals in paleoclimatology started after the existence of density bands in their skeletons was discovered [*Knutson et al.*, 1972]. These massive so-called "stony corals" build their skeletons of aragonite ($CaCO_3$) and grow at rates of millimeters to centimeters per year. The skeleton is extended by growth at the outermost surface of a coral colony within the living tissue layer. The tissue remains as a thin band at the outer surface of a colony because its lower margin is abruptly lifted at approximately monthly intervals [*Barnes and Lough*, 1993]. In general, these corals reveal a skeletal density banding pattern of alternating bands of high and low density, with one year being represented by a high and low density-band pair. The annual density-band pairs in coral skeletons are comparable to growth rings in trees and provide a first chronometer for the stable isotope record.

The first long (30 years) seasonal resolution coral stable isotope record was shown by *Emiliani et al.* [1978], which was followed by the works of *Fairbanks and Dodge* [1979] and *Pätzold* [1984]. The first century-long coral stable isotope record in annual resolution was shown by *Pätzold* [1984, 1986]. The reconstruction of ocean-atmosphere variability

using century-long coral stable isotope records in monthly resolution started with the work of *Cole et al.* [1993]. The field of coral paleoclimatology is rapidly growing since the NOAA workshop on coral paleoclimate reconstruction in 1992 [*Dunbar and Cole*, 1993] with an increasing number of publications coming out recently. Until now coral stable isotope records are common which provide paleoenvironmental information about the past 100-300 years on the seasonal timescale with chronology age errors of a few years only (in the worst case). The most commonly used corals in paleoclimatology are those of the genus *Porites* owing to their dense skeletons built mostly of vertical skeletal elements [*Barnes and Lough*, 1993].

Corals precipitate their aragonitic skeletons out of isotopic equilibrium with ambient seawaters. The skeletons are depleted in ^{18}O and ^{13}C with respect to isotopic equilibrium. This isotopic disequilibrium is attributed to "kinetic" isotope effects which apparently result from discrimination against the heavy isotopes of oxygen and carbon during the hydration and hydroxylation of CO_2 [*McConnaughey*, 1989a, b]. The isotopic disequilibrium is believed to be constant along the major growth axis of a coral, where growth rates are at their maximum [*McConnaughey*, 1989a]. Samples for stable isotope analysis are therefore always taken along the major axis of coral growth.

1.2.2. Coral stable oxygen isotopes - paleoclimatic interpretation

During growth, massive corals incorporate isotopic species of oxygen and carbon into their skeletons. The ratio of coral skeletal $^{18}O/^{16}O$, reported as $\delta^{18}O$, reflects the environmental conditions in the ambient seawater during skeleton precipitation. The primary influences on coral skeletal $\delta^{18}O$ variability are (1) the temperature of aragonite formation and (2) the $\delta^{18}O$ of the seawater. (1) As temperature increases, there is a decrease in the $\delta^{18}O$ (depletion in ^{18}O) of the coral skeletal aragonite. That coral $\delta^{18}O$ is a function of temperature is derived from the concept of the paleotemperature equation based on the work of *Epstein et al.* [1953]. Near-weekly resolution calibrations of *Porites* coral $\delta^{18}O$ variability suggest a temperature dependence of 0.18‰ (relative to the Pee Dee belemnite "PDB" isotopic standard) per 1°C [*Gagan et al.*, 1994]. A recent regression of 13 annually-averaged Indo-Pacific coral $\delta^{18}O$ records against gridded estimates of local SST anomaly revealed a relationship of 0.19‰/°C [*Evans et al.*, submitted 1998]. (2) Coral $\delta^{18}O$ is also a function of variations in the $\delta^{18}O$ of the seawater which can result from evaporation (enrichment in ^{18}O), precipitation (depletion in ^{18}O), or runoff (depletion in ^{18}O). High evaporation results in both an enrichment in the $\delta^{18}O$ of the seawater and a higher salinity, high precipitation (or runoff) has opposing effects. Because of this, salinity variations, if driven through evaporation, precipitation or runoff, closely covary with the $\delta^{18}O$ variations of the seawater. In localities where one of these two environmental factors dominates the other, coral $\delta^{18}O$ records can provide information either on SST (e.g., Kiritimati, central equatorial Pacific) [*Evans et al.*, 1998a] or on sea surface salinity (SSS) (e.g., Tarawa, western equatorial Pacific) [*Cole et*

al., 1993] variations. In localities where variations in both SST and SSS occur simultaneously and work in the same direction (with respect to $\delta^{18}O$) an amplified coral $\delta^{18}O$ signal can result (e.g., Dahlak, southern Red Sea) [*Klein et al.*, 1997]. However, to define the relative contribution of variations in both SST and SSS on a coral record multiple proxies (e.g., combined Sr/Ca and $\delta^{18}O$) have to be applied.

1.2.3. Coral stable carbon isotopes - paleoclimatic interpretation

The interpretation of the coral skeletal $^{13}C/^{12}C$ variations in environmental terms is still a topic of debate [*Swart et al.*, 1996a] because of complicated interactions with physiological processes such as symbiont photosynthesis and respiration. Therefore the applicability of the $\delta^{13}C$ signal measured in coral skeletons has been hampered in paleoclimatic research. A long-term decreasing trend is indicated by several coral $\delta^{13}C$ records (depletion in ^{13}C) for the past several hundred years [e.g., *Nozaki et al.*, 1978; *Pätzold*, 1986; *Quinn et al.*, 1998]. This trend is usually attributed to the corresponding decrease in the $\delta^{13}C$ of atmospheric CO_2 owing to an increased anthropogenic release of ^{13}C-depleted CO_2 resulting from fossil fuel combustion. However, the slopes of this trend differ among the coral records making quantifications difficult. Coral $\delta^{13}C$ variations on the seasonal timescale are thought to be mainly controlled by the photosynthetic activity of the coral's endosymbiotic algae, and are therefore attributed to the seasonal light cycle, cloudiness or water column transparency [*Fairbanks and Dodge*, 1979; *Pätzold*, 1984; *McConnaughey*, 1989a; *Wellington and Dunbar*, 1995]. Endosymbiotic photosynthesis preferentially fixes ^{12}C relative to ^{13}C into organic carbon, thus enriching the internal dissolved inorganic carbon (DIC) "pool" from which calcification in corals takes place with ^{13}C. In general, periods of higher photosynthesis should lead to increased concentrations of ^{13}C in coral skeletons [*Fairbanks and Dodge*, 1979; *Swart*, 1983; *McConnaughey*, 1989a]. Variations in the $\delta^{13}C$ of the DIC of the seawater have also been shown to affect the coral skeletal $\delta^{13}C$ signal [*Swart et al.*, 1996a]. On the other hand, the possible importance of changes in the autotrophy-heterotrophy diet of corals on the $\delta^{13}C$ signal in their skeletons has also been pointed out [*Carriquiry et al.*, 1994; *Swart et al.*, 1996a]. Relative changes of the proportion of autotrophic and heterotrophic food sources is assumed to influence the isotopic composition of the coral's internal DIC pool from which calcification takes place [*Swart et al.*, 1996a]. Recently *Gagan et al.* [1994, 1996] reported that ^{13}C enrichments in the skeleton of corals from Australia culminate sharply at the time of the annual coral spawning event. This was explained with the rapid sequestering of ^{12}C required to build the reproductive tissue prior to spawning.

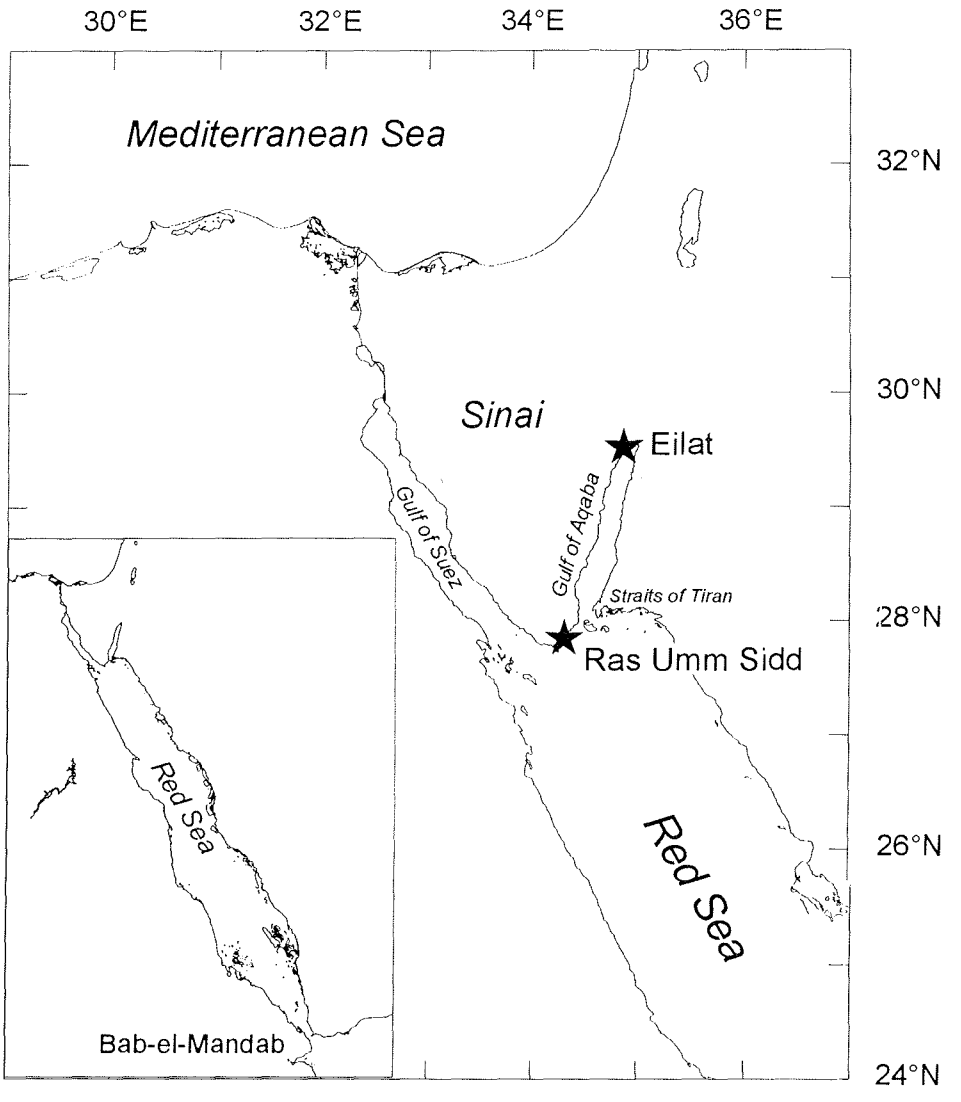

Figure 1.3. Study area in the Red Sea. The sampling locations of the coral cores are indicated by 'star' symbols. Core RUS-95 was collected at Ras Umm Sidd (Ras Mohammed National Park, Egypt), core EILAT-1 was collected at Eilat (Israel).

1.3. Study area

The study area is located near latitudes 28°-29°N at the northern rim of the African-Asian desert belt in the northernmost Red Sea. Within this thesis two coral stable isotope records from fringing reefs of the Sinai Peninsula are discussed. One from Ras Umm Sidd (Egypt) near the southern tip of the peninsula at the northern end of the Red Sea proper, and one from Eilat (Israel) near the northern end of the Gulf of Aqaba (Figure 1.3). The climate of the region is dominated by the subtropical high-pressure belt and therefore by the descending branch of the northern Hadley cell, where large-scale descending motions warm and dry the atmospheric boundary layer. In general, the warming and drying of this subsiding air near latitudes 30° is considered as the major cause of aridity in the subtropics. Above the subtropical high-pressure belt and the descending limb of the Hadley cell the subtropical westerly jet stream is located at about 12 km height. However,

the climate regime of the Mediterranean Sea with its winter rains resulting from the moisture bringing North Atlantic westerlies is located in a distance of less than 300-500 km to the north [*Buckle*, 1996; *Barry and Chorley*, 1998].

The Red Sea is a long (~2000 km) and narrow (~280 km) desert-enclosed basin with depths of up to 2800 m (Figure 1.3). It is connected to the Indian Ocean in the south by the narrow and shallow (~140 m) Strait of Bab-el-Mandab. The climate is extremely arid with high evaporation and negligible precipitation and runoff. The estimated net evaporation is ~200 cm/yr [*Morcos*, 1970; *Ahmad and Sultan*, 1989]. Therefore, the Red Sea is an evaporative basin. The Red Sea circulation is mostly driven by thermohaline forcing, wind forcing is secondary [*Eshel et al.*, 1994]. The excess of evaporation over precipitation causes a northward surface inflow through the Strait of Bab-el-Mandab. High evaporation in the northern Red Sea and low evaporation in the southern Red Sea depresses the sea level in the extreme north compared to the middle and southern part of the basin. This slope drives the thermohaline circulation and controls water mass formation [*Eshel and Naik*, 1997; *Eshel et al.*, submitted 1998]. At the northern end of the Red Sea deep water is formed and gives rise to a southward-flowing current [*Cember*, 1988].

The Gulf of Aqaba is a up to 1830-m-deep, narrow (180 km long, with 14 km average width), desert-surrounded basin forming the northeastern extension of the Red Sea proper (Figure 1.3). The climate is also arid, with high evaporation and negligible precipitation and runoff. Nutrient levels and primary production are very low and thus light penetration is deep [*Reiss and Hottinger*, 1984]. The evaporative loss is compensated by inflow from the Red Sea in the south. This inflow is confined to the upper warmer layer by a shallow sill at a water depth of 252 m (Straits of Tiran). This results in unusually high temperatures at depth, for example, 20.6°C at 1200 m. Consequently, the vertical stratification in the Gulf is unusually weak [*Klinker et al.*, 1976]. Winter cooling of the surface waters causes destabilization of the water column, which can result in deep convective mixing at the northern end of the Gulf, sometimes exceeding depths of 600-850 m [*Wolf-Vecht et al.*, 1992; *Genin et al.*, 1995], resulting in extraordinarily large plankton blooms in the surface waters [*Genin et al.*, 1995; *Lindell and Post*, 1995]. These deep vertical mixing events at the northern end of the Gulf of Aqaba are possibly unique to deep marginal seas with shallow sills [*Genin et al.*, 1995].

1.4. Material and methods

1.4.1. Coral core collection

A coral core (RUS-95) from Ras Umm Sidd (Egypt) near the southern tip of the Sinai Peninsula (Figure 1.3) was collected during the "Red Sea Program on Marine Sciences" (RSP) cruise-#1 of R/V *University I* in November-December 1995. The location is within the boundaries of the Ras Mohammed National Park [e.g., *Ormond et al.*, 1997]. A coral core (EILAT-1) from Eilat (Israel) near the northern end of the Gulf of Aqaba was collected in May 1993. Both cores were collected from large hemispherical *Porites* sp.

colonies by using a diver-operated underwater pneumatic drill with a 5-cm-diameter bit. Each core was drilled vertically, parallel to the major axis of coral growth, to the bottom of the colony. After drilling the Ras Umm Sidd core the borehole was sealed with a carbonate plug to prevent bioerosion. Visual inspection in March 1996 and December 1996 revealed that the drilling did not harm the huge coral and that the colony's living surface started to overgrow the plug. The borehole of the coral colony from Eilat was not sealed because it is still used for scientific experiments (B. Lazar, personal communication, 1997).

1.4.2. Sampling and stable isotope analysis

The drilled core segments were sliced into 3- to 5-mm-thick slabs parallel to the axis of coral growth. X radiograph positive prints of the slabs revealed a clear skeletal density-banding pattern of alternating bands of high and low density and were used as guides for spot-sampling along the axis of maximum coral growth, following precisely the major growth axis of single fans of corallites. This sampling technique limits the influence of "kinetic" isotope disequilibria effects [*McConnaughey*, 1989a, b]. According to the terminology of *Cohen and Hart* [1997] the sampling profile always followed the central axis of the highest bumps. Samples were collected by low-speed drilling using a dental tool with a 0.8-mm-diameter bit. The average growth rate of the corals and the average sample spacing provided an average resolution of more than 6 samples per year for both cores. X radiograph positive prints of the sampled coral slabs were used as controls for evaluating the position of the sampling profile. The control X radiographs revealed that the sampling profiles always followed precisely the major growth axis of single fans of corallites, i.e., the central axis of the highest bumps.

For isotopic analysis, we used a Finnigan MAT 251 mass spectrometer coupled to a Finnigan MAT automated carbonate device at the stable isotope laboratory of the Fachbereich Geowissenschaften, Universität Bremen, Germany. Long-term reproducibility, deduced from replicate measurements of an internal carbonate standard, is less than ±0.07‰ for $\delta^{18}O$ and ±0.05‰ for $\delta^{13}C$, respectively (1σ over a 3-year period). Isotopic values are reported relative to the Pee Dee belemnite (PDB) reference standard. The value of $\delta^{18}O$ and $\delta^{13}C$ are

$$\delta^{18}O = \{[(^{18}O/^{16}O)_{sample} / (^{18}O/^{16}O)_{standard}] - 1\} \times 1000$$

and

$$\delta^{13}C = \{[(^{13}C/^{12}C)_{sample} / (^{13}C/^{12}C)_{standard}] - 1\} \times 1000,$$

respectively. The RUS-95 and the EILAT-1 coral chronologies are based on 1530 and 150 stable isotope measurements, respectively.

1.4.3. Frequency domain analysis of the coral time series

For the time series analysis of the coral and climate data the AnalySeries (version 1.1) software package [*Paillard et al.*, 1996] was used. Periodicities are a recurrent and important feature in natural signals. Identifying such periodicities in a paleoclimatic time series and relating them to known oscillatory modes of the climate system is the goal of spectral and cross-spectral analysis. The Blackman-Tukey method [*Blackman and Tukey*, 1958; *Jenkins and Watts*, 1968] which is the classical method for spectral analysis was applied. This method is very robust, unlikely to present spurious spectral features. The algorithm computes first the autocovariance of the data, then applies a window (here a Tukey window), and finally Fourier-transforms the covariance functions to compute the power spectrum [e.g., *Paillard et al.*, 1996].

Singular spectrum analysis (SSA) [*Vautard and Ghil*, 1989; *Ghil and Vautard*, 1991; *Vautard et al.*, 1992] is designed to extract dominant oscillatory components from short, noisy time series without having to search for some nominally optimal band pass filter. SSA decomposes time series by data-adaptive spectral filters into nonlinear trends, oscillatory components (with anharmonic shapes) and noise. SSA is not truly a spectral analysis method because it does not decompose the signal into harmonic components. It is a form of principal component analysis and performs an empirical orthogonal function (EOF) analysis in the time domain, and thus represents the signal as a sum of components that are not necessarily oscillations, but more general, data adaptive functions [e.g., *Paillard et al.*, 1996; *Yiou et al.*, 1994; *Dettinger et al.*, 1995]. An important characteristic of SSA is the occurence of pairs of oscillatory components which have a similar shape and frequency but are in phase quadrature with each other. These two oscillatory components, which are never exactly equal, are associated with oscillatory phenomena in the time series. The associated oscillatory component is then reconstructed as the sum of the two components of an oscillatory pair [*Vautard and Ghil*, 1989; *Ghil and Vautard*, 1991; *Vautard et al.*, 1992; *Yiou et al.*, 1994].

SSA was used to reconstruct the most prominent oscillatory components (or modes) in the coral time series, to determine their relative contributions to the time series, and to detect the changes in their amplitude over time, using the AnalySeries (version 1.1) software package [*Paillard et al.*, 1996]. SSA was performed with several window lengths (25, 30, 35, 40, 50, 60, 75, and 80 years, respectively) to find the optimal window. For SSA two computers were run simultaneously for approximately 24 hours per day during a 2-week period. To determine the corresponding frequencies of the reconstructed oscillatory modes Blackman-Tukey spectral analysis was applied. Those periodicities which occured as prominent oscillations in both spectral analysis and SSA of the coral time series were interpreted as the most robust oscillatory signals. Before applying spectral analysis, cross-spectral analysis or SSA the individual time series were detrended by removing the linear trend and normalized to unit variance.

1.4.4. Data access via Internet

Instrumental and proxy climate data are available from several databases via Internet. These data are essential for the calibration and interpretation of every paleoclimatic record. For example, in addition to the datasets of instrumental SST observations in the northern Red Sea records of temperature and precipitation from about 80 weather stations (from Cyprus to Sudan, from Libya to Iraq) were investigated for the environmental interpretation of the coral records. A lot of datasets concerning instrumental climate observations and climate indices can be accessed via the server of the Lamont-Doherty Earth Observatory of Columbia University, Palisades, NY, USA (<http://ingrid.ldgo.columbia.edu/SOURCES/>). A good source for paleoclimatological data (corals, ice cores, tree rings, sediment cores, pollen) is the World Data Center-A for Paleoclimatology, NOAA/NGDC, Boulder, CO, USA (<http://www.ngdc.noaa.gov/paleo/paleo.html>). Another source for paleoclimatological data is the PANGAEA (PaleoNetwork for Geological and Environmental Data) database, AWI/MARUM, Bremerhaven/Bremen, Germany (<http://www.pangaea.de>). Supplementary datasets concerning publications in NATURE are available via <http://www.nature.com>. In addition to this more formal way of data collection several new paleoclimate datasets not available via Internet at this time were derived directly from colleagues by e-mail.

1.5. Focus of this thesis

The original focus of our coral-based work in the northern Red Sea was the reconstruction of climate variability. It was considered to use coral cores collected from the fringing reefs of the Sinai Peninsula [e.g., *Walther*, 1888; *Gvirtzman and Buchbinder*, 1978] for the generation of stable isotope records in annual to seasonal resolution [e.g., *Pätzold*, 1984; *Pätzold*, 1986]. Coral stable isotope-based paleoclimatological research in this subtropical region started with the pioneering works of *Klein et al.* [1992, 1993] which showed that on the seasonal timescale coral $\delta^{18}O$ variations in the northern Red Sea primarily reflect the seasonal SST cycle.

Every long seasonal resolution coral stable isotope record will extend the discontinuous instrumental observations of climate in the northern Red Sea region and therefore will hopefully provide a better understanding of Middle East climate variability during the past several hundred years. The work of *Genin et al.* [1995] which reported a deep vertical water mass mixing event at the northern end of the Gulf of Aqaba (the northeastern extension of the Red Sea proper) caused by a cold air-temperature anomaly following the large explosive volcanic eruption of Mount Pinatubo (Philippines, 1991) inspired us to detect such events in the stable isotopic composition of corals from that location. The focus of this thesis therefore is to reconstruct climate and ocean variability by using stable isotope records of modern corals from the reefs of the northern Red Sea.

1.6. Publications, manuscripts to be submitted

Chapters 2.-5. of this thesis are four manuscripts to be submitted to or already published in reviewed scientific journals.

Chapter 2.

Vertical water mass mixing and plankton blooms recorded in skeletal stable carbon isotopes of a Red Sea coral

Published as:

Felis, T., J. Pätzold, Y. Loya, and G. Wefer, Vertical water mass mixing and plankton blooms recorded in skeletal stable carbon isotopes of a Red Sea coral, *J. Geophys. Res.*, *103*, 30731-30739, 1998.

This publication provides new insight into the controls of the $\delta^{13}C$ signal in the skeletons of massive corals and therefore addresses a long standing problem in coral-based paleoclimate reconstructions. Constraints are placed on a relatively new idea that skeletal $\delta^{13}C$ variations are partially controlled by the coral's balance between autotrophic and heterotrophic food sources. Furthermore, the coral $\delta^{13}C$ record (EILAT-1) can be used to reconstruct oceanographic and climatic variability at the northern end of the Gulf of Aqaba (northern Red Sea) during a 19-year period (1974-1993). Evidence is presented for a coral response from the northern Red Sea to the cooling associated with the large explosive volcanic eruptions of El Chichón (Mexico, 1982) and Mount Pinatubo (Philippines, 1991). The publication promotes the applicability of seasonal skeletal $\delta^{13}C$ records of corals which change from autotrophy under normal conditions to increased heterotrophy during plankton bloom events as indicators of ocean paleoproductivity at interannual resolution, available from no other source.

Chapter 3.

First results of a coral-based history of recent climate in the northern Red Sea

Published as:

Felis, T., J. Pätzold, G. Wefer, M. Fine, Y. Loya, and A. H. Nawar, First results of a coral-based history of recent climate in the northern Red Sea, *Zbl. Geol. Paläont. Teil I*, *1997/1-2*, 197-207, 1998.

This publication discusses the most recent years (1990-1994) of the coral record from Ras Umm Sidd (RUS-95) in the northern Red Sea to test the applicability of the coral $\delta^{18}O$ signal of this specific colony for the reconstruction of large-scale sea surface temperature (SST) variability in this area on the seasonal and interannual timescale. The results are promising. For the first time correlation coefficients between a northern Red Sea coral $\delta^{18}O$ record and regional instrumental observations of SST are discussed.

Chapter 4.

A coral oxygen isotope record of temperature, aridity, and deep water formation from the northern Red Sea since the year 1750

To be submitted as:

Felis, T., J. Pätzold, Y. Loya, M. Fine, A. H. Nawar, and G. Wefer, A coral oxygen isotope record of temperature, aridity, and deep water formation from the northern Red Sea since the year 1750.

This manuscript discusses the entire coral $\delta^{18}O$ record from Ras Umm Sidd (RUS-95) in the northern Red Sea (1750-1995). The bimonthly resolution time series provides information on past climate and ocean variability during the past 245 years and reveals new aspects on large-scale Middle East climate variability on the interannual to interdecadal/multidecadal timescale. The coral $\delta^{18}O$-based SSTs suggest that mean annual northern Red Sea SSTs between 1751 and 1900 were ~0.3°C lower than the 20th century average. The northern Red Sea is probably the only site in the world oceans where water mass formation occurs and reef corals grow. The winter $\delta^{18}O$ values of the coral record can be used to detect episodic events of deep water formation of the Red Sea thermohaline circulation.

Chapter 5.

Interaction between the North Atlantic Oscillation and the El Niño-Southern Oscillation in a Middle East coral record

To be submitted as:

Felis, T., J. Pätzold, Y. Loya, and G. Wefer, Interaction between the North Atlantic Oscillation and the El Niño-Southern Oscillation in a Middle East coral record.

This manuscript discusses the coral $\delta^{18}O$ record from Ras Umm Sidd (RUS-95) in the frequency domain. Spectral analysis, cross-spectral analysis, and singular spectrum analysis (SSA) reveal that both the North Atlantic Oscillation (NAO) and the El Niño-Southern Oscillation (ENSO) contributed significantly to the climate variability of the Middle East during the past ~250 years on interannual to multidecadal timescales. The results suggest that interaction between extratropical and tropical modes of the global climate system via atmospheric teleconnections has an important control on subtropical climate variability. Furthermore a prominent cooling interval in the first half of the 19th century which is evident in several Northern Hemisphere temperature reconstructions can be related to a 70-year climate oscillation of most probably North Atlantic origin, at least for the Middle East region.

2. Vertical water mass mixing and plankton blooms recorded in skeletal stable carbon isotopes of a Red Sea coral

Published as:
Felis, T., J. Pätzold, Y. Loya, and G. Wefer, Vertical water mass mixing and plankton blooms recorded in skeletal stable carbon isotopes of a Red Sea coral, *J. Geophys. Res.*, *103*, 30731-30739, 1998.

2.1. Abstract

The environmental interpretation of the $^{13}C/^{12}C$ variations in the skeletons of massive corals is still a matter of debate. A 19-year seasonal skeletal $^{13}C/^{12}C$ record of a shallow-water *Porites* coral from the northern Red Sea (Gulf of Aqaba) documents interannual events of extraordinarily large plankton blooms, indicated by anomalous ^{13}C depletions in the coral skeleton. These blooms are caused by deep vertical water mass mixing, convectively driven in colder winters, which results in increased supplies of nutrients to the surface waters. The deep vertical mixings can sometimes be driven by the cooling occuring throughout the Middle East after large tropical volcanic eruptions. We therefore have evidence in our coral skeletal $^{13}C/^{12}C$ record for an indirect volcanic signal of the eruptions of El Chichón (1982) and Mount Pinatubo (1991). Deep mixing induced $^{13}C/^{12}C$ variations of the dissolved inorganic carbon in the surface waters can be neglected at this location. We therefore suggest that the ^{13}C skeletal depletions can be best explained by changes in the coral's autotrophy-heterotrophy diet, through increased

heterotrophic feeding on zooplankton during the blooms. Increased feeding on ^{13}C-depleted zooplankton or increased heterotrophy at the expense of autotrophy can both result in a ^{13}C-depleted coral skeleton. However, this suggestion requires more testing. If our conclusions are substantiated, seasonal skeletal $^{13}C/^{12}C$ records of corals which change from autotrophy under normal conditions to increased heterotrophy during bloom events may be used as indicators of ocean paleoproductivity at interannual resolution, available from no other source.

2.2. Introduction

The $^{18}O/^{16}O$ variations in the skeletons of massive corals have been shown to provide a high-resolution seasonal proxy for sea surface temperature (SST) and/or sea surface salinity (SSS) for the past several centuries [*Cole et al.*, 1993; *Linsley et al.*, 1994; *Quinn et al.*, 1996; *Charles et al.*, 1997; *Kuhnert et al.*, 1998]. The interpretation of seasonal coral skeletal $^{13}C/^{12}C$ variations in environmental terms is still a topic of debate [*Swart et al.*, 1996a] because of complicated interactions with physiological processes such as symbiont photosynthesis and respiration. Therefore the applicability of the seasonal $\delta^{13}C$ signal measured in coral skeletons as a recorder of past ocean-atmosphere variability has been hampered in paleoclimatic research. Exceptions include the work of *Shen et al.* [1992]. The most prevalent opinion is that skeletal $\delta^{13}C$ in photosynthetic corals on the seasonal timescale is mainly controlled by the photosynthetic activity of the coral's endosymbiotic algae, and it is therefore attributed to the seasonal light cycle, cloudiness or water column transparency [*Fairbanks and Dodge*, 1979; *Pätzold*, 1984; *McConnaughey*, 1989a; *Wellington and Dunbar*, 1995]. Endosymbiotic photosynthesis preferentially fixes ^{12}C relative to ^{13}C into organic carbon, thus enriching the internal dissolved inorganic carbon (DIC) "pool" from which calcification in corals takes place with ^{13}C. In general, periods of higher photosynthesis should lead to increased concentrations of ^{13}C in coral skeletons [*Fairbanks and Dodge*, 1979; *Swart*, 1983; *McConnaughey*, 1989a]. It is widely assumed that photosynthesis withdraws and respiration adds ^{13}C-depleted carbon to the internal DIC pool [*McConnaughey et al.*, 1997]. Variations in the $\delta^{13}C$ of the DIC of the seawater have also been shown to affect the coral skeletal $\delta^{13}C$ signal [*Swart et al.*, 1996a]. On the other hand, the possible importance of changes in the autotrophy-heterotrophy diet of corals on the $\delta^{13}C$ signal in their skeletons has also been pointed out [*Carriquiry et al.*, 1994; *Swart et al.*, 1996a]. Heterotrophy means coral feeding on allochthonous sources of organic carbon, mainly zooplankton with its typical ^{13}C-depleted isotopic signature, and a resulting contribution of ^{13}C-depleted respiratory CO_2 to the coral's internal DIC pool. This is opposite to the process where organic carbon is usually derived by photosynthetic corals, i.e., from photosynthesis of the endosymbiotic algae (autotrophy). Relative changes of the proportion of these two organic carbon food sources, with their different isotopic signatures, could influence the isotopic composition of the coral's internal DIC pool from

which calcification takes place [*Swart et al.*, 1996a]. Recently *Gagan et al.* [1994, 1996] reported that ^{13}C enrichments in the skeleton of corals from Australia culminate sharply at the time of the annual coral spawning event. This was explained with the rapid sequestering of ^{12}C required to build the reproductive tissue prior to spawning. Gagan et al. suggested that the reproductive modulation of the coral skeletal $\delta^{13}C$ signal can be used as an accurate time marker for constructing coral time series.

Here we present evidence from the moderately oligotrophic Gulf of Aqaba [*Reiss and Hottinger*, 1984] in the northern Red Sea that coral skeletal $\delta^{13}C$ variations record interannual oceanographic and climatic variability. A seasonal 19-yr skeletal $\delta^{13}C$ record derived from a shallow-water coral documents interannual events of extraordinarily large plankton blooms. These blooms are caused by deep vertical water mass mixing, which sometimes can be driven by the cooling following major tropical volcanic eruptions [*Genin et al.*, 1995].

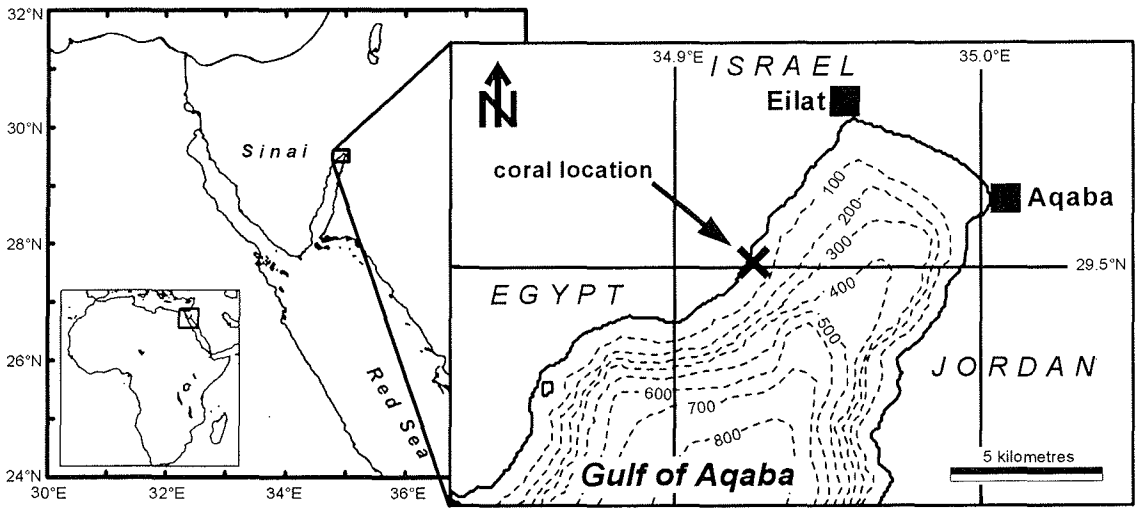

Figure 2.1. Sampling location of the coral core (EILAT-1) near the northern end of the Gulf of Aqaba (Red Sea). The coral colony is closely linked to open-sea conditions due to the narrow fringing reef and the steep submarine slope.

The Gulf of Aqaba is a 1830-m-deep, narrow (180 km long, with 14 km average width), desert-surrounded basin forming the northeastern extension of the Red Sea (Figure 2.1). The climate is arid, with high insolation, high evaporation (~400 cm/yr) and negligible precipitation (~2.2 cm/yr) and runoff. Nutrient levels and primary production are very low and thus light penetration is deep [*Reiss and Hottinger*, 1984]. The evaporative loss is compensated by inflow from the Red Sea in the south. This inflow is confined to the upper warmer layer by a shallow sill at a water depth of 252 m (Straits of Tiran). This results in unusually high temperatures at depth, for example, 20.6°C at 1200

m. Consequently, the vertical stratification in the Gulf is unusually weak [*Klinker et al.*, 1976]. During summer (April-October), an upper 200-300 m thermally stratified layer with temperatures between 21 and 26°C at the surface overlies a thermally homogenous layer of ~21°C [*Klinker et al.*, 1976; *Wolf-Vecht et al.*, 1992]. Winter cooling (November-March) of the surface waters causes destabilization of the water column, which can result in deep convective mixing in late winter (February/March) at the northern end of the Gulf [*Wolf-Vecht et al.*, 1992; *Genin et al.*, 1995]. Interannual variations in winter air temperature are directly linked to variations in maximum mixing depth [*Genin et al.*, 1995]. Anomalously cold winters drive the vertical mixing to depths exceeding 600-850 m [*Wolf-Vecht et al.*, 1992; *Genin et al.*, 1995]. During summer the stratified surface waters of the Gulf are depleted of nutrients. Because the concentration of nutrients increases with depth [*Reiss and Hottinger*, 1984; *Lindell and Post*, 1995], winters with deep vertical mixing result in increased supplies of nutrients to the surface waters, leading to extraordinarily large plankton blooms in spring (mid-March to mid-May) [*Genin et al.*, 1995; *Lindell and Post*, 1995].

Winters which drive a deep vertical mixing have only slightly lower SSTs than average winter minimum SSTs. This is made possible by the unusually weak water-column stratification of the Gulf of Aqaba. The contribution of salinity to vertical variations in water density is negligible in the Gulf; because of this, vertical profiles of density and potential temperature are almost mirror images of each other [*Reiss and Hottinger*, 1984; *Genin et al.*, 1995]. The average lowest daily SST from 1988-1995, a period encompassing winters with and without deep vertical mixing, had a range of only 0.7°C. The minimum mixing depth during that period occured in the winter of 1990-1991 (300 m), and the maximum mixing depth occured in the winter of 1991-1992 (>850 m). However, the mixing depth is also dependent on the length of the sea-cooling period during winter. The deep vertical mixing events at the northern end of the Gulf of Aqaba are amplifications of rather small-scale interannual variations in winter minimum SST, and they are possibly unique to deep marginal seas with shallow sills [*Genin et al.*, 1995].

2.3. Material and methods

A coral core (EILAT-1) was collected from a 0.85-m coral colony (*Porites* sp.) near the northern end of the Gulf of Aqaba (29°31'N, 34°56'E), using an underwater pneumatic drill (Figure 2.1). The coral is located at a water depth of 4.5 m in front of the reef crest near the H. Steinitz Marine Biology Laboratory at Eilat (Israel). The site is characterized by a steep submarine slope; the proximity to the 500- to 700-m-deep central-trough of the Gulf is ~3 km. The Gulf becomes increasingly deeper to the southwest; the location is therefore closely linked to open-sea conditions. We only analyzed the top 0.16 m of the core because changes in the coral's growth axis did not provide a continuous record below this depth.

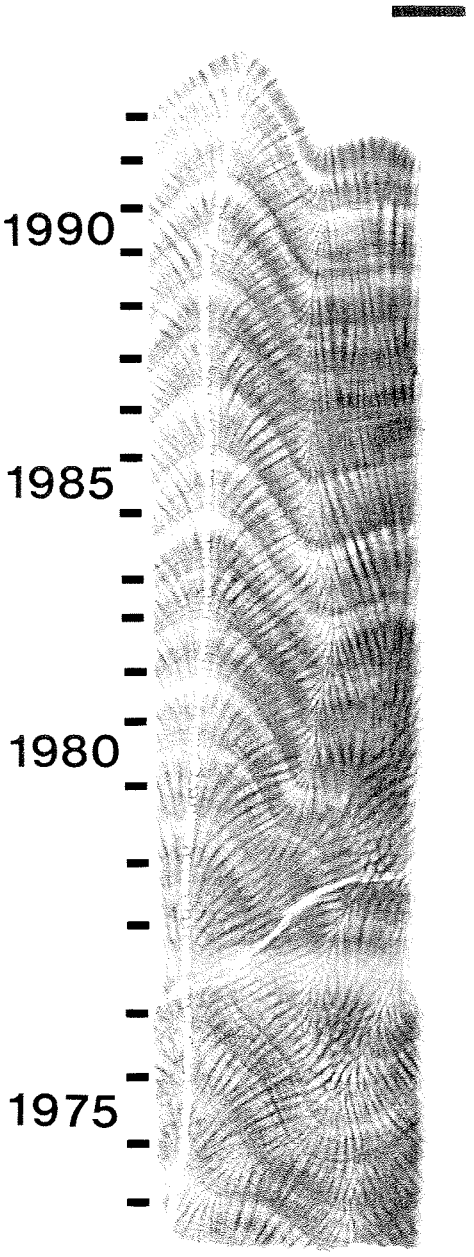

Figure 2.2. X radiograph positive print of the coral slab (*Porites* sp.). The skeletal density banding pattern of alternating bands of high (dark color) and low density (light color) can be clearly seen. One year is represented by a low and high density-band pair. Also shown are the corresponding years of skeleton precipitation. The sampling transect appears as white circles. The black bar in the upper right corner is 1 cm.

X radiograph positive prints of the sliced 5-cm-diameter coral core were used as guides for continuous spot sampling along the axis of maximum coral growth, following precisely the major growth axis of a single fan of corallites (Figure 2.2). This sampling technique limits the influence of "kinetic" isotope disequilibria effects [*McConnaughey*, 1989a,b]. Samples were collected by low-speed drilling using a dental tool with a 0.8-

mm-diameter bit. For isotopic analysis we used a Finnigan MAT 251 mass spectrometer coupled to a Finnigan MAT automated carbonate device at the stable isotope laboratory of the Department of Geosciences at Bremen University, Germany. Long-term reproducibility, deduced from replicate measurements of an internal carbonate standard, is less than ±0.07‰ for $\delta^{18}O$ and ±0.05‰ for $\delta^{13}C$, respectively (1σ over a 1-year period). Values are reported relative to the Pee Dee belemnite (PDB) reference standard.

The growth rate of the coral decreased more or less continuously from 10 (1974) to 4.5 mm/yr (1992). We sampled at approximately 1-mm intervals, which results in an average sampling frequency of 7-8 samples per year, providing approximately bimonthly resolution. Coral skeletal $\delta^{18}O$ variations at the northern end of the Gulf of Aqaba primarily reflect the seasonal SST cycle of ~5°C [*Klein et al.*, 1992; *Klein et al.*, 1993], SSS is nearly constant and varies by less than 0.5‰ throughout the year [*Wolf-Vecht et al.*, 1992). The coral chronology is constructed by setting the maximum $\delta^{18}O$ value in a given year equal to mid-March (on average, the time of winter minimum SST) and by assuming a constant coral growth rate between March of each year. Therefore we interpolated linearly between these fixed points for further age assignments.

Water samples for $\delta^{13}C$ analysis of the DIC were collected during the day in glass bottles (3-m water depth) and poisoned, and bottle caps were sealed with wax. Total dissolved inorganic carbon was extracted by acidification. The cryogenically purified, resultant gas was analyzed using a Finnigan MAT Delta-E mass spectrometer at the stable isotope laboratory, Department of Geosciences, Bremen University. Values are reported relative to PDB with an analytical error of ca. ±0.1‰ (1σ).

Before applying the least squares smoothing filter [*Savitzky and Golay*, 1964] to the $\delta^{13}C$ data in Figure 2.3b, the series was interpolated linearly to six equally spaced values per year for the filter to be optimal, providing a bimonthly resolution. All these procedures were performed using the AnalySeries (1.0a7) software package [*Paillard et al.*, 1996].

2.4. Results and discussion

2.4.1. Vertical mixing, plankton blooms, and volcanic eruptions recorded in coral skeletal $\delta^{13}C$

Figure 2.3b shows the skeletal $\delta^{18}O$ and $\delta^{13}C$ records obtained from the coral core. Coral skeletal $\delta^{18}O$ is not sensitive enough to detect the anomalously cold winters driving a deep vertical mixing at the northern end of the Gulf because these winters have only slightly lower SSTs than average winter minimum SSTs. Because the concentration of nutrients increases with water depth [*Reiss and Hottinger*, 1984; *Lindell and Post*, 1995], increasingly more nutrients are transported successively to the surface waters when mixing is reaching increasingly greater depths. Thus a vertical mixing exceeding a threshold depth of ~550 m results in extraordinarily large blooms (B. Lazar, personal communication, 1997). This critical depth is actually a band and can not be considered as

a definite depth limit (B. Lazar, personal communication, 1997). Figure 2.3c shows maximum winter mixing depths at the northern end of the Gulf of Aqaba. Figure 2.3d presents the average concentration of surface chlorophyll *a* during spring bloom, revealing the relationship between the critical mixing depth of 550 m and increased blooms [*Genin et al.*, 1995]. The coral skeletal $\delta^{13}C$ record shows anomalous ^{13}C depletions in the winters of 1975-1976, 1988-1989, 1991-1992, and 1992-1993, which correspond to all the available instrumentally documented deep vertical mixing and increased plankton bloom events, using the 550 m threshold depth as criterion (Figure 2.3c). These anomalous ^{13}C skeletal depletions rise up during winter from a ground level of a more or less clear seasonal skeletal $\delta^{13}C$ cycle in the coral record, as emphasized by smoothing of the $\delta^{13}C$ data (Figure 2.3b). On the other hand, in the winters of 1976-1977, 1989-1990, and 1990-1991, with only shallow to moderate maximum mixing depth, resulting in only minor spring blooms, no anomalous ^{13}C depletions can be identified in the coral record. The typical pattern of the anomalous ^{13}C skeletal depletions in the coral record can be described as (1) extraordinarily negative $\delta^{13}C$ values (<-2.5‰), (2) a strong decrease of >1.0‰ followed by a >1.4‰ increase producing pronounced spikes, and (3) the timing in late winter-early spring. In the winter of 1974-1975, vertical mixing exceeded 500 m [*Klinker et al.*, 1976] but probably not the 550-m threshold depth, as our coral skeletal $\delta^{13}C$ record indicates no deep vertical mixing and increased plankton bloom event.

Figure 2.3. Coral record (EILAT-1) and environmental parameters for the northern end of the Gulf of Aqaba (Red Sea). (a) Annual coral growth rate is calculated from mid-March to mid-March and plotted on mid-September. (b) Coral skeletal $\delta^{18}O$ and $\delta^{13}C$ records. The thick line represents a 21-point least squares smoothing filter [*Savitzky and Golay*, 1964]. The dotted bars indicate deep vertical mixing and increased plankton bloom events, derived from the coral $\delta^{13}C$ record. (c) Maximum winter mixing depth, mainly based on temperature versus depth profiles, is plotted on mid-March (1, *Klinker et al.* [1976]; 2, *Reiss et al.* [1976]; 3, *Reiss et al.* [1977]; 4, *Genin et al.* [1995] and *Wolf-Vecht et al.* [1992]; 5-7, *Genin et al.* [1995]; 8, *Genin et al.* [1995] and *Lindell and Post* [1995]). Arrows indicate that mixing exceeded the maximum depth that was measured. Mixings exceeding the critical depth band of ~550 m (horizontal dashed line) result in extraordinarily large spring blooms (B. Lazar, personal communication, 1997). (d) Average concentration of surface chlorophyll *a* during spring bloom [*Genin et al.*, 1995], as an indicator of bloom intensity and surface zooplankton concentration (A. Genin, personal communication, 1997), is plotted on mid-April. (e) Average monthly winter air temperature (December-February) for Eilat [*Baker et al.*, 1994], is plotted on mid-January; the horizontal solid line represents the average of this record. Vertical dashed lines indicate the two largest tropical volcanic eruptions during the record [*Robock and Mao*, 1992]. (f) Sunshine hours/month for Eilat (Israel Meteorological Service, unpublished data, 1991).

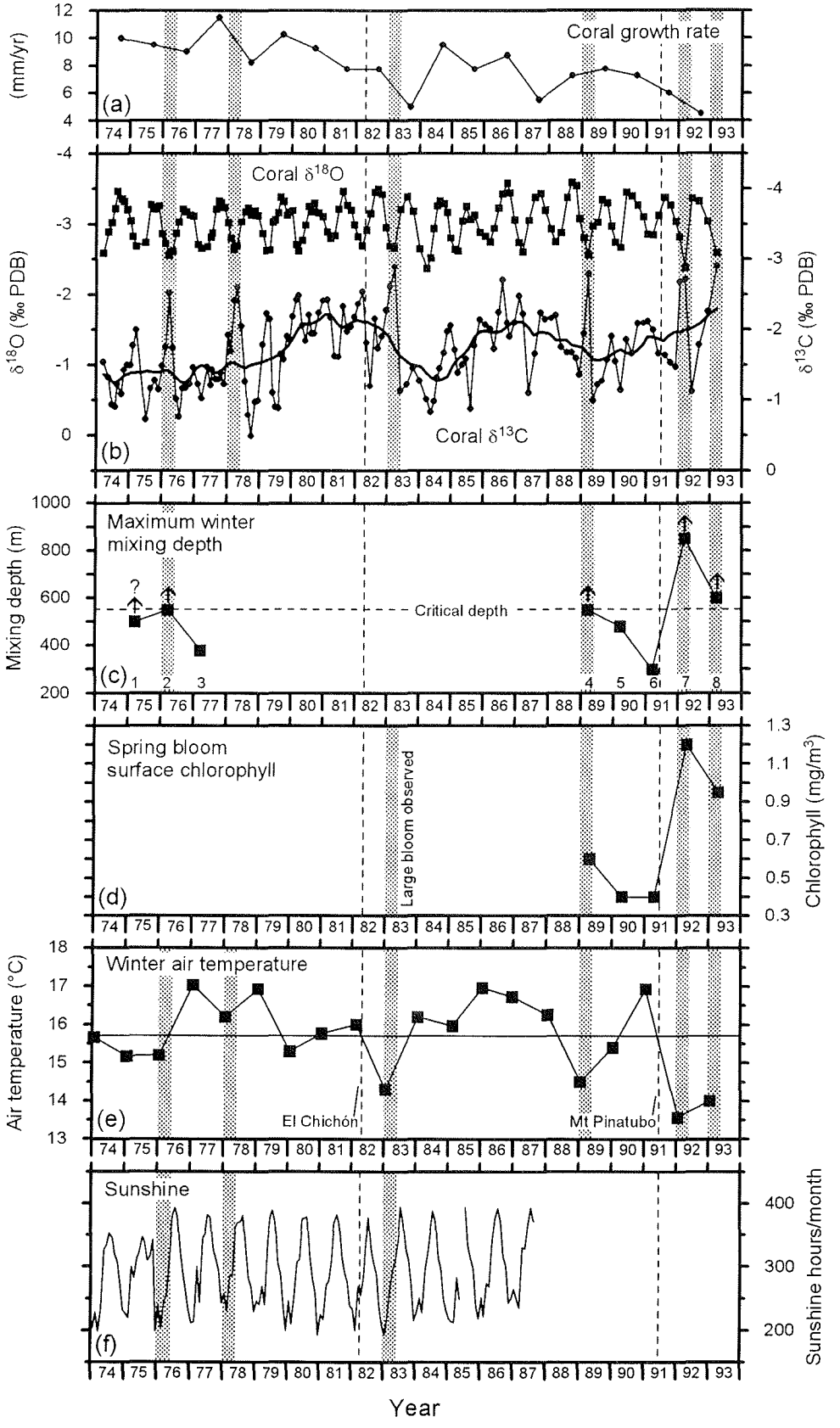
Coral growth rate
(mm/yr)
(a)
Coral δ18O
Coral δ13C
δ18O (‰ PDB)
δ13C (‰ PDB)
(b)
Maximum winter mixing depth
Critical depth
Mixing depth (m)
(c)
Spring bloom surface chlorophyll
Large bloom observed
Chlorophyll (mg/m3)
(d)
Winter air temperature
El Chichón
Mt Pinatubo
Air temperature (°C)
(e)
Sunshine
Sunshine hours/month
(f)
Year

Using these factors as criteria, we detected two more winters with a deep vertical mixing and increased plankton bloom event (1977-1978 and 1982-1983) during a period without available instrumental-based records (Figures 2.3b and 2.3c). The 1982-1983 event has been previously suggested because of an extraordinarily large spring bloom only observed by the naked eye and the anomalously cold winter air temperatures [*Genin et al.*, 1995] (Figures 2.3d and 2.3e). A common phenomenon throughout the Middle East is a cold air temperature anomaly occuring during the first winter after major tropical volcanic eruptions [*Robock and Mao*, 1992]. The 1991-1992 deep vertical mixing and increased plankton bloom event was driven by the anomalously cold air temperatures following the eruption of Mount Pinatubo (Philippines, June 1991) [*Genin et al.*, 1995]. The event in the winter of 1982-1983 followed the eruption of El Chichón (Mexico, April 1982). We therefore have evidence in our skeletal $\delta^{13}C$ record for a coral response from the northern Red Sea to the two largest tropical volcanic eruptions which occured during that period [*Robock and Mao*, 1992]. The effect of volcanism-induced cooling on coral skeletal $\delta^{18}O$ has recently been described [*Gagan and Chivas*, 1995; *Crowley et al.*, 1997]. *Crowley et al.* [1997] also discussed $\delta^{13}C$ enrichments coinciding with the $\delta^{18}O$ enrichments associated with volcanic eruptions in their coral record. However, we present evidence for an indirect volcanic signal in the skeletal $\delta^{13}C$ record of a coral from a location where coral $\delta^{18}O$ is not sensitive enough to detect such events.

Apparently, the deep vertical mixing and increased plankton bloom events occuring during the 1970s were not as strongly coupled to anomalously cold winter air temperatures as those which occured since the beginning of the 1980s. During the 1970s probably other forcing factors were driving the deep vertical mixing in the northern Gulf of Aqaba. The reason for this is beyond the scope of this paper. However, for the period 1988-1995 winter averages of other potential forcing parameters (solar radiation, relative humidity, wind speed, and cloud cover) were shown to be not significantly correlated with the maximum mixing depth of the water column [*Genin et al.*, 1995].

2.4.2. The seasonal coral skeletal $\delta^{13}C$ cycle

In many locations throughout the tropics and subtropics coral skeletal $\delta^{13}C$ variations on the seasonal timescale have been attributed to the seasonal cycle of light [*Fairbanks and Dodge*, 1979; *Pätzold*, 1984; *McConnaughey*, 1989a; *Shen et al.*, 1992; *Wellington and Dunbar*, 1995]. This has also been shown for the northern end of the Gulf of Aqaba [*Klein et al.*, 1992, 1993], where the warm summer season is more sunnier and the cold winter season is more cloudier. Light intensity and SST are positively correlated, with a time lag of about one to three months. Annual light intensity minima (December-February) precede SST minima (March), and light intensity maxima (July) precede SST maxima (August). For coral skeletal $\delta^{18}O$ and $\delta^{13}C$ variations this should result in a weak negative correlation at the seasonal scale and a shift in phase. A scatterplot of $\delta^{18}O$ versus $\delta^{13}C$ is shown in Figure 2.4. For the period 1974-1983, skeletal $\delta^{18}O$ and $\delta^{13}C$ in our

coral record reveal such a negative correlation (Figure 2.3b). The correlation coefficient r = -0.35 is significant at the 99.5% level. This negative correlation can be explained with increased endosymbiotic photosynthesis due to higher insolation during the warm summer season, resulting in a ^{13}C-enriched and ^{18}O-depleted coral skeleton, and vice versa for the winter season [*Fairbanks and Dodge*, 1979; *Swart*, 1983; *McConnaughey*, 1989a]. For the period 1984-1993 this correlation breaks down; there is no statistically significant correlation between skeletal $\delta^{18}O$ and $\delta^{13}C$ (r = -0.11), owing to changes in the pattern of the seasonal $\delta^{13}C$ cycle. This change in correlation, when interpreted as a decreased influence of the seasonal light cycle on coral skeletal $\delta^{13}C$, could be due to disturbances in the water-column transparency, probably caused by increased building activities along the shore since the early 1980s. In summary, the seasonal cycle of light probably affects the skeletal $\delta^{13}C$ variations of our coral, especially during 1974-1983, but it can not account for the variability in the seasonal amplitude, and in no case for the anomalous ^{13}C depletions which occur during the entire period of the coral record (Figures 2.3b and 2.3f). The ^{13}C depletions are superimposed on this more or less light-controlled coral skeletal $\delta^{13}C$ cycle. Therefore the process creating the ^{13}C skeletal depletions has to have its origin in the water column, as runoff-induced $\delta^{13}C$ variations of the surface water DIC should also be negligible in this desert-surrounded arid setting.

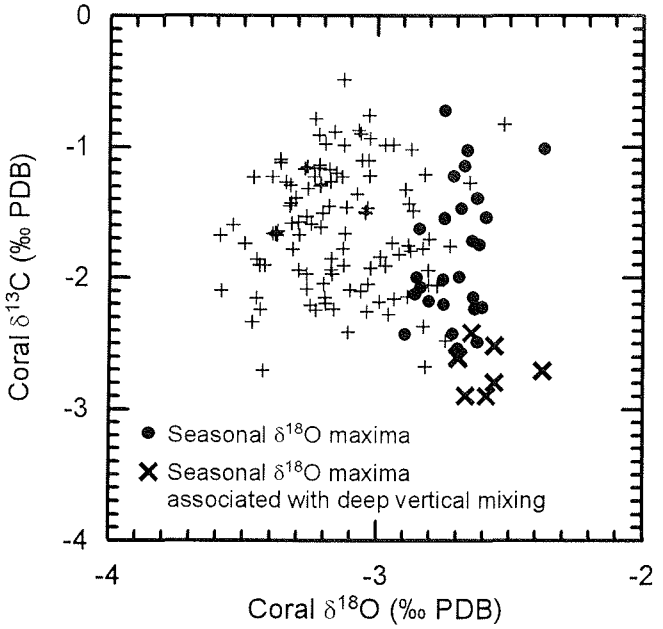

Figure 2.4. Scatterplot of coral skeletal $\delta^{18}O$ versus $\delta^{13}C$. Seasonal $\delta^{18}O$ maxima are labeled (most enriched $\delta^{18}O$ value in a given year including adjacent values $>\delta^{18}O_{max}$-0.1‰). Seasonal $\delta^{18}O$ maxima which are associated with deep vertical mixing and increased plankton bloom events are additionally labeled.

2.4.3. Causes for the anomalous ^{13}C depletions in the coral skeleton

The coral stable isotope record seems to be fairly robust with respect to "kinetic" isotope disequilibria effects [*McConnaughey*, 1989a,b]. Although the growth rate of the coral decreases from 10 (1974) to 4.5 mm/yr (1992), the isotope values do not show a corresponding enrichment in skeletal ^{18}O or ^{13}C as expected from kinetic isotope fractionations (Figures 2.3a and 2.3b). The calculated annual coral growth rate (mid-March to mid-March) reveals no pattern associated with the anomalous ^{13}C skeletal depletions. Two further methods of growth rate calculation were performed by fixing the coral chronology on mid-March and on mid-August simultaneously (on average, the time of minimum and maximum SSTs; results are not shown here). Also, in this calculated annual (mid-August to mid-August) as well as the seasonal growth rate (mid-August to mid-March and mid-March to mid-August), no pattern associated with the ^{13}C skeletal depletions was detected.

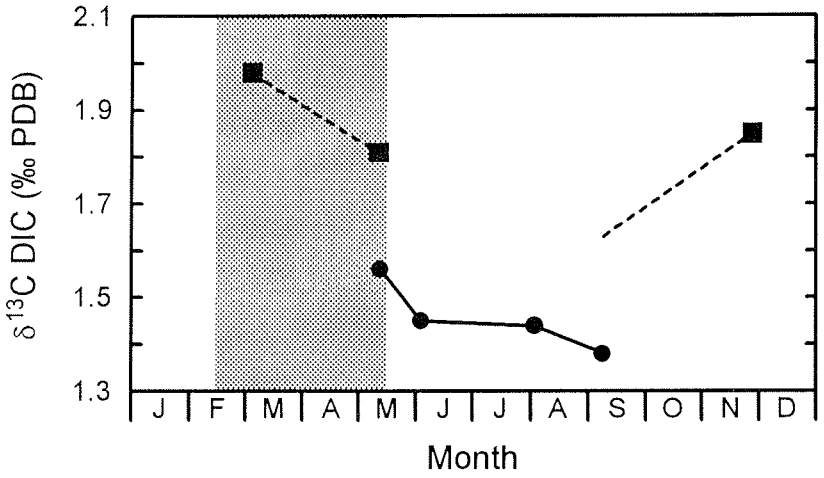

Figure 2.5. Composite record of the seasonal $\delta^{13}C$ cycle of the dissolved inorganic carbon (DIC) in the surface waters at the northern end of the Gulf of Aqaba (solid circles are from 1993, with 3-m depth and daytime sampling; solid squares are from 1979 to 1980, with the calculated average of daytime samples from the 0- to 10-m depth interval, derived from the data by *Shemesh et al.* [1994]). The dotted bar indicates the period of late winter-spring, where deep vertical mixing and increased plankton bloom events usually occur. The $\delta^{13}C$ of the surface water DIC has a seasonal cycle of probably less than 0.4‰, considering a correction for the 0.25‰ offset between the mid-May measurements from 1980 and 1993. This offset is probably due to an increased anthropogenic input of ^{13}C-depleted CO_2 into the atmosphere. For example, measurements of the $\delta^{13}C$ of the surface water DIC near Bermuda during the period 1984-1992 indicated an average decrease of ~0.022‰/yr [*Bacastow et al.*, 1996].

The $\delta^{13}C$ of the DIC in the upper waters (0-200 m) of the northern Gulf of Aqaba throughout the year (on average, 1.9‰) is controlled mainly by the process of isotopic equilibrium with the atmosphere [*Shemesh et al.*, 1994]. Vertical mixing in winter results

in a water mass with upper water $\delta^{13}C$-DIC characteristics. There is no imprint of the ^{13}C-depleted $\delta^{13}C$-DIC signature of the summer deep water (on average, 1.55‰ in 200-600 m) on the upper waters during vertical mixing [*Shemesh et al.*, 1994]. Deep mixing induced $\delta^{13}C$ variations of the surface water DIC therefore can be excluded to create the anomalous ^{13}C depletions in our coral skeletal $\delta^{13}C$ record. The $\delta^{13}C$ of the surface water DIC (0-10 m) shows a weak seasonal cycle of probably less than 0.4‰ (Figure 2.5), which has a roughly negative correlation to the average seasonal coral skeletal $\delta^{13}C$ variations. Thus it seems to be of minor influence on the $\delta^{13}C$ variability in the coral skeleton. The seasonal $\delta^{13}C$ variations of the surface water DIC are probably modulated by the seasonal cycle of productivity, resulting in ^{13}C enriched values during the period of increased productivity in winter and spring and ^{13}C-depleted values in summer due to increased oxidation of organic matter in the reef.

Three possible mechanisms, which are not mutually exclusive, are suggested to explain the anomalous ^{13}C depletions in the coral skeleton.

1. During the extraordinarily large plankton blooms following a deep vertical mixing, the water-column transparency at the northern end of the Gulf is reduced [*Genin et al.*, 1995]. Because of the reduced light availability and therefore decreased photosynthetically available radiation, the photosynthesis of the coral's endosymbiotic algae should decrease, resulting in a ^{13}C-depleted coral skeleton [*Fairbanks and Dodge*, 1979; *Swart*, 1983; *McConnaughey*, 1989a].
2. During the increased blooms, consequently, the concentration of surface zooplankton is unusually high (A. Genin, personal communication, 1997) and near-reef areas are strongly affected by zooplankton blooms at this location [*Echelman and Fishelson*, 1990]. In general, deep-water corals (>30 m), which are growing at lower light intensities compared with shallow-water corals, largely feed on allochthonous sources of carbon (e.g., zooplankton) [*Muscatine et al.*, 1989], owing to the attenuation of photosynthetically available radiation with depth and therefore lower photosynthetic rates. This has also been described for the reef at Eilat [*Muscatine et al.*, 1989]. Earlier studies in the Caribbean described typical feeding responses for *Porites* spp. corals on zooplankton [*Lewis and Price*, 1975]. Recently, controlled field experiments in the Caribbean demonstrated relatively high capture rates of massive corals for zooplankton [*Sebens et al.*, 1996]. The $\delta^{13}C$ of average marine plankton from the Gulf has values of about -21‰ [*Shemesh et al.*, 1994]. That the isotopic signature of a coral's food produces an imprint on the isotopic composition of a coral's skeleton has been shown by experiments, where ^{14}C-spiked foods were fed to corals and ^{14}C incorporation into skeletal carbonates was observed [*Pearse*, 1970]. We therefore suggest that the anomalous ^{13}C skeletal depletions in our coral record can be best explained by changes in the coral's autotrophy-heterotrophy diet through increased heterotrophic feeding on zooplankton during the extraordinarily large plankton blooms. It is assumed that the typical ^{13}C-depleted isotopic

signature of the zooplankton produces an imprint on the isotopic composition of the coral's skeleton through an increased contribution of ^{13}C-depleted respiratory CO_2 to the coral's internal DIC pool. Possible reasons for an increased feeding on zooplankton during the blooms are increased availability and/or decreased autotrophy due to a reduced photosynthetic activity of the coral's endosymbiotic algae during these periods of reduced water column transparency.

3. However, *McConnaughey et al.* [1997] postulated that not much ^{13}C-depleted respiratory CO_2 is incorporated into coral skeletons because corals calcify mainly during the daytime, which is the period of active photosynthesis when photosynthetic CO_2 uptake is several times faster than respiratory CO_2 release, while feeding on plankton occcurs mainly at night. The carbonate isotopic composition of coral skeletons should therefore reflect periods of maximum photosynthetic influence rather than periods of strong respiratory influence [*McConnaughey et al.*, 1997]. Therefore a third possible mechanism, which also postulates increased heterotrophy, is suggested to explain the anomalous ^{13}C skeletal depletions in our coral record. Increased heterotrophy at the expense of autotrophy by the coral during the extraordinarily large plankton blooms should reduce the "photosynthetic effect" described by *McConnaughey* [1989a] through reduced photosynthetic activity of the coral's endosymbiotic algae, and it should result in a ^{13}C-depleted coral skeleton without any need for incorporating more ^{13}C-depleted respiratory CO_2 from increased zooplankton feeding. In summary, we interpret our skeletal $\delta^{13}C$ record as being typical for a coral which is fluctuating between autotrophy and heterotrophy on the interannual scale, where increased heterotrophy during extraordinarily large plankton bloom events results in anomalous ^{13}C depletions in the coral skeleton.

That increased heterotrophy produces ^{13}C-depleted coral skeletons has been suggested to explain a general increase in the seasonal skeletal $\delta^{13}C$ variation with depth in coral records of *Porites lobata* from Costa Rica [*Carriquiry et al.*, 1994] because this pattern is contrary to the expected attenuation with depth in proportion to the decrease in light-intensity variation with depth [*Fairbanks and Dodge*, 1979]. In coral records (*Porites* spp.) from Eilat also no attenuation in the seasonal skeletal $\delta^{13}C$ variation with depth on a profile from 3 to 51 m is evident in the data of *Klein et al.* [1993], despite only 20-30% of the measured surface light values being available at 51-m depth [*Reiss and Hottinger*, 1984]. This additionally implies changes in the autotrophy-heterotrophy diet of Eilat *Porites* spp. corals on the seasonal scale and a resulting modulation of the seasonal $\delta^{13}C$ variations in their skeletons.

Additional geochemical tests to verify our hypothesis that the anomalous ^{13}C skeletal depletions are due to increased coral heterotrophy could include measurements of the $^{15}N/^{14}N$ ratio of the organic content of the coral skeleton. However, preliminary tests revealed a coral skeletal nitrogen content of a few ppm in a rough approximation (C. Gervais and M. Segl, personal communication, 1998). Because of this, $\delta^{15}N$ profiles

with a resolution of ~2-4 years only would be possible, not usable for verification. Further tests could include feeding experiments with $\delta^{13}C$ analysis of the zooplankton, coral tissue, endosymbiotic algae, and coral skeleton or, for example, feeding experiments with ^{14}C-spiked zooplankton.

We exclude the possibility that the extensive algal mat which covered broad sections of the underlying reef during the large 1991-1992 bloom event [*Genin et al.*, 1995] was responsible for the anomalous ^{13}C depletion in the coral skeleton that winter-spring, considering a possible covering of the coral colony and anerobic conditions at the base of the mat. The algal mat had a thickness of only ~15 cm above the bottom, and therefore corals growing on elevated substrates were not covered by algae [*Genin et al.*, 1995]. The coral colony from which the core for this study was recovered is 0.85 m high, growing solitary in front of the reef crest, and it can be assumed to have not been affected by the algal mat. Because the 1991-1992 bloom event is thought to be the largest during the last 48 years [*Genin et al.*, 1995], algae covering of our colony during the period of the coral record can therefore be excluded. Considering a possible effect of the algal mat on the DIC in the ambient water, an enrichment in $\delta^{13}C$ should be expected, which is opposite to the anomalous $\delta^{13}C$ depletions in the coral skeleton. On the other hand, the decay of the algal mat could have possibly caused a depletion in the $\delta^{13}C$ of the local DIC. However, as our coral colony is growing in front of the reef crest and closely linked to open sea conditions because of the steep submarine slope, we do not expect any significant depletion in the $\delta^{13}C$ of the local DIC owing to algal mat decay at this location.

Recently, *Spero et al.* [1997], on the basis of experiments with foraminifers and discussions of earlier results of *McConnaughey* [1989b], proposed that coral skeletal $\delta^{13}C$ possibly becomes more depleted in ^{13}C with increasing seawater $[CO_3^{2-}]$ and pH. In the surface waters of the northern Gulf of Aqaba there are no significant changes in pH, carbonate alkalinity, or total dissolved inorganic carbon during vertical mixing in winter [*Shemesh et al.*, 1994]. Therefore we can exclude deep mixing induced changes in the carbonate system of the surface waters to create the anomalous ^{13}C skeletal depletions in our coral record.

One would expect that the maximum coral skeletal $\delta^{18}O$ value in a given year, indicating the period of coldest SST (mid-March), always precedes an anomalous ^{13}C depletion, indicating extraordinarily large plankton blooms (mid-March to mid-May). However, as our resolution is approximately bimonthly, it can not be expected that the coral record preserves 1- to 2-month-scale time lags. Furthermore, differences in the proxy signal preservation of different environmental forcing factors during skeletogenesis, e.g. of sudden pulse events (plankton blooms) and annual cycles (SST), may complicate the preservation of such small-scale time lags in the coral skeletal $\delta^{18}O$ and $\delta^{13}C$ records [*Taylor et al.*, 1995; *Barnes et al.*, 1995]. This probably also explains the anomalous ^{13}C depletions apparently preceding the most positive $\delta^{18}O$ values in one or two winters with deep vertical mixing and increased plankton blooms in our coral record. Independent of these uncertainties in small-scale timing, our results show that the coral successfully

records large-scale late winter-spring conditions (February to mid-May) in the water column. In summary, the coral skeletal $\delta^{13}C$ record provides a proxy for the interannual oceanographic variability in the northern Gulf of Aqaba, which can sometimes be influenced by the cooling following large tropical volcanic eruptions.

2.5. Conclusions

Our findings provide support for the idea that changes in the autotrophy-heterotrophy diet of corals play an important role in the $\delta^{13}C$ variability of their skeletons. The anomalous ^{13}C skeletal depletions in our coral record, indicating deep vertical mixing and increased plankton bloom events in the northern Gulf of Aqaba (Red Sea), can be best explained by increased heterotrophic feeding on zooplankton during extraordinarily large plankton blooms. Increased heterotrophic feeding on ^{13}C-depleted zooplankton or increased heterotrophy at the expense of autotrophy by the coral can both result in a ^{13}C-depleted coral skeleton. Validation of our conclusions awaits testing with coral records from other locations and experimental evidence. If our conclusions are substantiated, then our results promote the applicability of seasonal skeletal $\delta^{13}C$ records from corals which change from autotrophy under normal conditions to increased heterotrophy during extraordinary bloom events as potential indicator of ocean paleoproductivity at interannual resolution. Of course, there will be a restriction to specific oceanographic settings with bloom events at the interannual scale (e.g., regions with monsoon-driven upwelling) and where instrumental data of the past several years (insolation, plankton or chlorophyll, and $\delta^{13}C$ of DIC) are available for calibration with the coral record. Because ocean productivity variations are always linked to oceanographic and climatic changes, the study of long skeletal $\delta^{13}C$ records of these specific corals, modern and fossil colonies, may lead to a better understanding of past climate variability, available from no other source.

2.6. Acknowledgments

We thank M. Segl and her team for stable isotope analysis; R. Klein and M. Fine for drilling the core; T. J. Crowley, A. Genin, and B. Lazar for helpful comments on earlier versions of the manuscript; T. A. McConnaughey for fruitful discussions; two anonymous reviewers for helpful comments and suggestions; C. Moos for water isotopic analysis; C. Gervais and M. Segl for nitrogen tests; the H. Steinitz Marine Biology Laboratory of the Interuniversity Institute at Eilat (Israel) for logistic support; and the Israel Meteorological Service for providing climatological data. This work is part of the Red Sea Program on Marine Sciences (RSP), funded by the BMBF (German Ministry for Education, Science, Research, and Technology) through grant 03F0151A.

3. First results of a coral-based history of recent climate in the northern Red Sea

Published as:
Felis, T., J. Pätzold, G. Wefer, M. Fine, Y. Loya, and A. H. Nawar, First results of a coral-based history of recent climate in the northern Red Sea, *Zbl. Geol. Paläont. Teil I, 1997/1-2*, 197-207, 1998.

3.1. Abstract

The oxygen isotopic composition of a *Porites* sp. coral from the Sinai peninsula successfully records the large-scale seasonal variability in sea surface temperature of the northern Red Sea. The 5-year oxygen isotope record strongly correlates with a record of sea surface temperature at the monthly timescale (r = -0.85). The seasonality of the coral oxygen isotope record reveals about 78% of the seasonal sea surface temperature cycle. The coral isotopic signal is probably reduced by about 12% due to seasonal changes in the isotopic composition of the seawater. Also the mean annual oxygen isotopic signal follows the sea surface temperature record. These first results demonstrate the applicability of the oxygen isotopic composition of this *Porites* sp. colony for reconstructing past climate variability in this region.

3.2. Zusammenfassung

Die Sauerstoffisotopenzusammensetzung einer *Porites* sp. Koralle von der Sinai-Halbinsel zeichnet die großräumige saisonale Variabilität der Oberflächenwassertemperaturen im nördlichen Roten Meer erfolgreich auf. Der Sauerstoffisotopenverlauf über 5 Jahre zeigt eine hohe Korrelation mit aufgezeichneten Oberflächenwassertemperaturen (r = -0.85), bezogen auf monatliche Werte. Die Saisonalität des Isotopenverlaufs in der Koralle beschreibt etwa 78% des saisonalen Zyklus der Oberflächenwassertemperaturen. Das Sauerstoffisotopensignal der Koralle ist aufgrund von saisonalen Änderungen in der Isotopenzusammensetzung des Meerwassers möglicherweise um etwa 12% reduziert. Auch die Jahresmittelwerte des Sauerstoffisotopensignals folgen den aufgezeichneten Oberflächenwassertemperaturen. Diese ersten Ergebnisse zeigen, daß sich die Sauerstoffisotopenzusammensetzung dieser *Porites* sp. Kolonie zur Rekonstruktion der Klimavariabilität der Vergangenheit in dieser Region eignet.

3.3. Introduction

Instrumental observations of climate in the northeast Africa/Middle East region only extend back to around 1870, starting with the opening of the Suez Canal in 1869. These records of air temperature or precipitation from weather stations [*Baker et al.*, 1994] in Cairo, Jerusalem and Suakin (Sudan), and ship-based observations of sea surface temperature (SST) in the Red Sea [*Slutz et al.*, 1985], are discontinuous. Continuous observations of SST in the northern Red Sea rarely span more than 20 years (Figure 3.1). But centuries-long continuous climate records are essential for the reconstruction of regional climate variability, as well as for understanding the interactions of the different modes of the global climate system, as the El Niño-Southern Oscillation (ENSO) phenomenon, the Asian monsoon, the North Atlantic Oscillation (NAO) or the Atlantic SST dipole. On the other hand, records from varied proxy sources (tree rings, banded corals, varved sediments, ice cores) provide a tool for reconstructing past seasonal to centennial-scale climate variability. These paleoclimatic records are also a central issue for climate predictability as well as for the assessment of perturbations to the natural climate variability through the anthropogenic injection of fossil fuel CO_2 into the atmosphere.

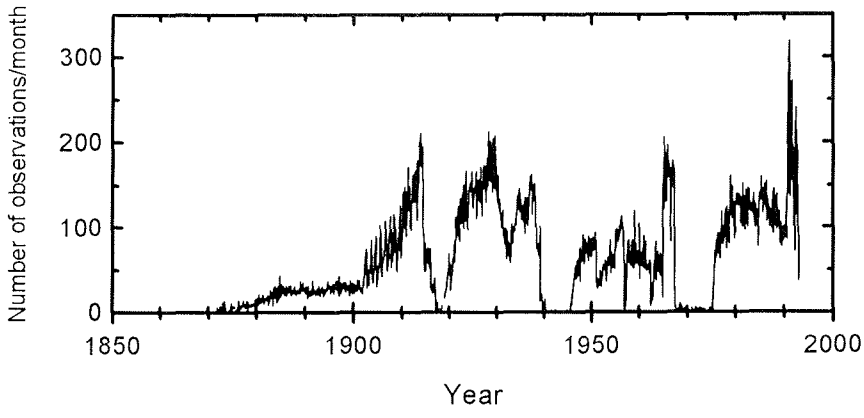

Figure 3.1. Time series of the number of ship-based instrumental SST observations per month [*Slutz et al.*, 1985] in a 2°×2° grid box located in the northern Red Sea, centered at 27.0°N/35.0°E (Figure 3.2). Significant data gaps occur during the war years (1916-1920, 1939-1946 and 1967-1975) and before 1903.

The stable oxygen isotopic composition of century-old, annually banded massive corals has been widely used for high-resolution paleoenvironmental reconstructions of SST and/or sea surface salinity variability of the past several hundred years in tropical and subtropical regions [*Nozaki et al.*, 1978; *Pätzold*, 1986; *Cole et al.*, 1993; *Druffel and Griffin*, 1993; *Quinn et al.*, 1993; *Dunbar et al.*, 1994; *Heiss*, 1994; *Linsley et al.*, 1994; *Quinn et al.*, 1996; *Swart et al.*, 1996b, c; *Charles et al.*, 1997; *Crowley et al.*, 1997]. The Red Sea coast is fringed by a narrow belt of modern coral reefs, which are among the most impressive reefs in the world. However, coral-based paleoenvironmental records from the Red Sea are limited to a few studies, including *Heiss* [1994], *Klein et al.* [1997] and *Schrag et al.* [1997].

Corals build their skeleton of aragonite ($CaCO_3$) and grow at rates of millimeters to centimeters per year. During growth, they incorporate isotopic species of oxygen into their skeleton. The ratio of coral skeletal $^{18}O/^{16}O$, reported as $\delta^{18}O$, reflects the environmental conditions in the ambient seawater during skeleton precipitation. The primary influences on coral skeletal $\delta^{18}O$ variability are the temperature of aragonite formation and the $\delta^{18}O$ of seawater. As temperature increases, there is a decrease in the $\delta^{18}O$ (depletion in ^{18}O) of the coral skeletal aragonite. In the tropical and subtropical oceans, variations in the $\delta^{18}O$ of the seawater can result from evaporation (enrichment in ^{18}O), precipitation (depletion in ^{18}O), or runoff (depletion in ^{18}O). In the arid, desert-surrounded northern Red Sea the latter two factors can be neglected. In this region coral skeletal $\delta^{18}O$ variations have been shown to reflect primarily the seasonal SST cycle [*Klein et al.*, 1992; *Schrag et al.*, 1997].

Here we present first results of a $\delta^{18}O$-based chronology of the last approximately 250 years from a northern Red Sea coral. The youngest 5 years of the record are investigated to test the applicability of the $\delta^{18}O$ signal of this specific coral for the reconstruction of large-scale SST variability in this region at the seasonal and interannual scale.

3.4. Material and methods

On a "Red Sea Program on Marine Sciences"-cruise a coral core was recently recovered from a fringing reef site at Ras Umm Sidd/Egypt (27°50.9'N, 34°18.6'E) near the southern tip of the Sinai peninsula (Figure 3.2). The location is within the boundaries of the Ras Mohammed National Park. The site is characterized by a narrow fringing reef in shallow water which terminates abruptly. The morphology creates a steep reef wall descending down to about 10-20 m, followed by a steep submarine slope down to the depths of the Red Sea. The coral core was collected from a large hemispherical 2.6-m-high *Porites* sp. colony, using an underwater pneumatic drill with a 5-cm-diameter bit. The core was drilled vertically, parallel to the main axis of coral growth. After drilling, the hole was sealed with a carbonate plug to prevent bioerosion. The coral is still growing at a water depth of about 5.5 m, located 20 m inside the reef front in a huge lagoon, which is half-open to the sea. The location Ras Umm Sidd faces the Red Sea proper, sheltering barrier reefs or islands do not exist (Figure 3.3). Therefore, the coral can be considered to be closely linked to open-sea conditions in the northern Red Sea.

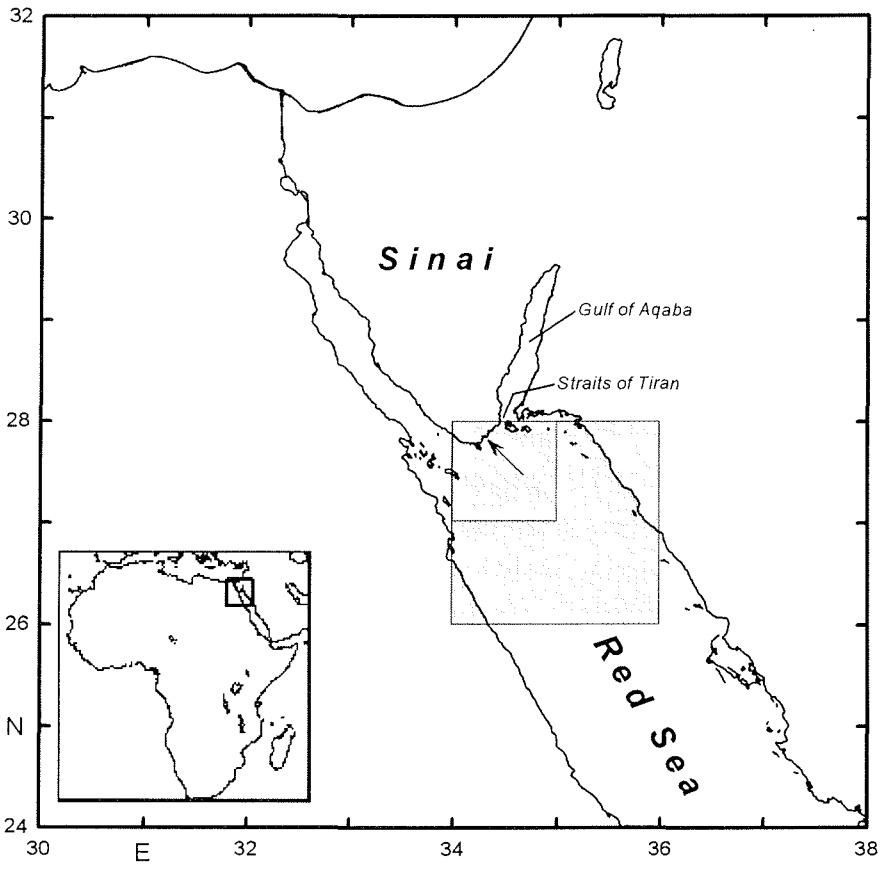

Figure 3.2. Map of the northern Red Sea. The arrow indicates the sampling location of the coral core at Ras Umm Sidd (Egypt) near the southern tip of the Sinai peninsula. The shaded boxes indicate the locations of the grid boxes for which coarse-gridded instrumental SST observations are available. The light-shaded box (2°×2°) represents the grid box for the SST data from *Slutz et al.* [1985], the dark-shaded box (1°×1°) represents the grid box for the SST data from *Reynolds and Smith* [1994] (see also Figure 3.5b and 3.6).

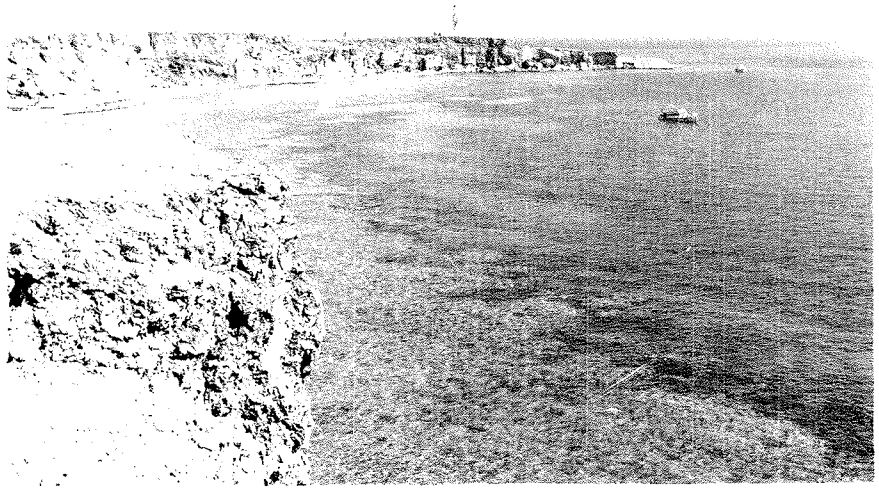

Figure 3.3. Ras Umm Sidd (Sinai/Egypt, northern Red Sea), view looking eastward. The narrow fringing reef in shallow water which terminates abruptly can be clearly seen. The location of the *Porites* sp. colony from which the coral core was recovered is indicated by the white arrow. The Ras Umm Sidd lighthouse is located on emerged fossil reef terraces, these reefs developed during periods of sea level high-stand in the Late Quaternary [*Gvirtzman et al.*, 1992; *Gvirtzman* 1994].

The coral core was sliced into 3- to 5-mm-thick slabs parallel to the axis of growth. X-radiograph positive prints of the slabs were used as a guide for continuous spot-sampling along the axis of maximum coral growth, following precisely the major growth axis of a single fan of corallites (Figure 3.4). Carbonate powder samples were collected by low-speed drilling using a dental tool with a 0.8-mm-diameter bit. The drilling depth for sampling was about 2 mm. The growth rate of the coral averages 10 mm per year and varies by about 4 mm. Samples were taken at approximately 1-mm intervals along the profile, providing nearly monthly resolution.

For isotopic analysis, we used a Finnigan MAT 251 mass spectrometer coupled to a Finnigan automated carbonate device at the Fachbereich Geowissenschaften, Universität Bremen (Germany). Long-term reproducibility, deduced from replicate measurements of an internal carbonate standard (Solnhofen limestone of 63-80 μm), is less than ±0.07‰ for $\delta^{18}O$ (1σ over a 1-year period). The value of $\delta^{18}O$ is

$$\delta^{18}O = \{[(^{18}O/^{16}O)_{sample} / (^{18}O/^{16}O)_{standard}] - 1\} \times 1000.$$

All measurements are reported relative to the Pee Dee belemnite (PDB) reference standard. Calibrations of *Porites* $\delta^{18}O$ variability suggest a temperature dependence of about 0.18‰/°C [*Gagan et al.*, 1994]. This relation is going to be more and more used for the temperature interpretation of century-long *Porites*-based $\delta^{18}O$ records [e.g.,

Charles et al., 1997], taking the place of the *Epstein et al.* [1953] equation in coral-based paleoclimatic research, which suggests that the $\delta^{18}O$ of biogenic calcium carbonate decreases by about 0.22‰ for every 1°C rise in water temperature.

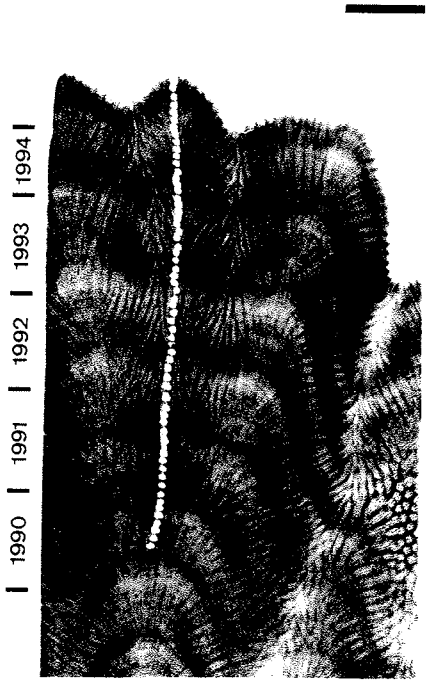

Figure 3.4. X-radiograph positive print of the slab from the youngest segment of the core from the annually banded *Porites* sp. coral from Ras Umm Sidd. The skeletal density banding pattern of alternating bands of high (dark colour) and low (light colour) density can be clearly identified. One year is represented by a low/high density-band couple. The sampling profile for stable isotope analysis appears as white dots. Also shown are the corresponding years of skeleton precipitation. The black bar in the upper right corner is 1 cm.

The coral $\delta^{18}O$ time series is constructed by setting the most positive $\delta^{18}O$ values equal to February of every year (on average, the coldest month of the year), assuming a constant coral growth rate between February of every year, and interpolating linearly between these fixed points for all further age assignments. This approach creates the potential for a 1- to 2-month time-scale error in any given year, but it is the most objective method for century-long coral $\delta^{18}O$ records [*Charles et al.*, 1997]. The 8 to 13 coral $\delta^{18}O$ values per year were interpolated linearly to 12 equally spaced values per year, using the AnalySeries(1.0a7) software package [*Paillard et al.*, 1996], providing a monthly resolution for comparison with SST data.

The monthly SST data which are used for comparison with the coral $\delta^{18}O$ record are coarse-gridded SST observations in a 1°×1° grid box in the northern Red Sea, including the sampling location at Ras Umm Sidd (Figure 3.2). These data are based on SST fields blended from ship, buoy and bias-corrected satellite data [*Reynolds and Smith*, 1994].

3.5. Results and discussion

For the northern Red Sea it has been shown that the seasonal SST variability (of about 7°C) is the major controlling factor of seasonal coral $\delta^{18}O$ variations [*Klein et al.*, 1992; *Schrag et al.*, 1997], because the $\delta^{18}O$ of the seawater is nearly constant throughout the year. In this arid, desert-surrounded region, with high insolation, high evaporation (~400 cm $year^{-1}$) and negligible precipitation (~2.2 cm $year^{-1}$) and runoff [*Reiss and Hottinger*, 1984], the seasonal salinity variability in the upper waters is about 0.5‰ [*Paldor and Anati*, 1979; *Wolf-Vecht et al.*, 1992].

The coral $\delta^{18}O$ record is shown in Figure 3.5 as a time series. Coral $\delta^{18}O$ strongly correlates with the observed monthly SST record. The correlation coefficient of $r = -0.85$ is significant at the 99.5% level. The SST record shows an average seasonal cycle of about 7.4°C. When the calibration of *Gagan et al.* [1994] for coral $\delta^{18}O$-temperature dependence is used (0.18‰/°C), the average coral $\delta^{18}O$ seasonality of 1.04‰ reveals a temperature change of about 5.8°C, which is about 78% of the average seasonal SST cycle.

The seasonal salinity cycle in the upper waters of the northern Red Sea is positively correlated to the seasonal cycle of SST (Figure 3.5). This means highest salinity occurs during periods of highest SST and strongest ^{18}O depletions in the coral skeleton (summer), and vice versa. High evaporation results in both a higher salinity and an enrichment in the ^{18}O of the seawater. Scaling of the 0.5‰ salinity variability [*Paldor and Anati*, 1979; *Wolf-Vecht et al.*, 1992] by means of the standard $\delta^{18}O$-salinity relation for Red Sea waters [*Craig*, 1966] results in less than 0.15‰ seasonal $\delta^{18}O$ seawater change. This calculated seasonal variation in the $\delta^{18}O$ of the seawater and the seasonal SST cycle should have opposing effects on the $\delta^{18}O$ in the coral skeleton, resulting in a reduced coral skeletal $\delta^{18}O$ signal (Figure 3.5). The seasonal $\delta^{18}O$ variability of the seawater has a magnitude of about 14% of the seasonal coral skeletal $\delta^{18}O$ cycle. The coral $\delta^{18}O$ signal therefore is probably reduced by about 12%, due to seasonal changes in the isotopic composition of the seawater. That means without seasonal $\delta^{18}O$ variations of the seawater the coral skeletal $\delta^{18}O$ record would have predicted about 89% of the average seasonal SST cycle. Minor but significant contributions from variations in seawater $\delta^{18}O$ on the seasonal $\delta^{18}O$ cycle of northern Red Sea corals were recently reported by *Schrag et al.* [1997].

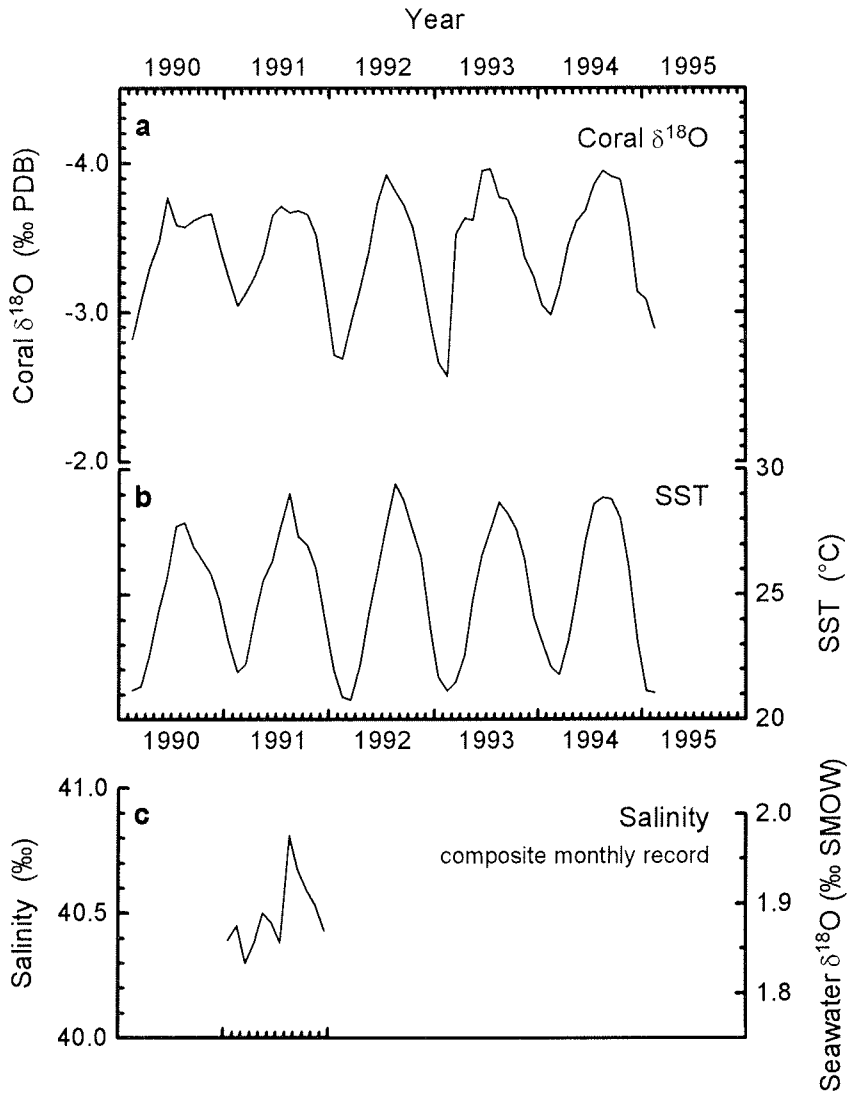

Figure 3.5. Time series of coral $\delta^{18}O$, SST, and salinity in the upper waters. The coral $\delta^{18}O$ record strongly correlates with the observed monthly SST record (correlation coefficient r = 0.85, significant at the 99.5% level). The seasonal salinity variability of the seawater of about 0.5‰ corresponds to less than 0.15‰ seasonal $\delta^{18}O$ seawater change [*Craig*, 1966]. This variation in seawater $\delta^{18}O$ and the seasonal SST cycle should have opposing effects on the $\delta^{18}O$ in the coral skeleton, resulting in a reduced coral skeletal $\delta^{18}O$ signal on the seasonal scale. For locations see Figure 3.2. (a) Coral $\delta^{18}O$ record from Ras Umm Sidd. Note that the ‰-PDB axis is inverted for better comparison with temperatures. (b) Monthly SST record in a 1°×1° grid box located in the northern Red Sea [*Reynolds and Smith*, 1994], including the sampling location. (c) Composite record of the monthly variation in salinity for the upper 150 m of the Straits of Tiran, derived from measurements during 1974-1977, 1 average year is shown [*Paldor and Anati*, 1979]; same timescale as in (a) and (b). The corresponding $\delta^{18}O$ seawater values are indicated by the y-axis on the right, calculated from its relation with salinity [*Craig*, 1966]; SMOW is the mean ocean water standard.

For comparison of the interannual variability in coral $\delta^{18}O$ and SST, the monthly data of every year were averaged into one value per year. The mean annual coral $\delta^{18}O$ values and the mean annual SST record show a good visual correlation at the interannual scale (Figure 3.6), but the correlation coefficient of r = -0.73 is not statistically significant because of only 4 data points. The range of the interannual variations in coral $\delta^{18}O$ is high compared to changes in SST. The range of the interannual SST variability over the period 1991-1994 is about 0.5°C. Coral $\delta^{18}O$ variations predict a much higher interannual SST variability of about 1°C over this period, although the coral $\delta^{18}O$ seasonality reveals only about 78% of the seasonal SST cycle, as discussed before. The average seasonal variations in the isotopic composition of the seawater cannot account for this amplification of the mean annual coral $\delta^{18}O$ signal in terms of temperature interpretation.

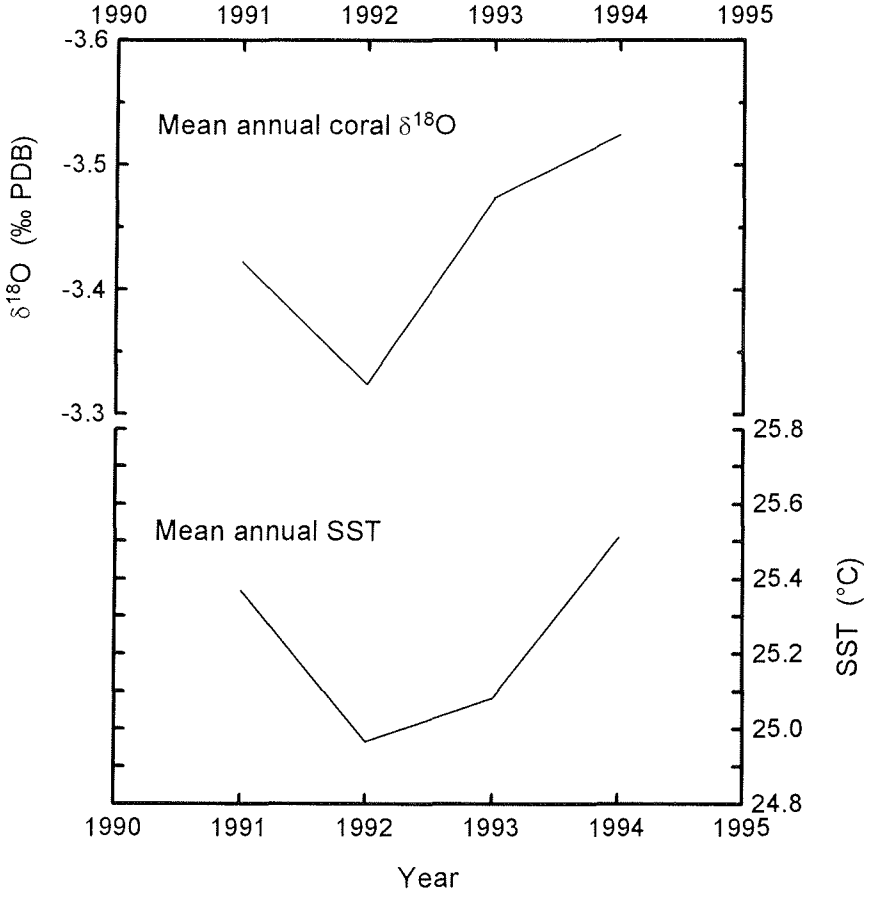

Figure 3.6. Time series of the interannual coral $\delta^{18}O$ and SST [*Reynolds and Smith*, 1994] variability over the period 1991-1994. The mean annual coral $\delta^{18}O$ and SST values show a good visual (but statistically not significant) correlation.

Apparently a different process works here. Probably a significant proportion of the mean annual coral $\delta^{18}O$ signal is the result of large-scale regional changes in the isotopic composition of the seawater of the northern Red Sea at the interannual scale. Southern

Red Sea and especially northern Indian Ocean surface waters are depleted in ^{18}O relative to the northern Red Sea [*Ganssen and Kroon*, 1991]. Variations in the intensity of lateral input of ^{18}O-depleted surface seawater by the northward currents from the southern Red Sea/Indian Ocean region at the interannual scale could be a possible explanation for the amplified coral $\delta^{18}O$ signal. *Klein et al.* [1997] recently reported for southern Red Sea corals, that over the seasonal cycle, changes in SST and surface water $\delta^{18}O$ work in opposite directions, resulting in a reduced coral $\delta^{18}O$ signal, whereas on the interannual timescale changes in SST and water isotopic composition combine to produce an amplified coral $\delta^{18}O$ climate signal. This signal is driven by interannual variations in the intensity of surface water influx from the Indian Ocean to the Red Sea. However, before drawing a conclusion on this aspect for our northern Red Sea coral, there is the need of extending the coral $\delta^{18}O$ record from Ras Umm Sidd.

In summary, these first results demonstrate that the seasonal $\delta^{18}O$ variations of our coral successfully record the seasonal SST variability in the northern Red Sea. Also at the interannual scale the mean annual coral $\delta^{18}O$ signal follows the mean annual SST variations. The record will be extended back to approximately 1750, this date is deduced from density-band counting of the entire coral core. The Ras Umm Sidd coral core will provide a continuous record of climate variability over the last 250 years for the northeast Africa/Middle East region, thereby extending the discontinuous instrumental observations and supporting other proxy records from the area.

3.6. Acknowledgments

We thank M. Segl and her team for stable isotope analysis; an anonymous reviewer for comments; H. Kuhnert for fruitful discussions; and the Government of Egypt and the Egyptian Environmental Affairs Agency (EEAA) for support and permission to sample in the Ras Mohammed National Park. This work is part of the Egyptian, Israeli, Palestinian and German Red Sea Program on Marine Sciences (RSP), funded by the BMBF (German Ministry for Education, Science, Research, and Technology) through grant 03F0151A.

4. A coral oxygen isotope record of temperature, aridity, and deep water formation from the northern Red Sea since the year 1750

To be submitted as:
Felis, T., J. Pätzold, Y. Loya, M. Fine, A. H. Nawar, and G. Wefer, A coral oxygen isotope record of temperature, aridity, and deep water formation from the northern Red Sea since the year 1750.

4.1. Abstract

A 245-year coral oxygen isotope record from Ras Umm Sidd (Egypt) near the southern tip of the Sinai Peninsula in the desert-surrounded northern Red Sea is presented. The record provides a bimonthly-resolution time series from a subtropical location (~28°N) at the northern rim of the African-Asian arid belt. The coral $\delta^{18}O$-based sea surface temperatures (SSTs) suggest that mean annual SSTs between 1751 and 1900 were ~0.3°C lower than the 20th century average. The coral record, supported by instrumental and proxy records of climate, reveals new aspects on large-scale Middle East climate variability on the interannual to interdecadal/multidecadal timescale. During colder periods the northern Red Sea region is more arid (higher evaporation) whereas the eastern Mediterranean region in the north is wetter. During warmer periods the northern Red Sea region is less arid (lower evaporation) whereas the eastern Mediterranean region is drier. This pattern is explained by variations in the latitudinal position of the subtropical westerly jet stream, the associated subtropical high-pressure belt, and therefore the

descending branch of the northern Hadley cell with its subsiding air, as well as of the moisture bringing North Atlantic westerlies which are located in the north of this system. The northern Red Sea is probably the only site in the world oceans where water mass formation occurs and reef corals grow. The winter $\delta^{18}O$ values of the coral record can be used to detect episodic events of deep water formation of the Red Sea thermohaline circulation during anomalously arid and cold winters, which are sometimes associated with El Niño events and large volcanic eruptions. The Ras Umm Sidd coral record therefore provides a valuable source of information on Middle East climate and Red Sea ocean history and may also support reconstructions of past climate variability on much larger timescales from the region.

4.2. Introduction

In most areas of the tropics and subtropics continuous instrumental observations of climate rarely span more than 30-40 years and therefore cannot resolve the full range of interannual- to interdecadal-/multidecadal-scale climate variability. Coral records from the tropical and subtropical reefs provide a tool for reconstructing continuously the climate variability of the past several hundred years, thereby extending the instrumental records. The stable oxygen isotopic composition of centuries-old, annually banded, massive corals has been widely used for high-resolution (annual to near monthly) reconstructions of sea surface temperature (SST) and/or sea surface salinity [e.g., *Pätzold*, 1984, 1986; *Cole et al.*, 1993; *Dunbar et al.*, 1994; *Heiss*, 1994; *Quinn et al.*, 1996; *Charles et al.*, 1997; *Crowley et al.*, 1997; *Quinn et al.*, 1998; *Kuhnert et al.*, 1999]. Massive corals build their skeletons of aragonite and grow at rates of millimeters to centimeters per year. During growth, they incorporate isotopic species of oxygen into their skeletons. The ratio of coral skeletal $^{18}O/^{16}O$, reported as $\delta^{18}O$, reflects the environmental conditions in the ambient seawater during skeleton precipitation. The primary influences on coral $\delta^{18}O$ variability are (1) the temperature of aragonite formation and (2) the $\delta^{18}O$ of the seawater. (1) As temperature increases, there is a decrease in the $\delta^{18}O$ (depletion in ^{18}O) of the coral skeletal aragonite. (2) Variations in the $\delta^{18}O$ of the seawater can result from evaporation (enrichment in ^{18}O), precipitation (depletion in ^{18}O), or runoff (depletion in ^{18}O). High evaporation results in both an enrichment in the $\delta^{18}O$ of the seawater and a higher salinity, high precipitation or runoff has opposing effects. Because of this, salinity variations, if driven through evaporation, precipitation or runoff, closely covary with the $\delta^{18}O$ variations of the seawater.

Here we present results from a 245-year coral $\delta^{18}O$ record from a subtropical northern hemisphere site (~28°N). The location Ras Umm Sidd near the southern tip of the Sinai Peninsula in the desert-surrounded northern Red Sea can be considered as unique under several aspects. (1) Despite the extremely arid environment at the northern rim of the African-Asian desert belt, the climate regime of the Mediterranean Sea with its wet winters is located in a distance of less than 500 km to the north. (2) The narrow fringing

reefs of the northern Red Sea are directly exposed to open-sea conditions owing to a steep submarine slope. Depths of >900 m are reached within 2 km from the sampling site. (3) The deep water formation of the Red Sea thermohaline circulation occurs here at the extreme north of the basin. To the best of our knowledge the northern Red Sea is the only site in the world oceans where water mass formation occurs and reef corals grow. (4) In contrast to other coral-based paleoclimatic studies from remote tropical/subtropical locations instrumental observations of climate in the Middle East extend further back into the past owing to the existence of old cities in the region (Cairo, Jerusalem, Alexandria). These instrumental records, though not continuous, provide a unique opportunity for the verification of the large-scale regional climatic information derived from the coral proxy record during parts of the second half of the 19th century. (5) Furthermore, due to the subtropical setting also a tree-ring chronology is available for supporting some of the climatic information derived from the coral record.

4.3. Study area

4.3.1. Climate and oceanography

The study area is located near latitude 28°N at the northern rim of the African-Asian arid belt, near the southern tip of the Sinai Peninsula which represents the northern boundary of the Red Sea proper (Figure 4.1). The climate of the region is dominated by the subtropical high-pressure belt and therefore by the descending branch of the northern Hadley cell, where large-scale descending motions warm and dry the atmospheric boundary layer. In general, the warming and drying of this subsiding air near latitudes 30° is considered as the major cause of aridity in the subtropics. Above the subtropical high-pressure belt and the descending limb of the Hadley cell the subtropical westerly jet stream is located at about 12 km height [*Buckle*, 1996; *Barry and Chorley*, 1998].

The Red Sea is a long (~2000 km) and narrow (~280 km) desert-enclosed basin with depths of up to 2800 m (Figure 4.2). It is connected to the Indian Ocean in the south by the narrow and shallow (~140 m) Strait of Bab-el-Mandab. The climate is extremely arid with high evaporation and negligible precipitation and runoff. The estimated net evaporation is ~200 cm/yr [*Morcos*, 1970; *Ahmad and Sultan*, 1989]. Therefore, the Red Sea is an evaporative basin. The Red Sea circulation is mostly driven by thermohaline forcing, wind forcing is secondary [*Eshel et al.*, 1994]. The excess of evaporation over precipitation causes a northward surface inflow through the Strait of Bab-el-Mandab. High evaporation in the northern Red Sea and low evaporation in the southern Red Sea depresses the sea level in the extreme north compared to the middle and southern part of the basin. This slope drives the thermohaline circulation and controls water mass formation [*Eshel and Naik*, 1997; *Eshel et al.*, submitted 1998]. At the northern end of the Red Sea deep water is formed and gives rise to a southward-flowing current [*Cember*, 1988].

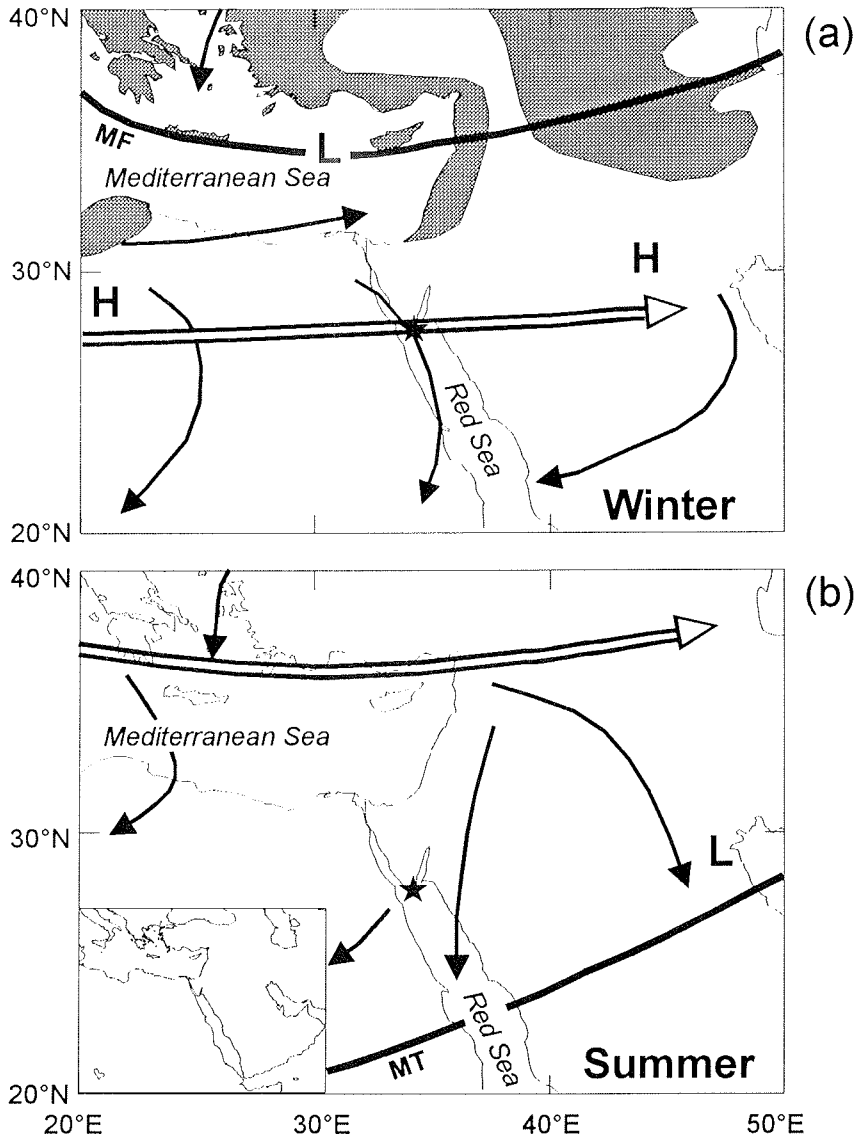

Figure 4.1. Map of the large-scale atmospheric phenomena that influence Middle East climate. The distribution of surface pressure (H, L), winds (solid arrows), and precipitation is shown; dotted areas indicate a monthly precipitation of 50-400 mm. The average positions of the subtropical westerly jet stream (open arrow), together with the Mediterranean Front (MF) and the Monsoon Trough (MT), are also shown. (a) Winter conditions (January). (b) Summer conditions (July). (Modified from *Barry and Chorley*, 1998). The location Ras Umm Sidd is indicated by a star.

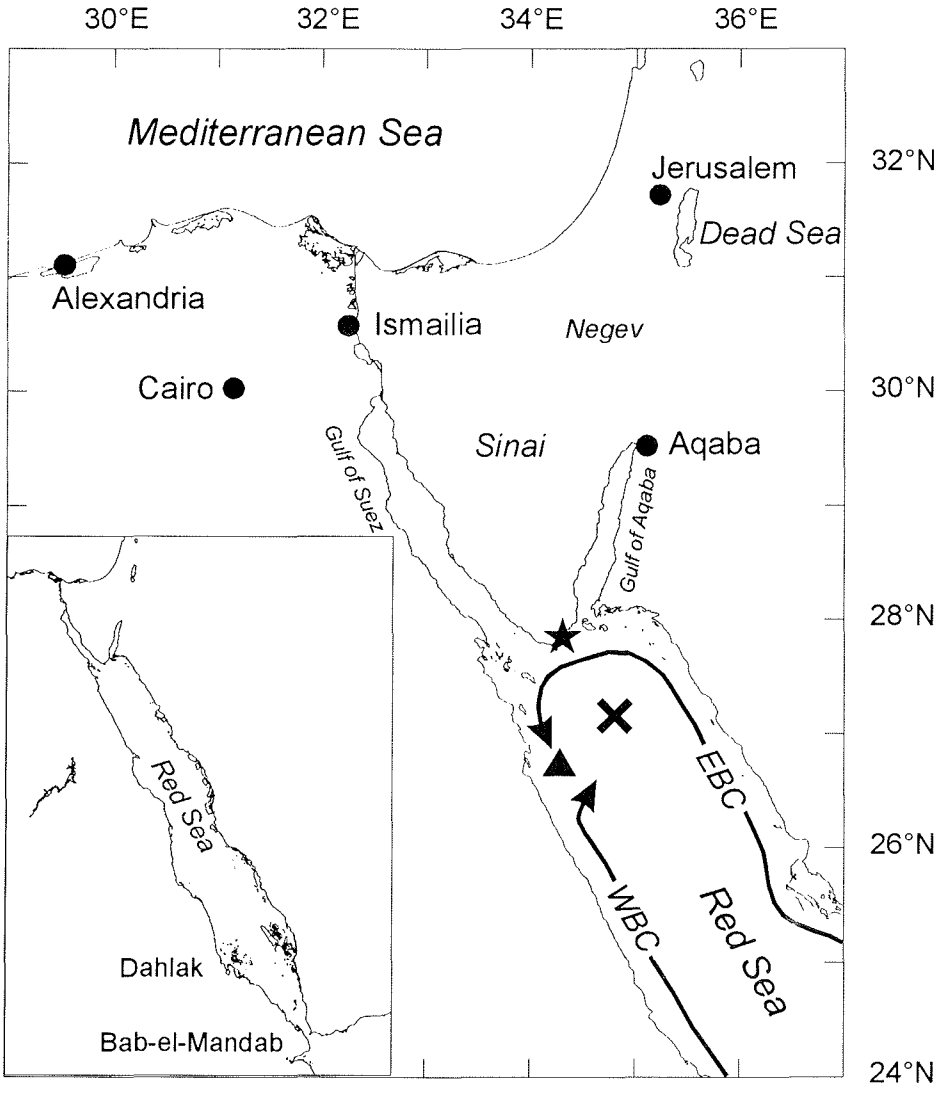

Figure 4.2. Map of the northern Red Sea. The location Ras Umm Sidd is indicated by a star. The suggested site of episodic, intermittent deep water formation located in the center of the cyclonic gyre [*Eshel and Naik*, 1997; *Clifford et al.*, 1997] is indicated by a cross. The suggested collision site of the (former) eastern boundary current (EBC) and the western boundary current (WBC) where intermediate water is formed [*Eshel and Naik*, 1997] is indicated by a triangle.

A numerical model [*Eshel and Naik*, 1997] shows that northward-flowing boundary currents are the major elements of the Red Sea surface circulation. In the northern Red Sea the main dynamical features are two boundary currents which flow north along the eastern and western coasts (Figure 4.2). The collision of these two currents takes place slightly south of the northwest corner of the Red Sea near the western coast (~26°N). At this location northward and southward flowing western boundary currents collide, after the one which originally flows to the north along the eastern boundary turns cyclonically, follows the northern boundary, and flows to the south along the western boundary. The southward flowing western boundary current is somewhat denser, due to haline

preconditioning of the upper-layer water, which occurs throughout the entire northward journey of the surface water from the Strait of Bab-el-Mandab, and a resulting longer path. Therefore this former eastern boundary current subducts under the lighter western boundary current at the collision site, and intermediate water (≤1 km) is formed. The subduction forces the western boundary current eastward into the interior. The process ceases in summer [*Eshel and Naik*, 1997].

In addition to this shallow-convective, subductive mode of intermediate water formation, which is the regular process in the climatology, Eshel and Naik speculate on an episodic, deep-convective formation process, which is entirely absent from the climatological conditions. It is related to short-lived intense atmospheric events, which are suppressed in climatological forcing, and is thought to occur in the center of the cyclonic gyre in the northern Red Sea, where the climatological winter stratification is the weakest [*Eshel and Naik*, 1997]. The existence of a cyclonic gyre in the northern Red Sea is further supported by observed tracks of surface drifters [*Clifford et al.*, 1997]. Clifford et al. also speculate on the center of this gyre as a location of intermittent deep convection during wintertime, because deep convection occurs preferentially in cyclones due to the fact that the shallower thermocline and halocline in the center of the vortex are more easily eroded by the wintertime heat loss and evaporation to the atmosphere. That the deep water formation of the Red Sea is intermittent rather than continuous every winter was first shown by the work of *Woelk and Quadfasel* [1996], which suggests that the event-like character of the deep water formation is strongly linked to interannual variations of the meteorological forcing. However, Woelk and Quadfasel suggest that slope convection from the Gulf of Suez and not open ocean convection in the northern Red Sea is the process responsible for Red Sea deep water formation.

4.3.2. Seasonal climatology

Gridded SST observations from the northern Red Sea show a seasonal cycle of nearly 6°C [*Levitus and Boyer*, 1994] to 7°C [*Reynolds and Smith*, 1994] for the grid box including Ras Umm Sidd (Figure 4.3a). Winter minimum SSTs are ~22°C (February) and summer maximum SSTs are ~28°C (August). The seasonal cycle of sea surface salinity is ~1.9 practical salinity units (psu) in the corresponding grid box [*Levitus et al.*, 1994]. However, according to a composite record (1974-1977) from the upper 150 m of the nearby Straits of Tiran the seasonal cycle of salinity is only ~0.5‰ [*Paldor and Anati*, 1979]. Both records show maximum salinities during the summer months (August, September) and minimum salinity values during the rest of the season (Figure 4.3c). Scaling of the seasonal salinity variability of 1.9‰ [*Levitus et al.*, 1994] and 0.5‰ [*Paldor and Anati*, 1979] by means of the standard $\delta^{18}O_{SMOW}$-salinity relations for Red Sea waters (slopes: 0.29; 0.291) [*Craig*, 1966; *Andrié and Merlivat*, 1989] results in ~0.54‰ and ~0.14‰ seasonal $\delta^{18}O_{PDB}$ seawater change, respectively. Considering the mean of these two values as the best approximation, the amplitude of the seasonal

changes in the $\delta^{18}O$ composition of the surface waters is small compared to the seasonal SST changes. Both seasonal cycles should have opposing effects on the $\delta^{18}O$ composition in coral skeletons, resulting in a reduced coral $\delta^{18}O$ signal on the seasonal timescale. Several studies showed that in the northern Red Sea coral $\delta^{18}O$ variations on the seasonal timescale primarily reflect the seasonal SST cycle [*Klein et al.*, 1992; *Felis et al.*, 1998a], with minor but significant contributions from variations in salinity [*Schrag et al.*, 1997; *Eshel et al.*, submitted 1998].

The evaporation minus precipitation climatology calculated by *da Silva* [1994] for the northern Red Sea shows a clear seasonal cycle (Figure 4.3b) with maximum values during the cold winter season (December-January-February). The seasonal cycle of precipitation with its maximum in April is negligible. Earlier calculations also identified the winter (January) as the evaporative season in the northern Red Sea [*Privett*, 1959], and more recent calculations come to the same conclusion [*Ahmed and Sultan*, 1989]. The work of *Eshel* [1996] explains this evaporation pattern with the stronger Hadley circulation in the winter hemisphere. During northern winter, the large-scale descending motions over the northern Red Sea intensify, warming and drying the atmospheric boundary layer [*Eshel*, 1996].

An additional explanation for the winter as the evaporative season could be the latitudinal shift of the descending branch of the Hadley cell, the associated subtropical high-pressure belt, and the associated subtropical westerly jet stream in the upper troposphere on the seasonal timescale. The subtropical high-pressure belt with its subsiding air moves a few degrees equatorwards in winter and polewards in summer [*Buckle*, 1996; *Barry and Chorley*, 1998]. During the winter season its location over the northernmost Red Sea is in coincidence with the maximum evaporation in this region (Figures 4.1a and 4.3b), which is arid throughout the year. At the same time the Mediterranean region in the north is under the influence of the North Atlantic westerlies and the associated storm tracks which provide much of the atmospheric moisture transport to this region, resulting in the typical Mediterranean winter rains. During the summer season the subtropical high-pressure belt shifts north, accompanied by a northward shift of the North Atlantic westerlies (Figure 4.1b). This brings dry and hot conditions to the Mediterranean region in summer [*Barry and Chorley*, 1998]. The lower evaporation in the northern Red Sea during the summer season is therefore probably in addition to the weaker Hadley circulation also due to the northward shift of the zone of maximum atmospheric subsidence which is associated with the subtropical high-pressure belt. The seasonal change in the position of the subtropical high-pressure belt at the surface and the associated subtropical westerly jet stream in the upper troposphere is shown in Figures 4.1a and 4.1b.

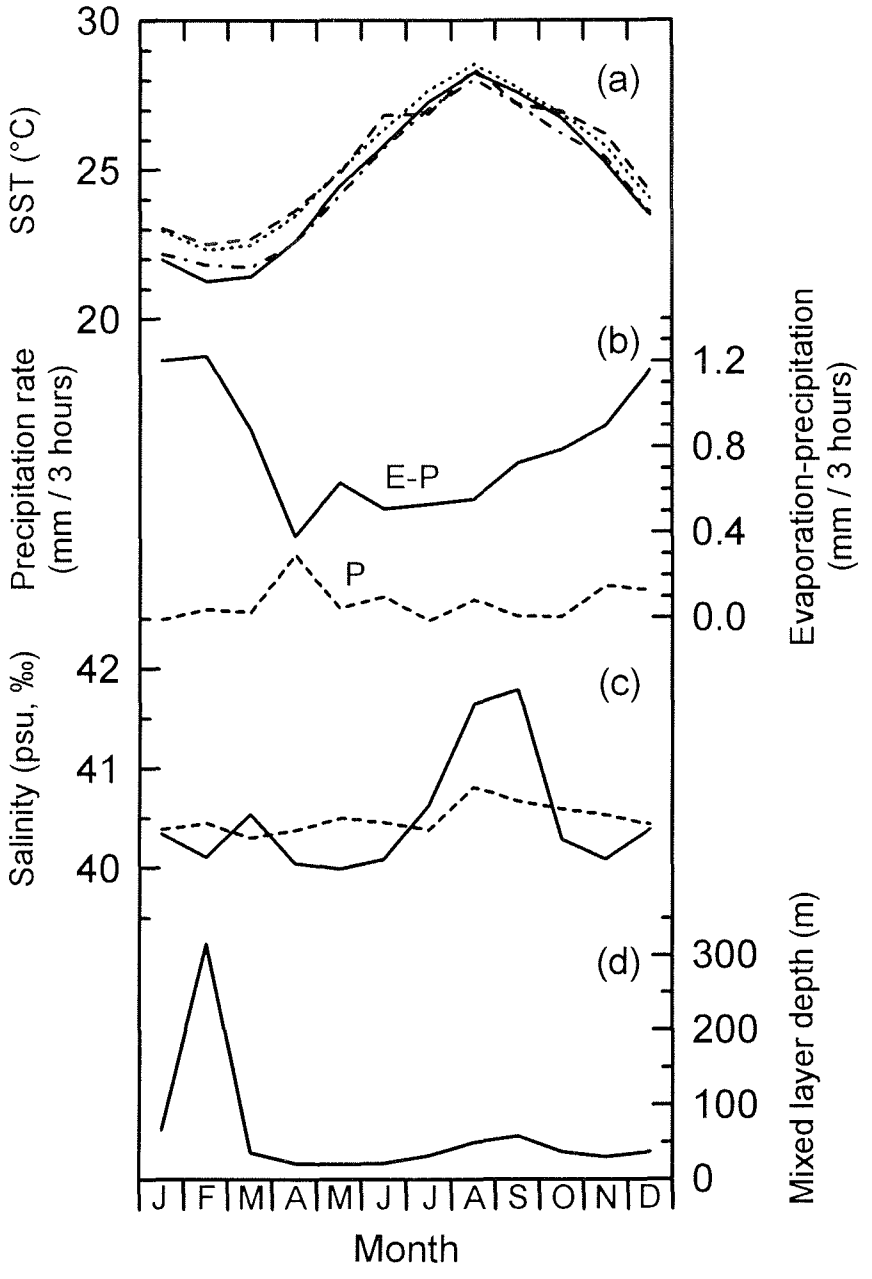

Figure 4.3. Monthly climatology for environmental parameters from grid boxes located in the northern Red Sea, including the sampling location Ras Umm Sidd. (a) Sea surface temperature (SST); solid line: U.S. National Meteorological Center (NMC)/IGOSS dataset [*Reynolds and Smith*, 1994], slash-dotted line: *da Silva et al.* [1994], dotted line: COADS dataset [*Slutz et al.*, 1985; *Woodruff et al.*, 1993], broken line: *Levitus and Boyer* [1994]. (b) Constrained evaporation minus precipitation (solid line), and precipitation (broken line) [*da Silva et al.*, 1994]. (c) Sea surface salinity (solid line) [*Levitus et al.*, 1994] and salinity in the upper 150 m of the Straits of Tiran (broken line) [*Paldor and Anati*, 1979]. (d) Mixed layer depth (IGOSS sio climatology). "psu" is practical salinity units.

In the northern Red Sea the summer is the season of maximum salinity in the surface waters whereas the winter is the season of maximum evaporation (Figure 4.3b and 4.3c). This apparent contradiction is probably due to the fact that during the summer the upper ocean is highly thermally stratified and therefore the effect of evaporation is concentrated on the upper waters, resulting in high salinities in the surface waters. The higher evaporation during the winter is probably masked in the salinity signature of the surface waters due to water column overturn during that season. In the climatology the maximum net evaporation coincides with the timing of the maximum mixed layer depth of more than 300 m in February and shows no effect on the corresponding salinity signature of the surface waters (Figure 4.3b, 4.3c and 4.3d).

4.3.3. Instrumental observations of climate in the region

Instrumental observations of SST in the northern Red Sea started with the opening of the Suez Canal in 1869. These measurements are taken by ships of opportunity, primarily along the major shipping route from Suez to the Strait of Bab-el-Mandab in the south. These observations are available as coarse-gridded SST time series [*Slutz et al.*, 1985; *Woodruff et al.*, 1993]. However, significant data gaps occur during the war years and before 1903 (Figure 4.4a). Therefore, continuous instrumental observations of SST variability from the region rarely span more than 20 years and do not extend reliably into the 19th century. Long land-based instrumental observations of air temperature/precipitation are available from weather stations in Cairo, Jerusalem, and Alexandria [*Baker et al.*, 1994] to the north of the sampling site. Some of these records extend back into the second half of the 19th century but are also discontinuous. However, during the second half of the 19th century these records are possibly more reliable than the rare ship-based SST observations in the northern Red Sea. To the south of the sampling location no long instrumental records from weather stations are available in a comparable distance.

4.4. Material and methods

4.4.1. Coral core collection and sampling site

A coral core (RUS-95) was recovered in the end of November 1995 from a fringing reef site at Ras Umm Sidd (27°50.9'N, 34°18.6'E) near the southern tip of the Sinai Peninsula (Egypt) at the northern end of the Red Sea proper (Figure 2), as part of the "Red Sea Program on Marine Sciences" [e.g., *Kaiser*, 1998]. The location can be considered to be affected by the northwestward-flowing eastern boundary current, now flowing to the southwest following the northern coast after turning cyclonically [*Eshel and Naik*, 1997]. The sampling site is located in the Ras Mohammed National Park [e.g., *Ormond et al.*, 1997]. The core was collected from a hemispherical 2.6-m-high coral colony (*Porites* sp.), using an underwater pneumatic drill with a 5-cm-diameter bit. The core was drilled vertically, parallel to the major axis of coral growth, to the bottom of the

colony. After the drilling procedure the borehole was sealed with a carbonate plug to prevent bioerosion. Visual inspection in March 1996 and December 1996 revealed that the drilling did not harm the huge coral and that the colony's living surface started to overgrow the plug.

The location Ras Umm Sidd is characterized by a narrow fringing reef in shallow water which terminates abruptly. The morphology creates a steep reef wall descending to about 10-20 m, followed by a steep submarine slope down to the depths of the Red Sea. Depths of >900 m are reached within 2 km from the sampling site. The coral colony is growing at a water depth of ~5.5 m, located 20 m inside the reef front in a huge lagoon (relative to the narrow fringing reef), which is half-open to the sea. The reef faces the Red Sea proper to the southeast, sheltering barrier reefs or islands do not exist. Therefore the coral can be considered to be directly exposed to open-sea conditions in the northern Red Sea.

4.4.2. Sampling, chronology construction, and stable isotope analysis

The drilled segments provide a 2.6-m-long continuous core without any gaps between the segments. The core was sliced into 3- to 5-mm-thick slabs parallel to the axis of coral growth. X radiograph positive prints of the slabs revealed a clear skeletal density-banding pattern of alternating bands of high and low density and were used as guides for spot-sampling along the axis of maximum coral growth, following precisely the major growth axis of single fans of corallites. This sampling technique limits the influence of "kinetic" isotope disequilibria effects [*McConnaughey*, 1989a, b]. According to the terminology of *Cohen and Hart* [1997] the sampling profile always followed the central axis of the highest bumps. Samples were collected by low-speed drilling using a dental tool with a 0.8-mm-diameter bit. The average growth rate of the coral is ~10 mm/yr and our average sample spacing of ~1.5 mm provides an average resolution of more than 6 samples per year. The drilling depth for sampling was controlled to be ~2 mm, to minimize the amount of sampled aragonite powder and therefore the range of age integration for a specific sample owing to possible changes in colony topography within the thickness of the slab. After each sample collection the slab and the bit were cleaned with pressure air and the latter was additionally cleaned with a brush. The bit was inspected under a microscope each 10 samples and replaced by a new one if necessary. The sampling laboratory was cleaned each 50 samples with a hoover. X radiograph positive prints of the sampled coral slabs were used as controls for evaluating the position of the sampling profile. The control X radiographs revealed that the sampling profile follows precisely the major growth axis of single fans of corallites, i.e., the central axis of the highest bumps, during the entire coral record.

The coral chronology is constructed by setting the maximum $\delta^{18}O$ value in a given year equal to mid-February (consistent with the climatological minima in SST) and assuming a constant coral growth rate between February of every year. Therefore we interpolated linearly between these fixed points for further age assignments. This

assumption can produce a 1- to 2-month time-scale error in any given year, but it is the most objective method [e.g., *Charles et al.*, 1997]. The resulting values were interpolated linearly to 6 equally spaced values per year, using the AnalySeries 1.1 software package [*Paillard et al.*, 1996], providing a bimonthly resolution (January-February, March-April, May-June, etc.) for comparison with environmental data. Mean annual values were calculated as the average of the six bimonthly interpolated values of a given year. In all cases were correlation coefficients are given the environmental/proxy data were bimonthly interpolated, and mean annual values were calculated from the bimonthly values. The strong seasonal cycle in $\delta^{18}O$ was used to count annual layers in the coral, supported by the density-banding pattern. The coral shows a consistent pattern of low-density-band creation during the winter season and high-density-band creation during the summer season. According to this combined method the Ras Umm Sidd coral record extends from fall 1750 to fall 1995. We assigned an age estimate error of ±0 years to the interval 1925-1995, of ±1 years to 1783-1924, and of additionally ±1 years to 1750-1782, respectively. Therefore the chronology is assigned a maximum cumulative error of ±2 years at the bottom of the core. The annual coral growth rate (e.g., for the year 1990) was calculated as the distance from a maximum $\delta^{18}O$ value in a given year (1990) to the maximum value of the following year (1991), i.e., from mid-February (1990) to mid-February (1991) according to our age model.

For oxygen isotopic analysis, we used a Finnigan MAT 251 mass spectrometer coupled to a Finnigan MAT automated carbonate device at the stable isotope laboratory of the Department of Geosciences at Bremen University, Germany. Long-term reproducibility for $\delta^{18}O$, deduced from replicate measurements of an internal carbonate standard, is less than ±0.07‰ (1σ over a 3-year period). Isotopic values are reported relative to the Pee Dee belemnite (PDB) reference standard. The coral stable carbon isotope data ($\delta^{13}C$) will be discussed elsewhere. The Ras Umm Sidd coral $\delta^{18}O$ data will be archived in digital form at the PANGAEA (PaleoNetwork for Geological and Environmental Data) database, AWI/MARUM, Bremerhaven/Bremen, Germany (<http://www.pangaea.de>) and at the World Data Center-A for Paleoclimatology, NOAA/NGDC, Boulder CO, USA (<http://www.ngdc.noaa.gov/paleo/paleo.html>).

Figure 4.4. (a) Number of ship-based sea surface temperature (SST) observations per month in the northern Red Sea (COADS dataset [*Slutz et al.*, 1985; *Woodruff et al.*, 1993]) in the grid box (2°×2°, centered at 27.0°N, 35.0°E) including Ras Umm Sidd. Significant data gaps occur around the war years (1917-1918, 1940-1945, 1967-1975) and before 1903. High numbers in the early 1990s are possibly due to increased activities during the Gulf War? (b) Comparison of the bimonthly Ras Umm Sidd coral $\delta^{18}O$ record and corresponding SST observations (same grid box as in (a)). (c) Same as in (b), but for mean annual values (January-December). (d) Same as in (b), but for summer values (July-October). (e) Same as in (b), but for winter values (January-April). Correlation coefficients are given for intervals of continuous SST observations (significant at the 99.5%, *99%, **97.5%, ***95%, and ****90% level, respectively; § = not significant) which are indicated by shading. The y-axes have been scaled so that 1°C = 0.2‰ PDB.

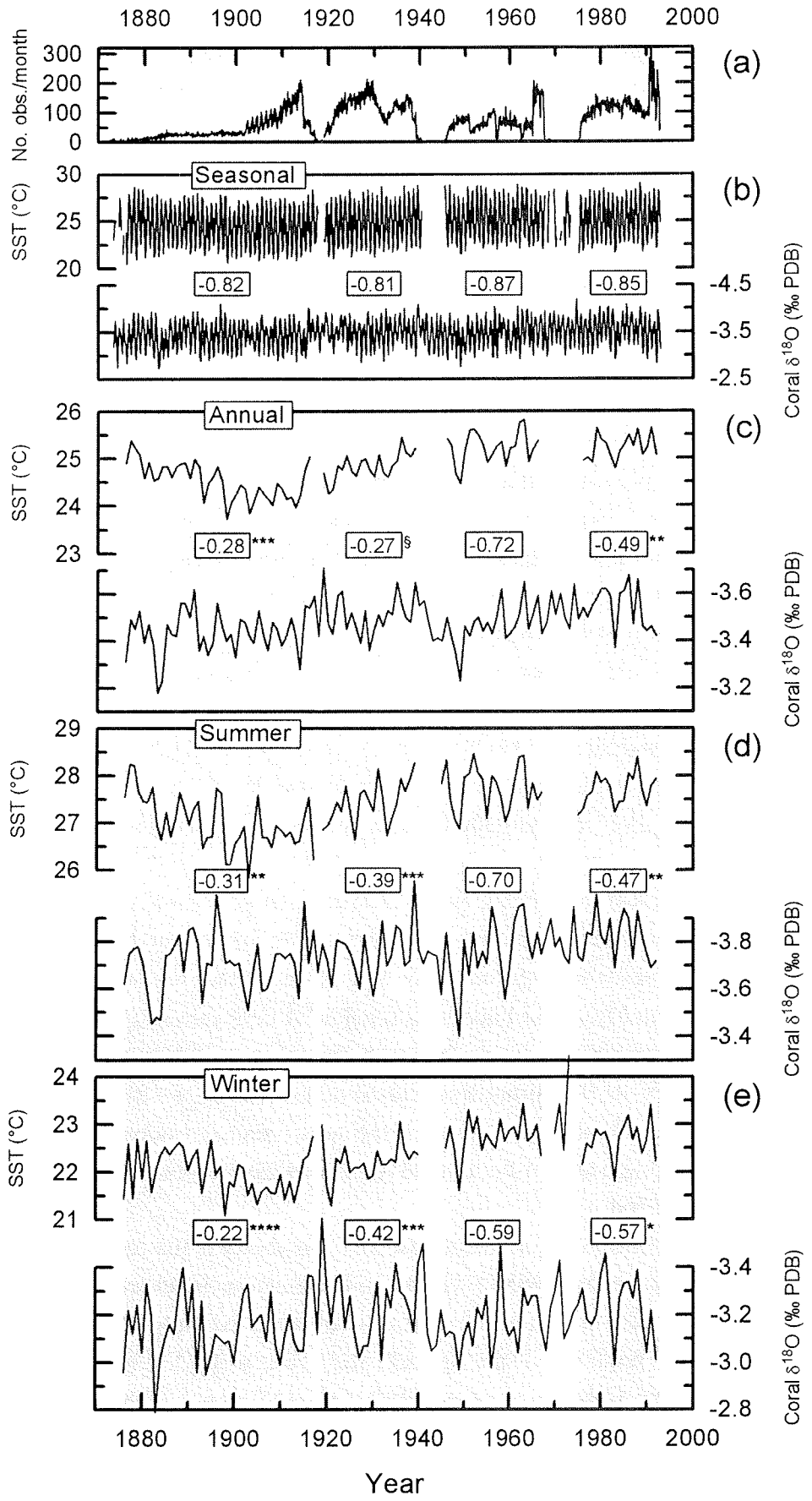
1880
1900
1920
1940
1960
1980
2000
No. obs./month
300
200
100
0
(a)
SST (°C)
30
25
20
Seasonal
(b)
-0.82
-0.81
-0.87
-0.85
-4.5
-3.5
-2.5
Coral δ18O (‰ PDB)
SST (°C)
26
25
24
23
Annual
(c)
-0.28***
-0.27§
-0.72
-0.49**
-3.6
-3.4
-3.2
Coral δ18O (‰ PDB)
SST (°C)
29
28
27
26
Summer
(d)
-0.31**
-0.39***
-0.70
-0.47**
-3.8
-3.6
-3.4
Coral δ18O (‰ PDB)
SST (°C)
24
23
22
21
Winter
(e)
-0.22****
-0.42***
-0.59
-0.57*
-3.4
-3.2
-3.0
-2.8
Coral δ18O (‰ PDB)
1880
1900
1920
1940
1960
1980
2000
Year

4.5. Results and discussion

4.5.1. Comparison with instrumental temperature observations

A preliminary study to test the applicability of the Ras Umm Sidd (RUS-95) coral core for paleoclimatic studies [*Felis et al.*, 1998a], providing a monthly-resolution time series for the interval of 1990-1994, revealed a clear seasonal coral $\delta^{18}O$ cycle which strongly correlates with northern Red Sea SST observations (r = -0.85, significant at the 99.5% level). A comparison of the coral $\delta^{18}O$ record and coarse-gridded SST observations from the northern Red Sea (COADS dataset [*Slutz et al.*, 1985; *Woodruff et al.*, 1993]) is presented in Figure 4.4. At the seasonal (bimonthly) timescale (Figure 4.4b) there is a strong (r = -0.81 to -0.87) and highly significant correlation (99.5% level) between coral $\delta^{18}O$ and SST during the intervals of overlap (1876-1916, 1919-1939, 1946-1966, and 1976-1992). We therefore conclude that on the seasonal timescale the coral is primarily recording information on SSTs.

However, correlation exercises on the seasonal timescale tend to inflate correlation coefficients and do not imply much on the quality of the reconstructed interannual-scale SST variabilty derived from coral records. A rigorous test for the applicabilty of the coral $\delta^{18}O$ data in reconstructing interannual-scale SST variability is the correlation of the mean annual values (Figure 4.4c). For the interval of 1976-1992 the correlation is only moderate (r = -0.49, 97.5% level). However, for the interval of 1946-1966 there is a strong and highly significant correlation (r = -0.72, 99.5% level). Before 1939 the correlation is not significant (1919-1939) or only weak (1876-1916), which could possibly reflect biases in the quality of the COADS-based SST observations during these intervals and before 1903 additionally the low number of observations, but this remains speculative.

The great advantage of climate proxy records derived from coral stable isotopes compared with dendroclimatic studies is the potential of reconstructing climate variability at the seasonal timescale. Figures 4.4d and 4.4e show the summer and winter reconstructions derived from the bimonthly coral $\delta^{18}O$ time series. The strong and highly significant correlations (99.5% level) for mean annual (r = -0.72), summer (r = -0.70), and winter values (r = -0.59) during the interval of 1946-1966 are striking. It can be also seen that the only moderate correlation of the mean annual values in the most recent interval (1976-1992) appears to be a result of the moderate correlation of the summer values during that period.

Another source of information about past SST variability is the reduced space optimal smoother analysis of the MOHSST5 global SST anomalies [*Kaplan et al.*, 1998]. This analysis uses present-day temperature patterns to enhance the meager data available in the past and has been applied to the global SST record MOHSST5 from the U.K. Meteorological Office [*Bottomley et al.*, 1990; *Parker et al.*, 1994], which has more thorough corrections for long-term trends caused by instrumental changes and a more careful quality control compared with the COADS dataset of *Slutz et al.* [1985] and *Woodruff et al.* [1993]. A comparison between the results of this analysis for the northern

Red Sea and the coral $\delta^{18}O$ data is presented in Figure 4.5. The correlation between the mean annual values is weak (r = -0.37) but highly significant (99.5% level). For the periods of continuous COADS SST observations (see also Figure 4.4) there is a comparable strong correlation during the 1946-1966 interval (r = -0.72, 99.5% level). As for COADS SSTs, there is no significant correlation during the 1919-1939 interval. In contrast to the correlation with COADS SSTs there is a stronger and more significant correlation (r = -0.42, 99.5% level) for the earliest period of SST reconstruction (1876-1916). We like to point out again that errors in the SST observations for the time before 1945 may be partly responsible for the weak correlations between SST and coral $\delta^{18}O$ on the interannual timescale.

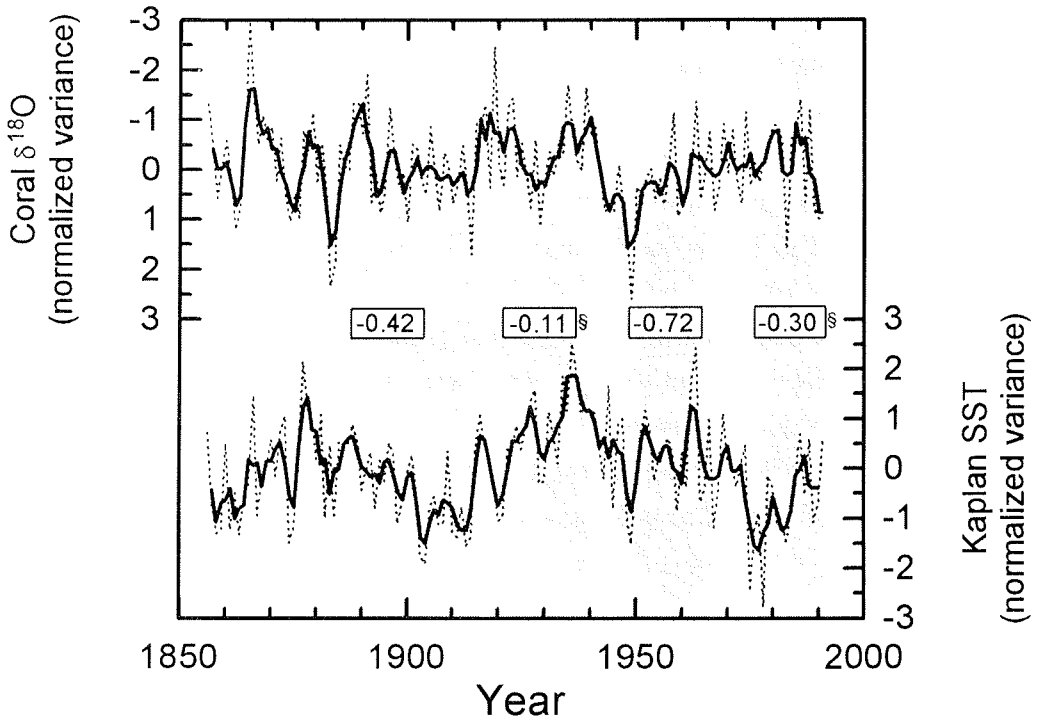

Figure 4.5. Comparison of the Ras Umm Sidd coral $\delta^{18}O$ record and the reduced space optimal smoother analysis of the MOHSST5 SST anomaly [*Kaplan et al.*, 1998] for the grid box including the northern Red Sea and Ras Umm Sidd (5°×5°, centered at 27.5°N, 32.5°E), for mean annual values (thin broken line). The correlation coefficient for the entire period (1856-1991) is -0.37, significant at the 99.5% level. Correlation coefficients are additionally given for the same intervals as in Figure 4.4, which are indicated by shading (99.5% level; § = not significant). The bold solid line represents a 3-year running average.

The reason for the weak correlation between the mean annual coral $\delta^{18}O$ values and SSTs during the most recent interval remains obscure (Figure 4.4c and 4.5). With respect to the COADS-based SSTs (1976-1992) the correlation is moderate (-0.49, 97.5% level),

with respect to the KAPLAN-based SSTs (1976-1991) the correlation is not significant. However, we like to point out that during the interval of 1982-1992 the correlation coefficient (r) between the mean annual coral $\delta^{18}O$ values and the COADS-based SSTs is -0.53, significant at the 95% level; whereas no significant correlation (r = -0.19) exists with the corresponding SSTs from the U.S. National Meteorological Center (NMC)/IGOSS dataset [*Reynolds and Smith*, 1994] (results not shown here). We are left with the conclusion that even the different datasets of SST observations show discrepancies for the northern Red Sea, which is a narrow basin with respect to the world oceans. However, because of the weak (r = -0.37) but highly significant correlation (99.5% level) between mean annual coral $\delta^{18}O$ and the KAPLAN-based SSTs during the entire period of overlap (1856-1991), and because of the strong (r = -0.72) and highly significant (99.5% level) correlation with KAPLAN- and COADS-based SSTs during the interval of 1946-1966, we conclude that the Ras Umm Sidd coral $\delta^{18}O$ record gives a reasonable approximation of the large-scale SST variability in the northern Red Sea at the interannual timescale.

A verification of this conclusion is provided by a comparison of the mean annual coral $\delta^{18}O$ record and long instrumental records of air temperature from weather stations [*Baker et al.*, 1994] in Cairo and Jerusalem (Figure 4.6a), old cities which are located several hundred kilometers to the north of Ras Umm Sidd (Figure 4.2). There are striking similarities in the interannual- to decadal-scale temperature variability especially during the second half of the 19th century, but also during the mid-20th century. This suggests that the Ras Umm Sidd coral record captures the large-scale regional aspects of Middle East temperature variability and therefore provides a proxy record of climate which improves and extends the discontinuous and short instrumental observations from the region.

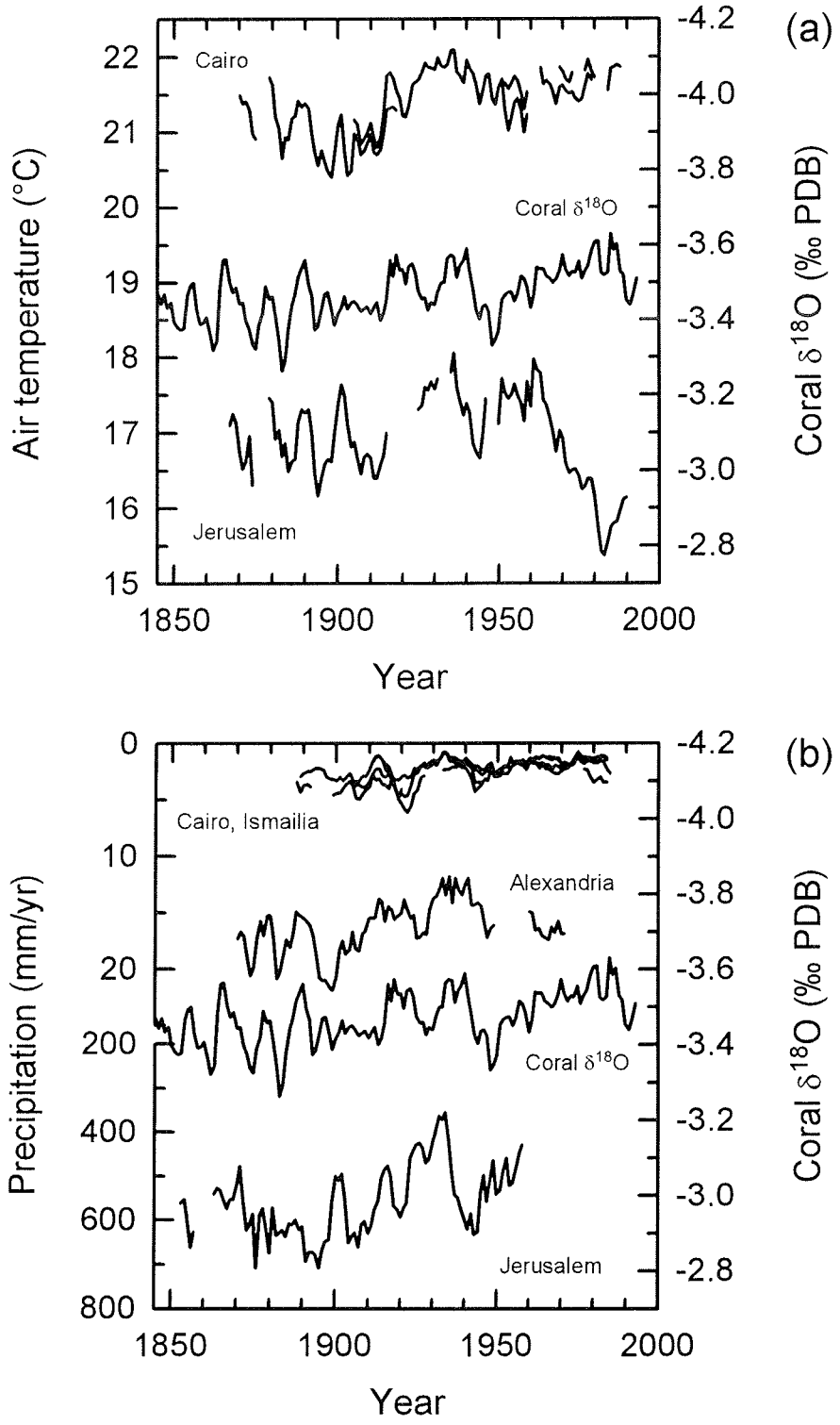

Figure 4.6. Comparison of the Ras Umm Sidd coral $\delta^{18}O$ record and instrumental observations of (a) air temperature and (b) precipitation [*Baker et al.*, 1994]; Jerusalem precipitation is derived from the work of *Rosenan* [1955]. 3-year running averages of mean annual values are shown, except for precipitation in (b) which are 5-year running averages. Records from the Cairo region include the World Meteorological Organization (WMO) stations Cairo, Cairo H.Q., Giza, and Helwan. Note that the precipitation scale (b) has been reversed for direct comparison with the coral record. See Figure 4.2 for locations.

4.5.2. Calibration with SSTs

High-resolution calibrations of *Porites* $\delta^{18}O$ variability suggest a temperature dependence of ~0.18‰/°C [*Gagan et al.*, 1994]. When this calibration is applied to the bimonthly coral time series, the $\delta^{18}O$ seasonality of the Ras Umm Sidd *Porites* reveals an average seasonal temperature change of ~4.3°C for the intervals of continuous SST observations. This is more than 74% of the average seasonal SST cycle of 5.8°C, according to the bimonthly interpolated data from the corresponding grid box of the COADS dataset [*Slutz et al.*, 1985; *Woodruff et al.*, 1993]. Calibrating the bimonthly coral $\delta^{18}O$ with these SSTs during the most recent intervals of continuous observations (1946-1966 and 1976-1992) reveals a SST-coral $\delta^{18}O$ relationship of -6.05°C/‰ (0.165‰/°C). The calculation of a Pearson's correlation coefficient (r) for the bimonthly values produces a relation that can be expressed by the equation

$$SST(°C) = -6.05\ (\delta^{18}O_{coral}) + 4.06 \qquad r = -0.86\ \ (99.5\%\ \text{level}) \qquad (1)$$

This relationship is different than the widely recognized "standard values" of -4.5°C/‰ (0.22‰/°C) for calcite [*Epstein et al.*, 1953] and -4.34°C/‰ (0.23‰/°C) for aragonite [*Grossman and Ku*, 1986]. However, our value shows a similarity to those recently determined by *Gagan et al.* [1994] for a Great Barrier Reef *Porites* at the near-weekly scale (-5.56°C/‰, 0.18‰/°C) and by *Quinn et al.* [1998] for a New Caledonia *Porites* at the monthly scale (-5.81°C/‰, 0.172‰/°C). We therefore interpret our relationship of -6.05°C/‰ (0.165‰/°C) to be reasonable, although some minor biasing due to the bimonthly sampling resolution and owing to the use of coarse-gridded SST data for the calibration cannot be totally excluded.

The mean annual SST/coral $\delta^{18}O$ calibration for these intervals (1946-1966 and 1976-1992) is different (-1.84°C/‰ or 0.543‰/°C). The calculation of a Pearson's correlation coefficient (r) for the mean annual values produces a relation that can be expressed by the equation

$$SST(°C) = -1.84\ (\delta^{18}O_{coral}) + 18.79 \qquad r = -0.58\ \ (99.5\%\ \text{level}) \qquad (2)$$

A comparable difference between the SST-coral $\delta^{18}O$ relationship for monthly and for mean annual values has been recently described for a multicentury coral record from New Caledonia in the southwestern Pacific Ocean [*Quinn et al.*, 1998]. Interestingly, only the mean annual SST/coral $\delta^{18}O$ calibration of this study provided the correct estimate for mean annual SSTs during an early 20th century verification interval and was therefore used for the interpretation of the entire coral record with respect to temperature.

4.5.3. Coral growth record

The growth rate of the Ras Umm Sidd coral varies from 0.45 cm/yr to 1.9 cm/yr, with an average value of 1 cm/yr (Figure 4.7c). There is no significant correlation between the annual values of coral growth rate and the mean annual values of coral $\delta^{18}O$. However,

for arbitrarily choosen intervals of 50-year length there are weak positive correlations. Correlation coefficients (r) are 0.35 (99% level) for 1801-1850, 0.22 (90% level) for 1901-1950, and 0.27 (95% level) for 1951-1994, respectively. During 1751-1800 and 1851-1900 there is no significant correlation. The weak but positive correlations indicate that the Ras Umm Sidd coral $\delta^{18}O$ record is fairly robust with respect to "kinetic" isotope disequilibria effects, which should result in a negative correlation [*McConnaughey*, 1989a, b]. A positive correlation between the coral growth rate and the coral $\delta^{18}O$ suggests an increased coral growth during years of colder SSTs. In general, the optimum temperature of coral growth is ~27°C with an upper limit of ~32-33°C and a lower limit of ~20°C [*Buddemeier and Kinzie*, 1976]. The average mean annual SSTs in the northern Red Sea are ~25°C, with a summer maximum of ~28°C and a winter minimum of ~22°C, which are in the range of optimum temperature conditions for coral growth. Therefore with respect to temperature there is no reason why colder conditions in the northern Red Sea should increase coral growth. A possible explanation could be that during colder years the mixed layer depth is deeper, resulting in a higher availability for nutrients and zooplankton in the upper waters. These nutrient/food rich conditions could probably result in an increased coral growth. A similar pattern was described for corals from Bermuda [*Pätzold and Wefer*, 1992; Pätzold, 1994].

4.5.4. Interpretation of the coral $\delta^{18}O$ record

The Ras Umm Sidd coral $\delta^{18}O$ record is shown in Figure 4.7 as time series for bimonthly, mean annual, summer, and winter values. As discussed earlier, on the seasonal timescale, represented by the bimonthly coral $\delta^{18}O$ record (Figure 4.7a), the coral primarily records information on SSTs. The amplitude of the seasonal cycle is fluctuating around an average value of 0.76‰ with no long-term trend evident. The mean annual coral record (Figure 4.7b) shows a long-term trend towards lower $\delta^{18}O$ values, significant at the 99.9% level. Application of the mean annual SST/$\delta^{18}O$ calibration (2) to the mean annual coral record indicates that average SSTs during the interval 1751-1900 were ~0.3°C lower than the average 20th century SSTs in the northern Red Sea. There is also interannual- to decadal-scale variability on the order of ~0.4°-0.8°C in the coral record.

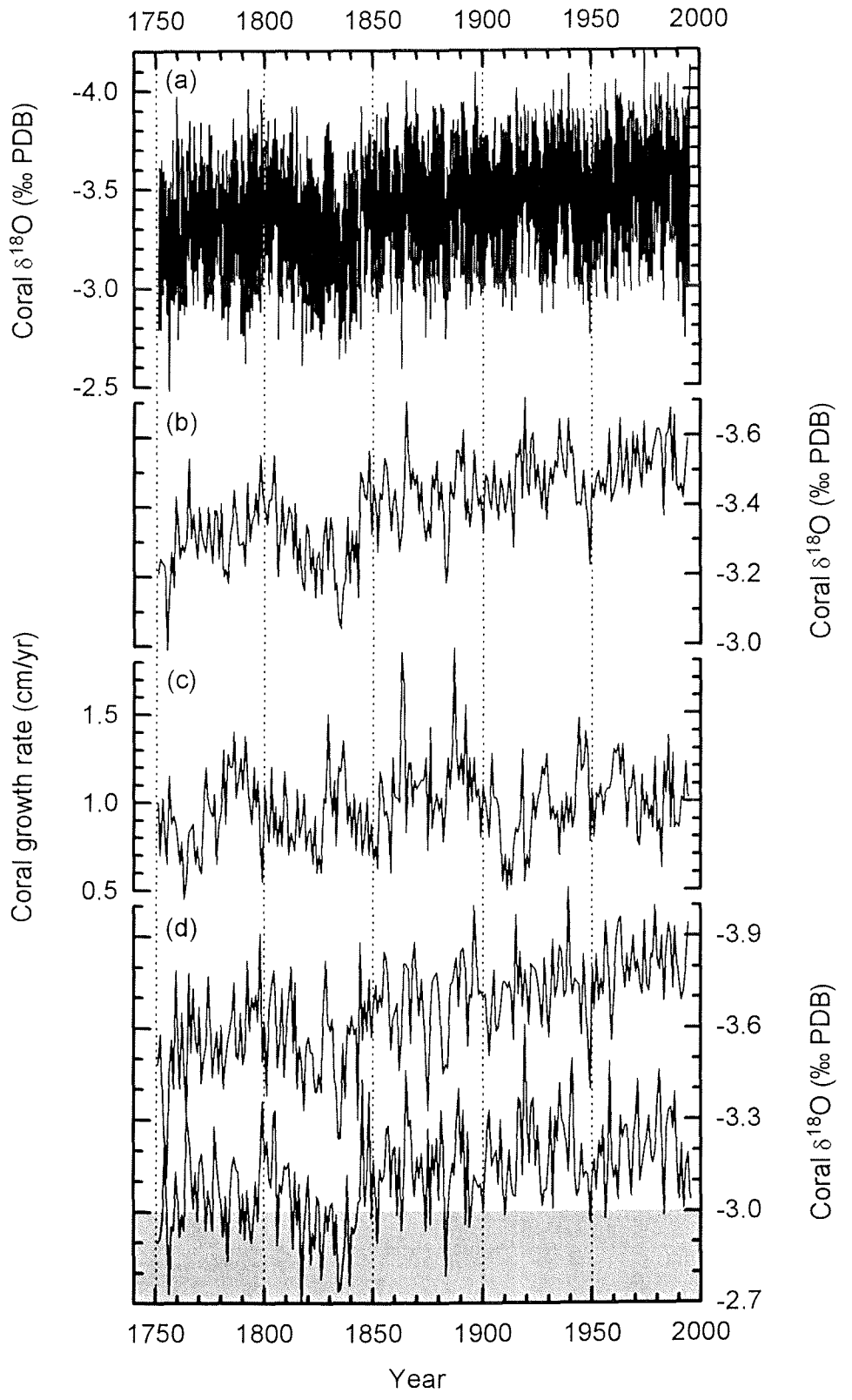

Figure 4.7. The Ras Umm Sidd coral $\delta^{18}O$ record (core RUS-95). (a) Bimonthly time series. (b) Mean annual time series. (c) Annual coral growth rate. (d) Summer (July-October) time series (upper line); winter (January-April) time series (lower line). The shading indicates winters in which most likely deep water formation occured (see text for discussions).

4.5.4.1. Prominent cooling events and volcanic eruptions

Large explosive volcanic eruptions reduce the incoming solar radiation owing to injections of sulphate aerosols into the stratosphere and can therefore cause cooling at the Earth's surface on a 2- to 3-year timescale [e.g., *Robock and Mao*, 1992]. Prominent cooling events in the mean annual Ras Umm Sidd coral record occur in 1755, 1834-1835, 1883-1884, and 1949 (Figure 4.7b). Following the approach of *Crowley et al.* [1997] some of these coolings coincide with or follow within one year large volcanic eruptions. Eruptions in 1754 (Taal, Philippines), 1835 (Coseguina, Nicaragua), and 1883 (Krakatau, Indonesia) have caused northern and/or southern hemisphere coolings, which is known from tree-ring [*Briffa et al.*, 1998] and/or coral records [*Crowley et al.*, 1997], although the climate effect of the 1754 eruption of Taal has recently been called into question [*Quinn et al.*, 1998]. Two less pronounced interannual cooling events in the coral record in 1914 and 1983 are probably associated with large eruptions in 1912 (Novarupta/Katmai, Alaska) and 1982 (El Chichón, Mexico). There is a known effect of volcanism on Middle East climate. For the period 1883-1992 it was shown that large volcanic eruptions were followed by a cold anomaly over the Middle East, independent of the hemisphere of the volcanoes [*Robock and Mao*, 1992].

However, the most prominent cooling event in the Ras Umm Sidd coral record (1834-1835), probably associated with the eruption of Coseguina (1835), is part of a longer cooling interval between 1805 and 1844. A comparable cooling interval in the first half of the 19th century can also be found in the northern hemisphere temperature reconstructions of *Mann et al.* [1998] and *Jones et al.* [1998], in a network of temperature-sensitive northern hemisphere tree-ring-density chronologies [*Briffa et al.*, 1998], in a multiproxy record of circum-Arctic temperature [*Overpeck et al.*, 1997], and in coral $\delta^{18}O$ proxy records of SST from the southwestern [*Quinn et al.*, 1996; *Crowley et al.*, 1997; *Quinn et al.*, 1998] and the equatorial eastern Pacific Ocean [*Dunbar et al.*, 1994]. In fact, most of these records show a warm-cold-warm-cold pattern of decadal-scale oscillations during this interval of prominent cooling (~1805-1840) which has recently been suggested to be of use in the refinement of coral chronologies [*Crowley et al.*, 1997]. This pattern is also evident in the Ras Umm Sidd coral record (Figure 4.7b).

The prominent cooling interval in the first half of the 19th century and the associated warm-cold-warm-cold pattern are thought to be related to a pulse of large explosive volanic eruptions that occurred during this time [*Crowley et al.*, 1997; *Mann et al.*, 1998]. The Ras Umm Sidd coral record shows minor cooling events superimposed on the generally cold pattern during that period in 1809, 1815, 1817-1818, 1823, and 1832 which are probably associated with large volcanic eruptions in 1809 (unknown), 1815 (Tambora, Indonesia), 1822 (Galungung, Indonesia), and 1831 (Babuyan, Philippines) [e.g., *Crowley et al.*, 1997]. However, there is also some evidence for a solar-induced cooling in the early 19th century [*Lean et al.*, 1995; *Crowley and Kim*, 1996].

4.5.4.2. Interannual salinity changes and mean annual coral $\delta^{18}O$

As discussed earlier (sections 4.5.1. and 4.5.2.) there is a weaker correlation between coral $\delta^{18}O$ and SST on the annual timescale (r = -0.58) relative to the bimonthly timescale (r = -0.86) for the Ras Umm Sidd coral record. The SST/coral $\delta^{18}O$ calibration for each timescale is also different, with a slope of -1.84°C/‰ (0.543‰/°C) on the annual timescale and of -6.05°C/‰ (0.165‰/°C) on the bimonthly timescale. A similar feature was described for the New Caledonia coral record [*Quinn et al.*, 1998], where the SST/coral $\delta^{18}O$ correlation changes from r = -0.87 on the monthly timescale to r = -0.53 on the annual timescale, and the SST/coral $\delta^{18}O$ calibration from -5.38°C/‰ (0.186‰/°C) to -1.72°C/‰ (0.581‰/°C), respectively. Despite the only moderate correlation between mean annual coral $\delta^{18}O$ and SSTs at New Caledonia the predicted SSTs using the mean annual calibration and the observed mean annual SSTs match well over a verification interval [*Quinn et al.*, 1998]. It was suggested that although the amplitude of the seasonal salinity changes at New Caledonia is small compared to SST changes, interannual changes in salinity may be proportionately larger (with respect to temperature) than seasonal changes. It was therefore suggested that salinity variations at the interannual timescale could be in part responsible for the degradation of the SST/coral $\delta^{18}O$ correlations and the difference in the slopes of the SST/coral $\delta^{18}O$ calibrations between monthly and mean annual regressions in this coral record (T. J. Crowley et al., manuscript in preparation, 1998).

We are therefore left with the conclusion that while on the seasonal timescale the Ras Umm Sidd coral is primarily recording information on SSTs, also in the northern Red Sea on the interannual timescale large-scale salinity variations in the surface waters probably affect coral $\delta^{18}O$ in addition to SST. However, it is important to recall that the mean annual Ras Umm Sidd coral $\delta^{18}O$ record can still be used for the reconstruction of the large-scale SST variability in the northern Red Sea, which for example is supported by the striking similarities between the coral record and regional records of air temperature during the late 19th century (Figure 4.6a) or the strong correlation with SSTs during the interval of 1946-1966 (Figure 4.4c).

The slope of the mean annual SST/coral $\delta^{18}O$ calibration of -1.84°C/‰ (0.543‰/°C) for the Ras Umm Sidd record implies an amplification of the mean annual coral $\delta^{18}O$ signal (with respect to temperature) relative to the seasonal signal. This suggests that on the interannual timescale colder SSTs in the northern Red Sea coincide with higher $\delta^{18}O_{seawater}$ values and therefore higher salinities in the surface waters, and warmer SSTs with lower $\delta^{18}O_{seawater}$ values and therefore lower salinities. Precipitation and runoff are negligible in this extremely arid environment (section 4.3.) and therefore can be excluded to have any effect on the $\delta^{18}O$ of the seawater on the interannual timescale. Another possible source is the lateral advection of surface water from the southern Red Sea by the northward-flowing currents. Southern Red Sea and especially northern Indian Ocean surface waters have lower $\delta^{18}O$ values relative to northern Red Sea waters [*Ganssen and Kroon*, 1991].

It was recently described for a coral record from the Dahlak Archipelago (Eritrea) that in the southern Red Sea (Figure 4.2) simultaneous changes in SST and $\delta^{18}O_{seawater}$ on the interannual timescale produce an amplified mean annual coral $\delta^{18}O$ signal (with respect to temperature) [*Klein et al.*, 1997]. This signal was suggested to be controlled by interannual variations in the intensity of surface water influx from the Indian Ocean to the Red Sea, which is more intense during periods of high Indian Ocean SSTs [*Klein et al.*, 1997]. An increased influx of warmer Indian Ocean water with its lower $\delta^{18}O$ signature through the Strait of Bab-el-Mandab could therefore probably also result in warmer SSTs and lower $\delta^{18}O_{seawater}$ values in the northern Red Sea a few years later relative to Eritrea, which is the timescale for the entire northward journey of the surface waters [*Eshel and Naik*, 1997]. However, there is no significant correlation between the mean annual $\delta^{18}O$ values of the coral records from Ras Umm Sidd and Eritrea. Correlations at different lag and lead times (-15 to +15 years; results are not shown here) reveal that the Ras Umm Sidd coral record apparently leads the Eritrea record by 4-6 years. The maximum correlation coefficient (r) is 0.44 for a lead time of 6 years; or 0.62 when 3-year running averages are used for the correlation (both are significant at the 99.5% level).

The reason for this apparent lead of the Ras Umm Sidd record is beyond the scope of this paper, but if interannual variations in the intensity of surface water influx from the Indian Ocean would have a control on northern Red Sea SST and $\delta^{18}O_{seawater}$ variability the opposite pattern should be expected. We therefore conclude that the processes and effects which were described for the southern Red Sea [*Klein et al.*, 1997] are most likely not responsible for the amplification of the mean annual coral $\delta^{18}O$ signal (with respect to temperature) in the Ras Umm Sidd coral record; and that the causes for the amplification are probably associated with processes occuring in the northern Red Sea.

4.5.4.3. Combined record of temperature and aridity

The dominant influence of the seasonal shift in the latitudinal position of the subtropical high-pressure belt and the associated subtropical westerly jet stream on the evaporation and salinity patterns in the northern Red Sea and on the precipitation pattern in the Mediterranean region was discussed earlier (section 4.3.2.). In general, the jet stream in the upper troposphere and the associated high-pressure belt at the surface separate the arid region in the south from the winter rainfall region in the north. Changes in the mean annual latitudinal position of the jet-stream axis on interannual or larger timescales should therefore have considerable effects on Middle East climate.

Model simulations of the Last Glacial Maximum (LGM; ~18 kyr BP) show a strengthening and southward shift of the jet stream relative to its present position and a resulting increased winter precipitation in the (eastern) Mediterranean region [*Lautenschlager and Herterich*, 1990; *Prentice et al.*, 1992]. The increased precipitation resulted in a higher lake level of Lake Lisan (the present-day Dead Sea) (Figure 4.2) during the LGM [*Begin et al.*, 1985; *Qin and Yu*, 1998] whereas for the northern Red

Sea increased arid conditions are indicated by the work of *Almogi-Labin et al.* [1986], *Locke and Thunell* [1988], and *Geiselhart et al.* [1998].

Recurring periods of wetter and drier climate during the last glacial period for the Dead Sea/Lake Lisan region are indicated by a series of palaeosols from the northern Negev desert [*Goodfriend and Magaritz*, 1988]. The major source area of precipitation during the wetter periods was identified in the north/northwest. The wetter periods were therefore interpreted to result from a southward shift of the northern boundary of the desert belt in the Middle East [*Goodfriend and Magaritz*, 1988], i.e., a southward shift of the subtropical high-pressure belt. New results from an U-Th-dated Lake Lisan sediment record (~70-18 kyr BP) reveal that this region was wetter during global cold periods and drier during warmer periods of the last glacial, on the timescales of Heinrich events and Dansgaard-Oeschger events [*Schramm et al.*, 1997; *Stein et al.*, 1998].

For the more recent Roman period ~2000 years ago less arid conditions in the Dead Sea region relative to present-day climate were inferred from the stable isotopic composition of ancient wood [*Yakir et al.*, 1994; *Lipp et al.*, 1996]. Lipp et al., discussing historical accounts on greater precipitation and cooler temperatures during the Roman period in this region, suggested that changing atmospheric circulation has played a role in climate change over the Middle East over the past two millennia. In summary, the paleorecords and model simulations show some evidence that during global cold periods the eastern Mediterranean region in the north was wetter and the northern Red Sea region in the south possibly drier, whereas during global warm periods the north was drier with no information available for the conditions in the south.

The climatic effects of the interactions of changes in the latitudinal temperature gradient, which governs the Hadley cell intensity, and the global mean temperature, which governs the Hadley cell extent, were recently investigated in several General Circulation Model (GCM) experiments [*Rind*, 1998]. However, a simplified point of view is that lower high-latitude temperatures (e.g., during the Little Ice Age period, ~1450-1850) raise the equator-pole temperature gradient, which results in an equatorwards shift of the main components of the atmospheric circulation. A southward displacement and intensification of the subtropical jet stream is accompanied by a southward shift of the circumpolar westerlies and the associated storm tracks. The corresponding southward shift of the subtropical high-pressure belt is accompanied by increased subsidence associated with an intensification of the Hadley cells.

We therefore suggest that the amplification of the mean annual $\delta^{18}O$ signal (with respect to temperature) in the Ras Umm Sidd coral record from the northern Red Sea can be best explained by variations in the mean annual latitudinal position of the subtropical westerly jet stream on the interannual timescale (Figure 4.8). During colder years the jet stream and the associated subtropical high-pressure belt are assumed to shift southward. Over the entire year the northern Red Sea would therefore predominantly experience atmospheric conditions which are typical for the present-day winter, i.e., a higher evaporation because the zone of maximum atmospheric subsidence stays a longer time of the year over the area. This should result in higher mean annual salinities in the surface

waters during colder years. The combined effect of colder SSTs and higher salinities would produce an amplified mean annual coral $\delta^{18}O$ signal (with respect to temperature). During warmer years the jet stream is assumed to shift northward. Over the entire year the northern Red Sea would then predominantly be affected by atmospheric conditions which are typical for the present-day summer, i.e., a lower evaporation because the zone of maximum atmospheric subsidence stays a shorter time of the year over the area. This should result in lower mean annual salinities in the surface waters during warmer years and again an amplified mean annual coral $\delta^{18}O$ signal (with respect to temperature) would result.

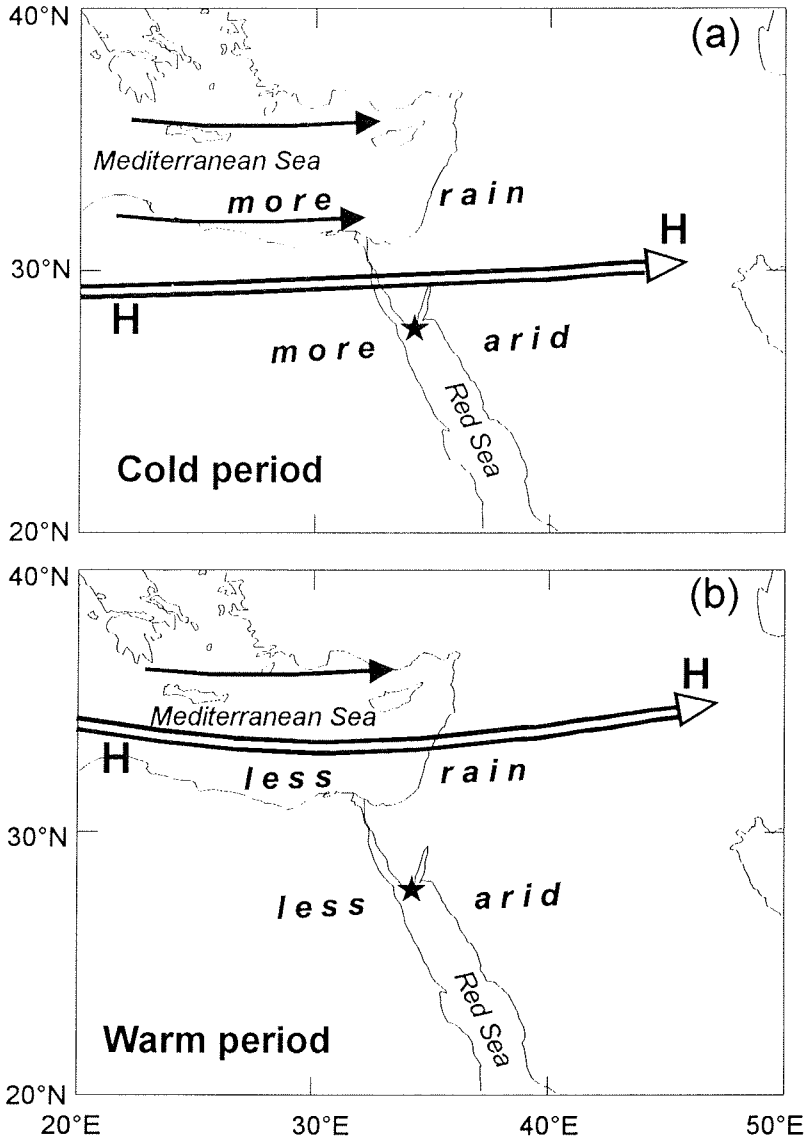

Figure 4.8. Schematic map of the Middle East and the large-scale atmospheric and surface conditions suggested for (a) colder years and (b) warmer years, as interpreted from the Ras Umm Sidd coral record and supported by instrumental and proxy records of climate. The hypothetical mean annual position of the subtropical westerly jet stream (open arrow) is shown. Suggested changes in aridity, rainfall, and surface winds (solid arrows) are also shown. The location Ras Umm Sidd is indicated by a star.

This hypothesis suggests that colder years in the northern Red Sea region are more arid (higher evaporation) and warmer years are less arid (lower evaporation) without any variations in the amount of precipitation which is a negligible factor in this desert region. The mean annual Ras Umm Sidd coral record (Figure 4.7b) should therefore be interpreted as a record of temperature and aridity. However, the record can still be used for the reconstruction of the large-scale SST variability in the northern Red Sea because simultaneous changes in temperature and aridity produce an amplified mean annual coral $\delta^{18}O$ signal with respect to temperature.

Direct multiyear measurements of $\delta^{18}O_{seawater}$ or salinity are not available from the northern Red Sea to verify our hypothesis. However, an indirect verification can be obtained from observations of rainfall in the Mediterranean region in the north. Our hypothesis that a southward shift of the jet stream during colder years results in more arid conditions in the northern Red Sea would imply increased rainfall in the eastern Mediterranean region due to the accompanied southward shift of the moisture bringing North Atlantic westerlies. During years with a southward-shifted jet stream the eastern Mediterranean region should predominantly experience atmospheric conditions which are typical for the present-day winter, i.e., the period of winter rainfall should be longer, resulting in an increased mean annual precipitation for the region. During warmer years with a northward-shifted jet stream and an accompanied northward shift of the North Atlantic westerlies the eastern Mediterranean region should predominantly be affected by atmospheric conditions which are typical for the present-day summer, i.e., drier conditions because the subtropical high-pressure belt stays a longer time of the year above the area.

A comparison of the Ras Umm Sidd coral record with instrumental observations of precipitation in Alexandria [*Baker et al.*, 1994] at the southern coast of the eastern Mediterranean Sea (Figure 4.2) reveals striking similarities (Figure 4.6b). Cold and arid conditions in the northern Red Sea, indicated by high coral $\delta^{18}O$ values, coincide with increased rainfall in Alexandria on the interannual to interdecadal timescale; and warm and less arid conditions in the northern Red Sea coincide with decreased rainfall in Alexandria. Inspection of the rainfall record for Jerusalem reveals a comparable pattern only for the 1930s-1950s. For the earlier part of the record there is no clear relationship evident. However, the Jerusalem rainfall record is not derived from a quality-controlled dataset [e.g., *Baker et al.*, 1994]. The problems associated with this record are discussed in the original reference [*Rosenan*, 1955].

A probably better source of information on past rainfall variablity in Jerusalem is a tree-ring chronology [*Liphschitz*, 1998]. The width of annual tree rings in the Jerusalem region is strongly dependent on the amount of annual rainfall, with increased rainfall resulting in an increased tree-ring width [*Yakir et al.*, 1996]. The Jerusalem tree-ring chronology and the Ras Umm Sidd coral record reveal similarities on the interannual to interdecadal timescale during most parts of overlap and show the expected relationship of cold/warm and arid/less arid conditions in the northern Red Sea coinciding with

increased/decreased rainfall in Jerusalem (Figure 4.9). The most striking similarities are evident for the 1830s with an extremely cold and arid climate in the northern Red Sea and large amounts of rainfall in Jerusalem. Our general conclusions are supported by recent results from Israel that during the last winters with increased precipitation the subtropical jet stream shifted southward [Y. Carmona and P. Alpert, personal communication, in *Price et al.*, 1998] and tree-ring growth was increased in Jerusalem [*Yakir et al.*, 1996].

The instrumental records of precipitation from Cairo/Ismailia and Alexandria reveal that both latitudes are affected by the Mediterranean winter rainfall regime (Figure 4.6b) but that there is sharp transition to extremely arid conditions towards the Red Sea in the south (Figure 4.2). This pattern excludes the possibility that Mediterranean winter rains significantly affect the northern Red Sea and the $\delta^{18}O$ signal of the Ras Umm Sidd coral record on interannual or larger timescales. Furthermore such an effect would result in a pattern opposite to the observed relationship between Ras Umm Sidd coral $\delta^{18}O$ and precipitation in Alexandria (Figure 4.6b).

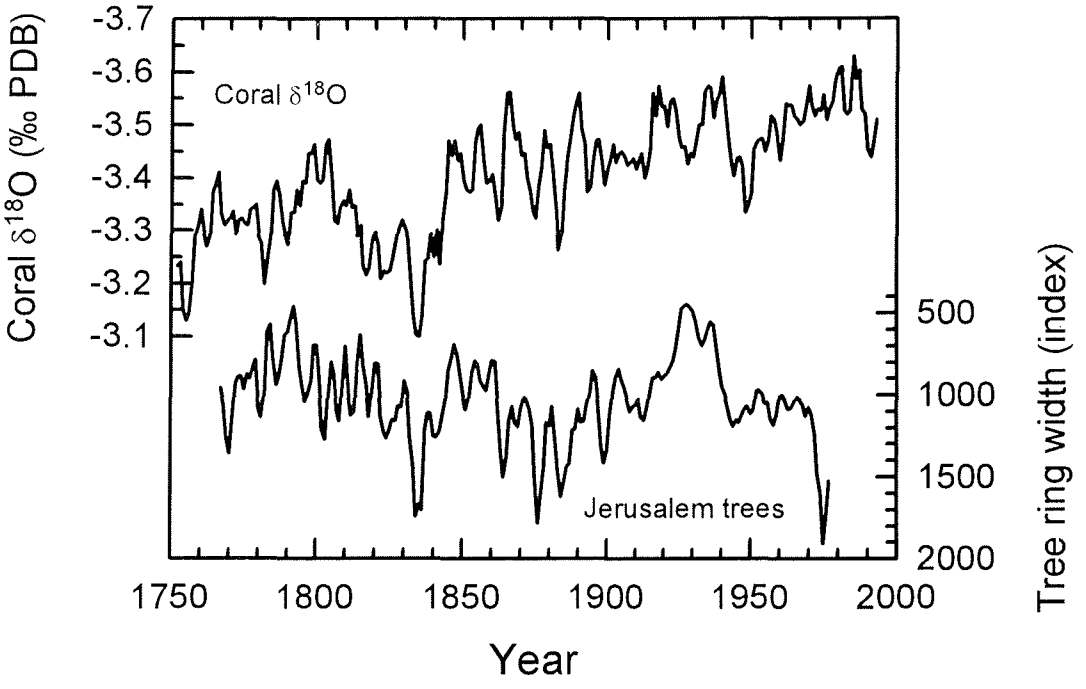

Figure 4.9. Comparison of the Ras Umm Sidd coral $\delta^{18}O$ record and a tree-ring chronology from Jerusalem. The chronology is a master curve derived from 5 trees. High index values indicate high annual tree-ring widths [*Liphschitz*, 1998]. In this region an increased tree-ring width indicates increased rainfall [*Yakir et al.*, 1996]. 3-year running averages of mean annual values are shown. Note that the tree-ring-width scale has been reversed for direct comparison with the coral record.

The paleoclimatic information derived from the Ras Umm Sidd coral $\delta^{18}O$ record in combination with regional instrumental and proxy records of climate suggests that cold periods in the Middle East are associated with increased arid conditions (higher evaporation) in the northern Red Sea and increased rainfall in the eastern Mediterranean region. Warm periods are associated with less arid conditions (lower evaporation) in the northern Red Sea and decreased rainfall in the eastern Mediterranean region. This pattern is suggested for the past nearly 250 years on the interannual to interdecadal/multidecadal timescale.

Simultaneous humid-arid variations during decadal- to multidecadal-scale cold/warm periods are also indicated by other proxy climate records along the northern rim of the African-Asian arid belt for the last 500 years [*Ji et al.*, 1993]. It was suggested that during a hemisphere-scale cold period the westerlies shift southwards bringing increased precipitation to the Mediterranean area whereas the arid region in the south becomes drier. During a warm period the westerlies were assumed to shift northwards resulting in decreased precipitation in the Mediterranean region whereas the arid region in the south becomes wetter [*Ji et al.*, 1993]. No physical mechanism was given to explain the dry-wet changes in the northern part of the arid belt. Our results on Middle East climate variability derived from the paleoclimatic interpretation of the Ras Umm Sidd coral record are in general agreement with the conclusions in the work of *Ji et al.* [1993]. However, our results suggest that the dry-wet changes assumed by Ji et al. for the northern part of the arid belt are in fact changes between a more arid (higher evaporation) and a less arid (lower evaporation) climate, i.e., changes in the strength of evaporation and not in the amount of precipitation, at least in the Middle East section.

4.5.4.4. Deep water formation in the northern Red Sea

The northern Red Sea is probably the only site in the world oceans where water mass formation occurs and reef corals grow. As discussed earlier (section 4.3.1.) there are two modes of water mass formation, both occur during the wintertime. The regular process in the climatology is the shallow-convective, subductive mode of intermediate water formation (≤1 km) which occurs slightly south of the northwest corner of the Red Sea near the western coast (~26°N) (Figure 4.2). The process ceases in summer [*Eshel and Naik*, 1997].

In contrast to this regular process the deep water of the Red Sea is formed during intermittent, episodic events [*Woelk and Quadfasel*, 1996; *Eshel and Naik*, 1997] in a deep-convective process which most likely occurs in the center of the cyclonic gyre in the northern Red Sea where the climatological winter stratification is the weakest [*Eshel and Naik*, 1997; *Clifford et al.*, 1997]. Eshel and Naik suggest that the episodic formation of deep water is related to short-lived intense atmospheric events. Also Woelk and Quadfasel suggest that the intermittent formation of deep water is strongly linked to interannual variations of the meteorological forcing like cooling and evaporation; and speculate on a possible relation to El Niño-Southern Oscillation (ENSO) events.

The only direct observation of deep water formation in the northern Red Sea in the winter 1982-1983 is provided by the work of *Woelk and Quadfasel* [1996]. However, it was recently demonstrated that the winter $\delta^{18}O$ values of northern Red Sea corals can be used to track water mass formation variability [*Eshel et al.*, submitted 1998]. It was suggested that the dominant process of Red Sea deep water formation is lower-tropospheric subsidence, which dries the boundary layer, increases surface evaporation and water surface density, and finally drives water mass formation [*Eshel et al.*, submitted 1998]. Eshel et al. successfully converted a coral $\delta^{18}O$ time series from the northern Red Sea (western Ras Mohammed area, ~17 km southwest of Ras Umm Sidd) to a proxy record of water surface density for the period 1973-1995. The record indicates that maximum water surface density anomalies and therefore most probably deep water formation occured in the winters of 1982-1983 and 1991-1992 [*Eshel et al.*, submitted 1998], with the first event being in coincidence with the observations of *Woelk and Quadfasel* [1996].

Both events are also documented in the Ras Umm Sidd coral record by the highest winter $\delta^{18}O$ values during the corresponding period (Figure 4.7d). We therefore assume that the winter $\delta^{18}O$ values of the Ras Umm Sidd coral record can be used to detect extraordinarily cold and/or arid winters when deep water formation in the northern Red Sea most probably occured. For the winters of 1982-1983 and 1991-1992 the coral record shows $\delta^{18}O$ values of -2.99‰ and -3.01‰, respectively. We therefore assign a threshold value to the record and interprete all winters with a higher coral $\delta^{18}O$ value than -3.00‰ as deep-water formation events in the northern Red Sea.

The Ras Umm Sidd coral record indicates 57 of such events (including 1991-1992) during the past 245 years (Figure 4.7d and Table 4.1). It cannot be excluded that this approach indicates to many events in the earlier part of the coral record owing to the generally colder conditions in the 18th and 19th century relative to the 20th century and taking not into account possible associated changes in the thermocline/halocline system. However, we assume it is the most objective method. When the linear trend is removed from the winter coral $\delta^{18}O$ record only 11 events are indicated (including 1991-1992) (Table 4.1), using again the winters 1982-1983 and 1991-1992 as criterion.

The two most recent events of deep water formation in the winters of 1982-1983 and most probably 1991-1992 both coincide with strong to moderate El Niño events but also with large tropical volcanic eruptions (El Chichón, 1982; Mount Pinatubo 1991) (Table 4.1). The signatures of volcanic eruptions in the mean annual coral record were discussed earlier (section 4.5.4.1.). The work of *Robock and Mao* [1992] showed for the period 1883-1992 that large volcanic eruptions are followed by a cold surface temperature anomaly over the Middle East, independent of the hemisphere of the volcanoes [*Robock and Mao*, 1992]. This cooling occured in the first winter after tropical eruptions, in the first or second winter after midlatitude eruptions, and in the second winter after high latitude eruptions [*Robock and Mao*, 1992]. Winter cooling in the Middle East after large explosive volcanic eruptions is also observed in GCM experiments [*Graf et al.*, 1993;

Kirchner and Graf, 1995]. Volcanism-induced cooling could therefore be partly responsible for the deep water formation in the winters of 1982-1983 and 1991-1992. Deep convective water mass mixing during these two winters is also documented in a coral record from the northern end of the nearby Gulf of Aqaba (Israel) (Figure 4.2) [*Felis et al.*, 1998b] and was attributed to the cold air temperature anomaly following the eruptions of El Chichón (1982) and Mount Pinatubo (1991) [*Genin et al.*, 1995; *Felis et al.*, 1998b].

El Niño events occured in both 1982-1983 and 1991-1992. A possible relationship between El Niño events and deep water formation in the northern Red Sea was already suggested in the work of *Woelk and Quadfasel* [1996], but no physical mechanism was given to explain a possible teleconnection. GCM experiments revealed that the winter cold anomaly in the Middle East after volcanic eruptions is weaker during El Niño years, but still exists [*Kirchner and Graf*, 1995]. However, a possible explanation for an El Niño teleconnection responsible for deep water formation could be a change in the latitudinal position of the subtropical westerly jet stream. In general, during an El Niño event the Hadley cell intensity is increased and the subtropical jet stream is intensified and displaced equatorward, especially in winter [*Philander*, 1990]. A southward displacement of the jet stream and the associated subtropical high-pressure belt during an El Niño winter, together with the increased Hadley cell intensity, should result in increased arid conditions (higher evaporation) in the northern Red Sea, which is favorable for deep water mass formation [*Eshel et al.*, submitted 1998]. This hypothesis is supported by recently reported evidence that the subtropical westerly jet stream in Israel shifted southward during the last El Niño years [Y. Carmona and P. Alpert, personal communication, in *Price et al.*, 1998].

To investigate a possible relationship between deep water formation in the northern Red Sea and volcanic eruptions/El Niños during the past nearly 250 years all events as inferred from the Ras Umm Sidd coral record are listed in Table 4.1. Also given are co-occuring large explosive volcanic eruptions and El Niño events if known. The coincidence of deep-water formation events and volcanic eruptions/El Niños is only moderate. Deep water formation occurs in at least 22 years of a total 57 event years without any co-occuring volcanic eruption/El Niño; or in at least 3 years of a total of 11 event years when the detrended record is considered. Of the 57 deep-water formation events 27 coincide with El Niños, at least 11 (probably 13 or 16) with volcanic eruptions, including at least 6 (probably 7 or 8) which coincide with both an El Niño and a volcanic eruption.

Table 4.1. Years with deep water formation in the northern Red Sea as inferred from the Ras Umm Sidd coral $\delta^{18}O$ record and co-occuring large volcanic eruptions and El Niño events

Year [a]	Volcano (year)[b]	El Niño[c]
1751		M +
1752		
1753	Little Sunda (1752)[d]	
1755	Taal (1754)[d]	S
1756		
1757		
1758		
1761		S
1762		S
1763		
1769	Cotopaxi (1768)	M +
1773	Papandajan (1772)	M
1776		M+
1781		
1783		VS
1789	unknown (1788)	
1791		VS
1793		VS
1794		M +
1795		M +
1797		M +
1806		M +
1813	Soufriere+Awu (1812)	
1815		
1817	Tambora (1815)[e]	M +
1818	Roung (1817)	
1821		M
1822		
1823	Galungung (1822)	
1826		
1827	Kelut (1826)	
1829		
1832	Babuyan (1831)	S +
1833		S +
1834		
1835		M
1836	Coseguina (1835)	M
1837		S
1839		S
1840		
1841		
1842		
1849		
1852		M
1861		
1863		
1874		M +
1876		
1883	Krakatau (1883)[e]	
1892		
1894		
1900		VS
1910	Ksudach (1907)[e]	
1949		
1956		
1983	El Chichón (1982)	VS
1992	Mount Pinatubo (1991)	M

[a] "Year" refers to the winter of the corresponding year, i.e., 1751 refers to the winter of 1750-1751. The deep-water formation chronology is derived from the winter $\delta^{18}O$ values (January-April) of the coral record. The criterion for a deep-water formation event is defined as a higher coral $\delta^{18}O$ value relative to a threshold value which is the calculated mean of the $\delta^{18}O$ values in the two "event winters" of 1983 and 1992, which are indicated by a frame. Bold years still indicate an event when the linear trend is removed from the winter coral $\delta^{18}O$ record. The age estimate error of the coral chronology is ±0 years in the interval of 1925-1995, ±1 years in 1783-1924, and ±2 years in 1750-1782, respectively.

[b] Only those eruptions were taken into account which resulted in a cooling signal in two recently published northern [*Briffa et al.*, 1998] and southern hemisphere [*Crowley et al.*, 1997] proxy records. A further selection was performed by using the criteria of *Robock and Mao* [1992] that cooling in the Middle East occurs in the first winter after tropical eruptions, in the first or second winter after midlatitude eruptions, and in the second winter after high latitude eruptions. For further details on the climatic significance of the eruptions and the latitude of the volcanoes see *Crowley et al.* [1997], *Briffa et al.* [1998], *Robock and Mao* [1992], and references therein.

[c] The El Niño years were derived from the event chronology of *Quinn et al.* [1992]. Strengths are moderate (M), strong (S), or very strong (VS); the + indicates intermediate values. The event in 1992 was added by us after inspection of several El Niño indices.

[d] The climate effect of the eruption has been recently called into question [*Quinn et al.*, 1998].

[e] The eruption occured to early/late to have any effect on Middle East climate in the year of deep water formation, according to the criteria of *Robock and Mao* [1992][b]. However, considering the age estimate error of the coral chronology a possible climate effect cannot totally be excluded.

On the other hand, not every large volcanic eruption (e.g., Santa Maria, 1902; Novarupta/Katmai, 1912; Agung, 1963) or strong El Niño (e.g., 1844-1846, 1877-1878, 1940-1941) which occured during the period of the coral record coincides with a deep-water formation event. We are therefore left with the conclusion that the episodic events of Red Sea deep water formation during winter are sometimes associated with El Niño events or large volcanic eruptions which can cause increased arid/cold conditions in the northern Red Sea favorable for deep water formation. However, deep water formation can also occur independent of these two forcing factors.

It was recently demonstrated that the skeletal $\delta^{13}C$ signal of a coral record (1974-1993) from the northern end of the nearby Gulf of Aqaba (Israel) (Figure 4.2) documents large plankton bloom events which are caused by deep vertical water mass mixing, convectively driven in colder winters. The signal was explained by changes in the coral's autotrophy-heterotrophy diet, through increased heterotrophic feeding on zooplankton during the blooms [*Felis et al.*, 1998b]. However, no comparable signals can be identified in the Ras Umm Sidd coral $\delta^{13}C$ record (results not shown here) during winters with deep-water formation events in the northern Red Sea as inferred from the coral $\delta^{18}O$ record.

4.5.4.5. Comparison with other coral records

There are now three long coral $\delta^{18}O$ records available from the Red Sea (Figure 4.10). The 63-year coral record from the Dahlak Archipelago (Eritrea) in the southern Red Sea [*Klein et al.*, 1997] has a bimonthly resolution and was discussed earlier (section 4.5.4.2.). The other record is an annual time series from Aqaba at the northern end of the Gulf of Aqaba (Jordan) [*Heiss*, 1994], which is in fact two records which were derived from the same coral colony. A vertically drilled core provides a 205-year record (AQ18) and a horizontally drilled core a 107-year record (AQ19).

The Gulf of Aqaba is a 1800-m-deep basin and is seperated from the Red Sea proper in the south by the narrow and shallow (~250 m) Straits of Tiran (Figure 4.2). The distance between Aqaba and Ras Umm Sidd is ~200 km and in general we would expect a similar coral $\delta^{18}O$ signal at both locations. However, the correlation of the mean annual Ras Umm Sidd record with the two Aqaba records is only weak with $r = 0.33$ for core AQ18 and 0.28 for core AQ19, respectively (99.5% level). Surprisingly there is no significant correlation between the two Aqaba cores itself. The correlation with the Ras Umm Sidd record increases to $r = 0.65$ and 0.74 for core AQ18 and 0.45 and 0.56 for core AQ19 when 5-year and 11-year running averages are used, respectively (99.5% level).

That data smoothing increases the correlation between the Ras Umm Sidd and the Aqaba records suggests that the coral $\delta^{18}O$ time series probably reflect a common climate signal on pentadal to decadal timescales. However, visual inspection of the coral records reveals no striking similarities on these timescales (Figure 4.10). An exception is that the

AQ18 record shows the highest coral $\delta^{18}O$ values in the 1830s, a decade which is also recorded as the coldest and most arid period in the Ras Umm Sidd record. Furthermore, a cooling interval in the first half of the 19th century with a superimposed warm-cold-warm-cold pattern is also documented in the AQ18 record. Hopefully a higher resolution coral record will become available from Aqaba in the near future to get better estimates of mean annual values from this latitude for the past several hundred years.

The Red Sea coral records together with a monthly coral record from the Seychelles in the western equatorial Indian Ocean [*Charles et al.*, 1997] now provide a transect of climate proxy records from ~30°N to ~5°S, considerably extending the discontinuous marine and terrestrial instrumental observations of climate in this region of the world.

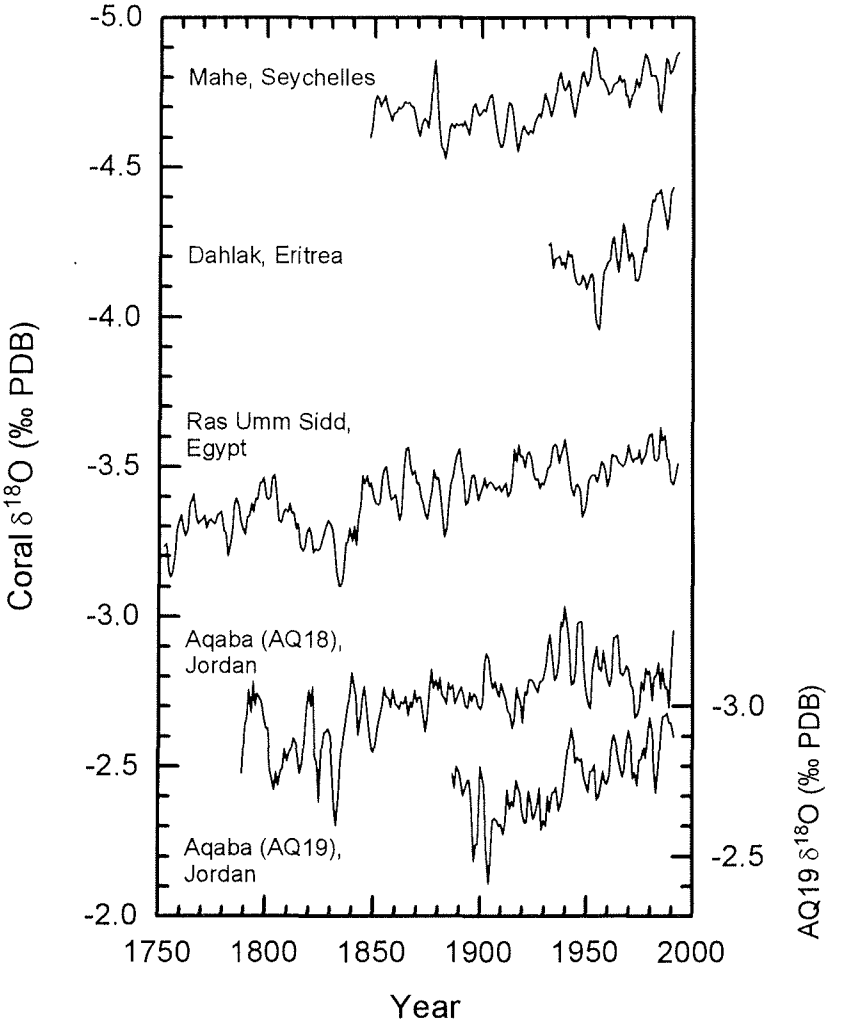

Figure 4.10. A comparison of long Red Sea and western Indian Ocean coral $\delta^{18}O$ records on a transect from ~30°N to ~5°S. All time series are plotted as 3-year running averages of mean annual values. Mahe, Seychelles (4.6°S) [*Charles et al.*, 1997]; Dahlak, Eritrea (15.7°N) [*Klein et al.*, 1997]; Ras Umm Sidd, Egypt (27.8°N) [*Felis et al.*, this study]; Aqaba, Jordan (29.5°N) [*Heiss*, 1994], two cores from the same colony. Resolution of the original time series is monthly (Seychelles), bimonthly (Dahlak and Ras Umm Sidd), and annual (Aqaba).

4.6. Conclusions

A coral $\delta^{18}O$ record from Ras Umm Sidd (Egypt) near the southern tip of the Sinai Peninsula in the northern Red Sea provides a bimonthly-resolution time series for the past 245 years (1750-1995) from this subtropical location (~28°N) at the northern rim of the African-Asian desert belt. The chronology is assigned an age estimate error of ±1 years to the interval 1783-1924 and of additionally ±1 years to the interval 1750-1782, resulting in a maximum cumulative error of ±2 years at the bottom of the core. The coral record seems to be fairly robust with respect to "kinetic" isotope disequilibria effects [*McConnaughey*, 1989a, b].

On the seasonal (bimonthly) timescale the coral $\delta^{18}O$ is primarily recording information on SSTs. The mean annual coral $\delta^{18}O$ signal reflects the large-scale variability of SSTs in the northern Red Sea and of air temperatures in the Middle East region. Application of the mean annual SST/coral $\delta^{18}O$ calibration indicates that average mean annual SSTs between 1751 and 1900 were ~0.3°C lower than the 20th century average. Prominent cooling events in 1755, 1834-1835, 1883-1884, and less pronounced events in 1914 and 1983 are probably associated with large explosive volcanic eruptions. The coral record indicates a prominent cooling interval in the first half of the 19th century with a superimposed warm-cold-warm-cold pattern which is also evident in northern hemisphere temperature reconstructions [e.g., *Mann et al.*, 1998] and southern hemisphere coral records [e.g., *Crowley et al.*, 1997; *Quinn et al.*, 1998].

The different SST/coral $\delta^{18}O$ calibrations for the annual and the seasonal (bimonthly) timescale suggest that similar as described for New Caledonia [*Quinn et al.*, 1998] changes in salinity may play a proportionately larger role on the interannual timescale resulting in an amplification of the mean annual coral $\delta^{18}O$ signal (with respect to temperature) relative to the seasonal signal. This suggests that on the interannual timescale colder SSTs in the northern Red Sea coincide with higher $\delta^{18}O_{seawater}$ values and therefore higher salinities in the surface waters, and warmer SSTs with lower $\delta^{18}O_{seawater}$ values and therefore lower salinities.

It is suggested that this amplification can be best explained by interannual variations in the latitudinal position of the subtropical westerly jet stream, the associated subtropical high-pressure belt, and therefore the descending branch of the northern Hadley cell with its subsiding air. During colder periods the jet stream is assumed to shift southward and the location of the associated high-pressure belt over the northern Red Sea results in an increased evaporation for this region and therefore in higher salinities in the surface waters. During warmer periods the jet stream and the high-pressure belt are assumed to shift northward resulting in less evaporative conditions in the northern Red Sea and therefore lower salinities surface waters. In summary, simultaneous changes in temperature and salinity on the interannual to interdecadal/multidecadal timescale are assumed to produce an amplified mean annual coral $\delta^{18}O$ signal which implies that colder periods in the northern Red Sea region are more arid (higher evaporation) and warmer

periods are less arid (lower evaporation), without any variations in the amount of precipitation which is a negligible factor in this desert region.

The paleoclimatic information derived from the Ras Umm Sidd coral record and the inspection of temperature and rainfall records from the eastern Mediterranean region in the north reveal that during colder periods in the Middle East on the interannual to interdecadal/multidecadal timescale the northern Red Sea region is more arid (higher evaporation) whereas the eastern Mediterranean region is wetter. During warmer periods in the Middle East the northern Red Sea region is less arid (lower evaporation) whereas the eastern Mediterranean region is drier. The pattern in the eastern Mediterranean region can also be explained by latitudinal shifts in the position of the subtropical jet stream. When the jet stream is shifted southward during a cold period the eastern Mediterranean region experiences increased rainfall owing to the associated southward shift of the North Atlantic westerlies. When the jet stream is shifted northward during a warm period rainfall in the north decreases due to the location of the subtropical high-pressure belt over the eastern Mediterranean region and the associated northward shift of the westerlies.

Results of other paleostudies indicate that the eastern Mediterranean region during the last glacial was wetter during global cold periods and drier during warm periods on the timescales of Heinrich events and Dansgaard-Oeschger events [*Schramm et al.*, 1997; *Stein et al.*, 1998], and ~2000 years ago wetter and possibly also colder [*Yakir et al.*, 1994; *Lipp et al.*, 1996]. We therefore suggest that comparable variations in the large-scale atmospheric circulation over the Middle East as described in this study may have also worked on much larger timescales during the last glacial period and possibly also during the Holocene.

The northern Red Sea is probably the only site in the world oceans where water mass formation occurs and reef corals grow. The winter $\delta^{18}O$ values of the Ras Umm Sidd coral record can be used to detect the intermittent, episodic events of deep water formation of the Red Sea thermohaline circulation during extraorinarily cold and/or arid winters. These events are sometimes associated with El Niño events or large volcanic eruptions which can result in increased arid/cold conditions in the northern Red Sea favorable for deep water formation.

In summary, the Ras Umm Sidd coral record (RUS-95) provides a valuable source of information on Middle East climate and Red Sea ocean history during the past nearly 250 years on the interannual to interdecadal/multidecadal timescale and may also support reconstructions of past climate variability on much larger timescales from the region.

4.7. Acknowledgments

We thank M. Segl and her team for stable isotope analysis; the Government of Egypt and the Egyptian Environmental Affairs Agency (EEAA) for support and permission to sample in the Ras Mohammed National Park; C. Gervais for giving a length scale to the sampling profile; and M. N. Evans, C. Price, G. Eshel, and A. Almogi-Labin for

discussions. This work is part of the Egyptian, Israeli, Palestinian, Jordanian and German Red Sea Program on Marine Sciences (RSP), funded by the BMBF (German Federal Ministry for Education, Science, Research, and Technology) through grant 03F0151A.

5. Interaction between the North Atlantic Oscillation and the El Niño-Southern Oscillation in a Middle East coral record

To be submitted as:
Felis, T., J. Pätzold, Y. Loya, and G. Wefer, Interaction between the North Atlantic Oscillation and the El Niño-Southern Oscillation in a Middle East coral record.

5.1. Abstract

The North Atlantic Oscillation (NAO) is one of the prominent modes of Northern Hemisphere climate variability primarily affecting the North Atlantic and its surrounding continents [*van Loon and Rogers*, 1978; *Rogers and van Loon*, 1979; *Hurrel*, 1995; *Hurrel*, 1996; *Hurrel and van Loon*, 1997]. The El Niño-Southern Oscillation (ENSO) phenomenon originates in the tropical Pacific Ocean but influences global climate via so-called "teleconnection" patterns [*Philander*, 1990; *Diaz and Kiladis*, 1992; *Evans et al.*, 1998a]. The oxygen isotopic composition of an annually banded reef coral from the northernmost Red Sea (~28°N) reveals that both the NAO and the ENSO contributed significantly to the climate variability of the Middle East during the past ~250 years on interannual to multidecadal timescales. The most prominent oscillation in the bimonthly coral time series with a period of 70 years and other periods of 22-23 and 8.6-8.7 years can be attributed to North Atlantic climate variability. Of considerable interest is a strong coherence with instrumental NAO [*Hurrel*, 1995] and ENSO [*Kaplan et al.*, 1998] indices at a period of ~5.7 years which is also the most prominent period in the

cospectrum of NAO and ENSO [*Rogers*, 1984]. The results suggest that interaction between extratropical and tropical modes of the global climate system has an important control on subtropical climate variability and that a prominent cooling interval in the first half of the 19th century evident in several Northern Hemisphere temperature reconstructions [*Mann et al.*, 1998; *Jones et al.*, 1998; *Overpeck et al.*, 1997] can be related to a 70-year climate oscillation of most probably North Atlantic origin, at least for the Middle East region.

5.2. Introduction

The North Atlantic Oscillation (NAO) has a strong influence on large-scale variations in the atmospheric circulation of the Northern Hemisphere controlling regional distributions of surface temperature and precipitation [*van Loon and Rogers*, 1978; *Rogers and van Loon*, 1979; *Hurrel*, 1995; *Hurrel*, 1996; *Hurrel and van Loon*, 1997]. The NAO is described with an index based on the difference of normalized winter sea-level atmospheric pressures between Lisbon, Portugal, and Stykkisholmur, Iceland [*Hurrel*, 1995]. Winters with a high NAO index are characterized by low pressures of the Icelandic low and high pressures of the Azores high (Figure 5.1).

During winters with a high NAO index the North Atlantic westerlies shift northward resulting in wetter and warmer conditions in northern Europe owing to the associated atmospheric moisture transport and the moderating influence of the ocean. This northward shift results in drier and colder conditions in southern Europe, the Mediterranean, North Africa, and the Middle East. During winters with a low NAO index a southward shift of the westerlies produces wetter and warmer conditions in the Mediterranean and the Middle East [*Hurrel*, 1995; *Hurrel and van Loon*, 1997]. The interannual variations in the atmospheric export of desert dust from North Africa are also NAO controlled with an increased export during high NAO index years owing to an increased uptake and transport during drier conditions [*Moulin et al.*, 1997]. The NAO is present throughout the year but is most pronounced during winter [*Barnston and Livezey*, 1987].

The El Niño-Southern Oscillation (ENSO) phenomenon is associated with variations in central and eastern equatorial Pacific sea surface temperatures. Tropical Pacific warm events are referred to as ENSO events. A commonly used measure of ENSO strength is the sea surface temperature (SST) anomaly of the eastern equatorial Pacific, averaged over 150°W-90°W, 5°N-5°S (NINO3 index). The ENSO can affect extratropical climate variability via atmospheric teleconnection patterns which induce variations in the intensity and latitudinal position of the subtropical westerly jet stream [*Philander*, 1990; *Hurrel*, 1996].

Enhanced winter precipitation in Israel during years with ENSO events was recently reported for the last 20-25 years [*Yakir et al.*, 1996; *Price et al.*, 1998]. There is evidence for a southward shift of the subtropical jet stream over Israel during the recent ENSO years [Y. Carmona and P. Alpert, personal communication, in *Price et al.*, 1998] which

would be accompanied by a southward shift of the moisture bringing North Atlantic westerlies explaining the increased precipitation.

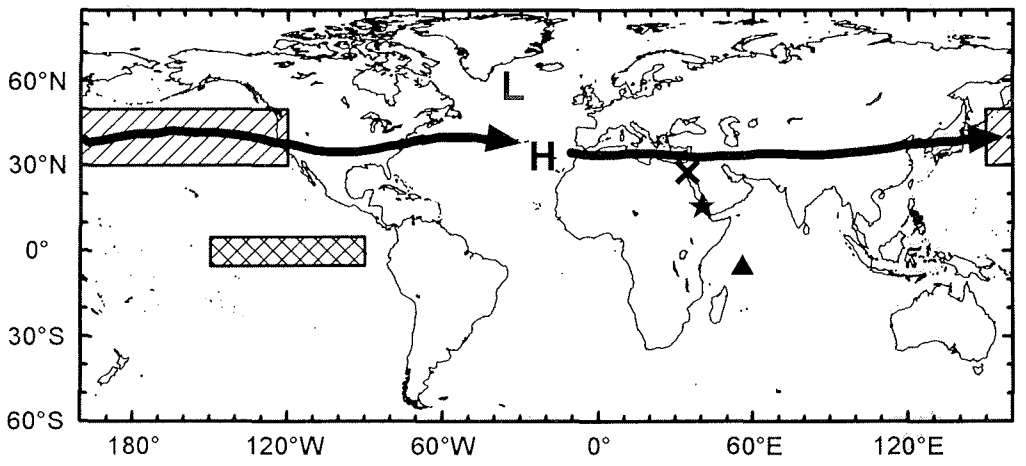

Figure 5.1. Map showing the positions of the Icelandic low (L) and the Azores high (H), the centers of action of the North Atlantic Oscillation (NAO); the locations of the NINO3 area index (150°W-90°W, 5°N-5°S) in the eastern equatorial Pacific (cross-hatched box) and the North Pacific (NP) area index (150°E-120°W, 50°N-30°N) in the North Pacific (hatched box); the position of the Northern Hemisphere's subtropical westerly jet stream (bold arrows); and the locations of coral records from the Seychelles (triangle) in the western equatorial Indian Ocean [*Charles et al.*, 1997], Dahlak (star) in the southern Red Sea [*Klein et al.*, 1997], and Ras Umm Sidd (cross) in the northern Red Sea [*Felis et al.*, this study].

5.3. Material

A coral core (RUS-95) was collected at Ras Umm Sidd (27°50.9'N, 34°18.6'E) near the southern tip of the Sinai Peninsula (Egypt) in the northernmost Red Sea (Ras Mohammed National Park). The subtropical location at the northern rim of the African-Asian desert belt is in a distance of less than 500 km to the climate regime of the Mediterranean Sea in the north. The stable oxygen isotope ($\delta^{18}O$) composition of the coral (*Porites* sp.) provides a bimonthly-resolution time series for the period 1750-1995. The seasonal and the mean annual coral $\delta^{18}O$ signals were shown to provide a proxy for the large-scale SST variability in the northern Red Sea [*Felis et al.*, to be submitted 1999].

The paleoclimatic information derived from the coral record, supported by instrumental and proxy records of climate from the region, revealed that during colder periods in the Middle East the northern Red Sea region is more arid (higher evaporation) whereas the eastern Mediterranean region in the north is wetter. During warmer periods the northern Red Sea region is less arid (lower evaporation) whereas the eastern

Mediterranean region is drier. This pattern was explained by variations in the latitudinal position of the subtropical westerly jet stream, the associated subtropical high-pressure belt, and therefore the descending branch of the northern Hadley cell with its subsiding air, as well as of the moisture bringing North Atlantic westerlies which are located in the north of this system [*Felis et al.*, to be submitted 1999].

During a cold period on interannual to interdecadal/multidecadal timescales the jet stream was assumed to shift southward with the location of the associated high-pressure belt over the northern Red Sea resulting in increased arid conditions for this region whereas the accompanied southward shift of the North Atlantic westerlies results in increased rainfall in the eastern Mediterranean region. During a warm period the jet stream was assumed to shift northward resulting in less arid conditions in the northern Red Sea whereas the location of the high-pressure belt over the eastern Mediterranean and the accompanied northward shift of the westerlies results in decreased rainfall for this region. The Ras Umm Sidd coral record was therefore interpreted as a proxy of Middle East temperature variability but also as a proxy of northern Red Sea aridity and indirectly of eastern Mediterranean rainfall [*Felis et al.*, to be submitted 1999].

5.4. Results and discussion

The detrended bimonthly coral $\delta^{18}O$ time series is shown in Figure 5.2a. The result of the spectral analysis of this time series is shown in Figure 5.2b. Significant spectral peaks (minimum of 80% level) are at periods of 70, 8.6, 5.7, 3.4, 2.7, 2.2., 2.0, and 1.7 years. A not significant peak at 22.2 years is of possible interest because a similar peak occurs in the singular spectrum analysis (SSA) [*Vautard and Ghil*, 1989] of the time series. We used SSA to reconstruct the most prominent oscillatory modes in the coral $\delta^{18}O$ time series. The most prominent mode (beside the seasonal cycle) has a period of 70 years and shows a decrease in amplitude over the last ~200 years (Figure 5.3a). The amplitude of the 22.8-year mode varies but is relatively constant throughout the record (Figure 5.3b). The amplitude of the 5.7-year mode becomes stronger during the 20th century (Figure 5.3c). Conversely, the 8.7-year mode becomes weaker during these times (Figure 5.3d). Because of the occurence in both spectral analysis and SSA we interpret periods of 70, 22-23, 5.7, and 8.6-8.7 years as the most robust signals in the Ras Umm Sidd coral $\delta^{18}O$ time series. Spectral analysis of the detrended mean annual coral $\delta^{18}O$ time series (not shown) also indicates significant peaks (minimum of 80% level) at periods of 69, 8.6, and 5.7 years and a not significant peak at 22.6 years.

Cross-spectral analysis between the Ras Umm Sidd mean annual coral $\delta^{18}O$ record and the commonly used winter (December-March) index of the NAO [*Hurrel*, 1995] indicates that the two time series are coherent at periods of 22.6, 7.6, and 5.7-5.8 years (Figure 5.4a). At these periods, 65-79% of the variance is linearly correlated between these time series. The prominent periods of 22-23 and 5.7 years which are identified by both spectral analysis and SSA of the entire coral time series can therefore be attributed

to the NAO. Despite the high coherency between coral $\delta^{18}O$ and the NAO at a period of 7.6 years, which is the most prominent peak in the instrumental NAO spectrum (1864-1994), this peak can not be identified in the spectrum of the entire coral record. However, spectral analysis of a proxy NAO index based on eastern North America and northwestern Europe tree ring data (1701-1980) indicates the most prominent peak in the

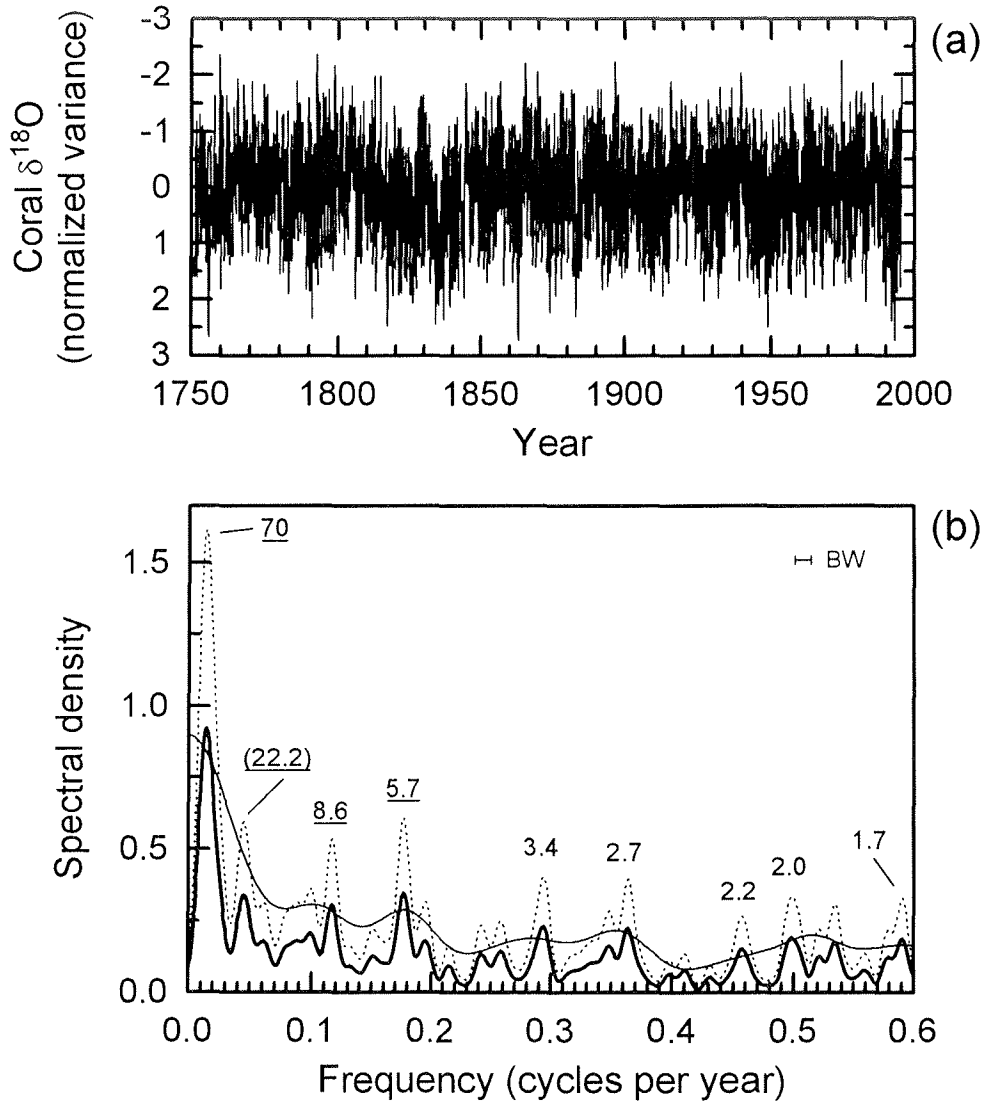

Figure 5.2. (a) Detrended bimonthly coral $\delta^{18}O$ time series from Ras Umm Sidd in the northernmost Red Sea (Egypt). Units are in ‰ relative to the Pee Dee belemnite (PDB) isotopic standard. (b) The results of Blackman-Tukey spectral analysis [*Jenkins and Watts*, 1968; *Paillard et al.*, 1996] of the time series. Spectral density equals variance divided by frequency. Those peaks of the spectrum (dotted line) are declared to be significant which rise above the low-resolution spectrum (thin solid line) by a distance greater than the one-sided confidence interval at the 80% level (thick solid line). The periods (in units of years) of statistically significant peaks are shown. Underlined periods occur as prominent oscillatory modes in the singular spectrum analysis (SSA) [*Vautard and Ghil*, 1989] of the time series. Periods in brackets are not significant but occur in the SSA. "BW" indicates bandwidth.

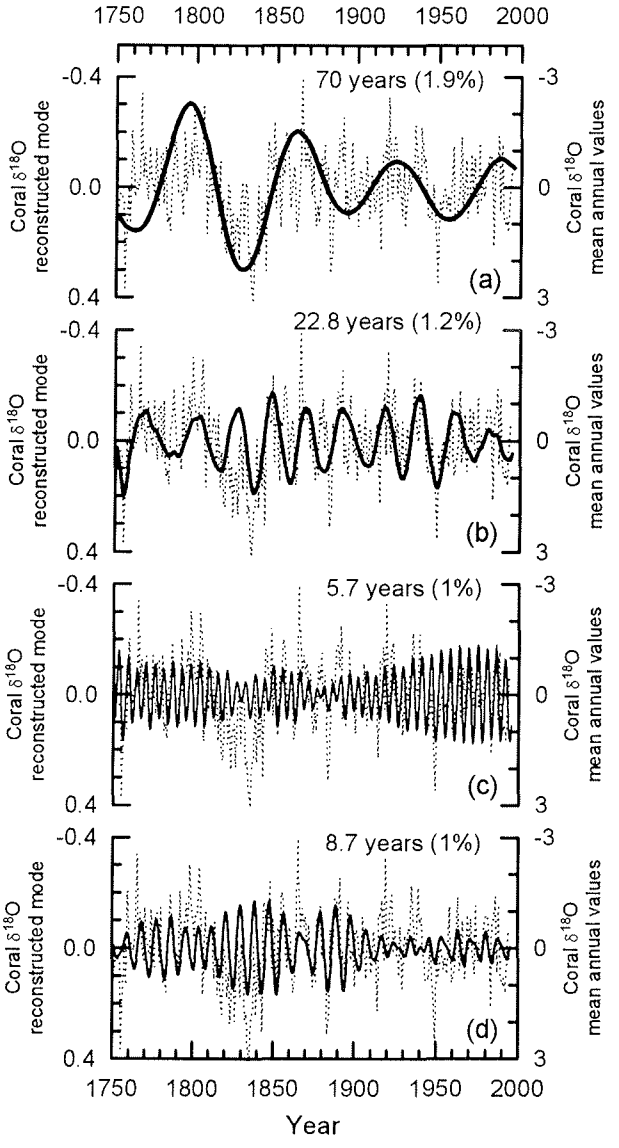

Figure 5.3. The results of singular spectrum analysis (SSA) [*Vautard and Ghil*, 1989; *Paillard et al.*, 1996] of the bimonthly coral $\delta^{18}O$ time series from Ras Umm Sidd. The most prominent oscillatory modes are shown (bold solid lines) with the period (in units of years) and percentage variance (of the detrended bimonthly time series) indicated. Each reconstruction is the sum of two modes of an oscillatory pair which are in phase quadrature; (a) modes 3 and 4, (b) modes 5 and 6, (c) modes 8 and 9, and (d) modes 10 and 11. The first 11 modes (with respect to the variance captured) were considered, except mode 7 which has no oscillatory counterpart. The remainder is interpreted here as noise. Not shown is the most prominent oscillation (mode 1 and 2) with a period of 1 year (65% of variance) which represents the seasonal cycle. For SSA a window lenght of 35 years was used; a 80-year window length was used to better resolve the 70-year mode. Also shown is the detrended mean annual coral $\delta^{18}O$ time series (thin dotted line) for direct comparison. High coral $\delta^{18}O$ values indicate low temperatures (note that the $\delta^{18}O$ scale has been reversed for direct comparison with temperatures) which are associated with increased aridity in the northern Red Sea and increased rainfall in the eastern Mediterranean region, and conversely for low coral $\delta^{18}O$ values which indicate high temperatures [*Felis et al.*, to be submitted 1999]. Units are in ‰ relative to the Pee Dee belemnite (PDB) isotopic standard.

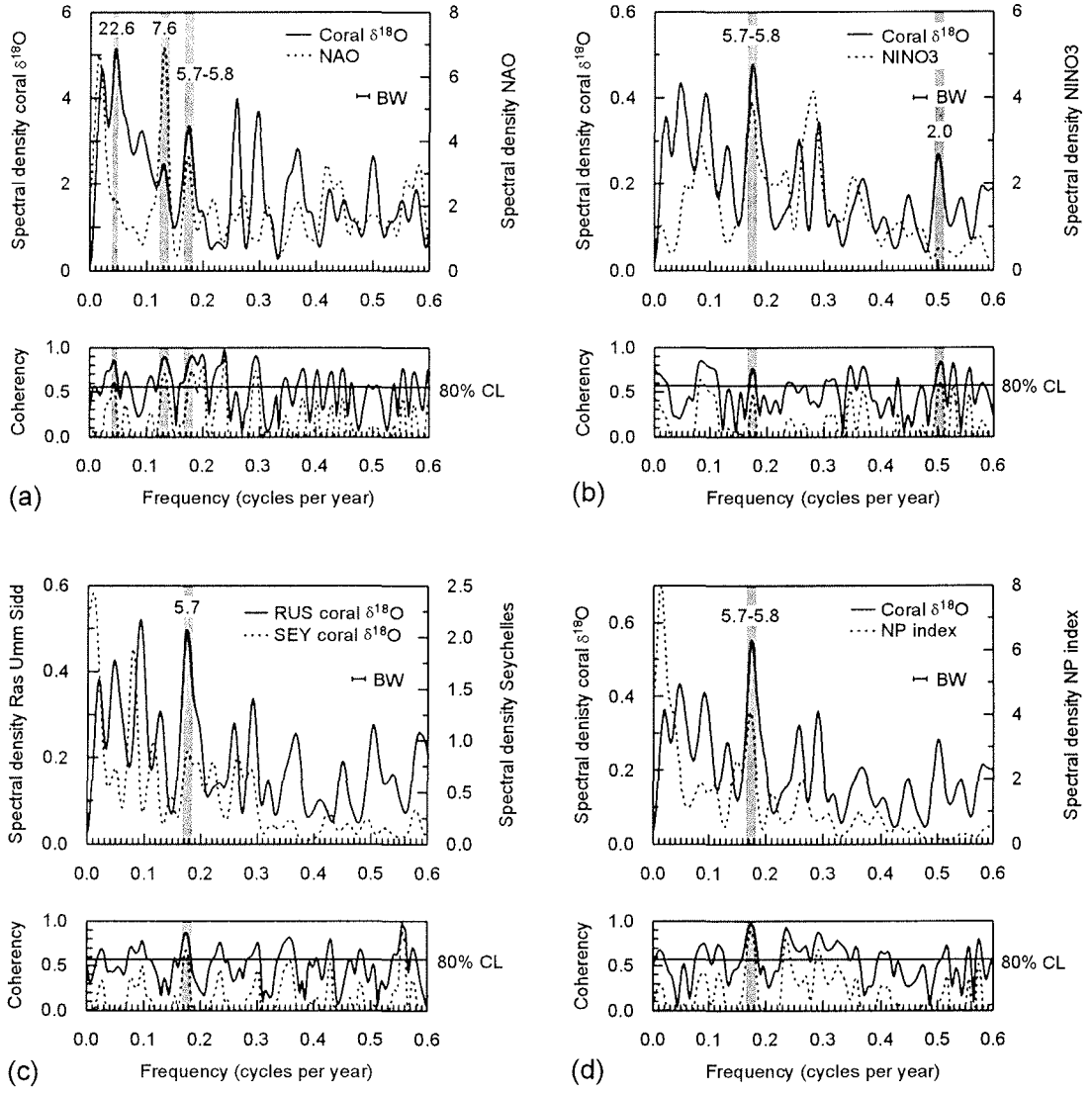

Figure 5.4. The results of Blackman-Tukey cross-spectral analysis [*Jenkins and Watts*, 1968; *Paillard et al.*, 1996] (a) between mean annual Ras Umm Sidd coral $\delta^{18}O$ and the winter (December-March) North Atlantic Oscillation (NAO) index [*Hurrel*, 1995] for the interval 1864-1994, (b) between bimonthly variations in Ras Umm Sidd coral $\delta^{18}O$ and the extended NINO3 SST anomaly index [*Kaplan et al.*, 1998; *Reynolds and Smith*, 1994], a measure of El Niño-Southern Oscillation (ENSO) strength, for the interval 1856-1995, (c) between bimonthly variations in Ras Umm Sidd coral $\delta^{18}O$ and Seychelles coral $\delta^{18}O$ [*Charles et al.*, 1997] for the interval 1846-1995, and (d) between bimonthly variations in Ras Umm Sidd coral $\delta^{18}O$ and the North Pacific (NP) SST anomaly index [*Kaplan et al.*, 1998] for the interval 1856-1991 (see Figure 1 for locations). Each upper panel shows the variance spectra of the individual time series, each lower panel shows the coherency (the correlation coefficient as a function of frequency) between these time series (bold solid line). The thin dotted line in the lower panel indicates the one-sided coherency confidence interval at the 80% level. Coherency values of >0.8 indicate that over 64% (0.8^2) of the variance at these periods is linearly correlated between these time series. The periods (in units of years) for which the two time series are coherent at the 80% level are shown. The criteria for this are that the variance peaks are aligned (in the upper panel) and that the corresponding coherency exceeds the 80% confidence level (CL, horizontal line in the lower panel). "BW" indicates bandwidth.

7-10 year frequency band at a period of 8 years [*Cook et al.*, 1998]. A further proxy NAO index based on Greenland ice core data (1648-1991) indicates maximum spectral power at periods of 5-7 and 9-11 years in the corresponding frequency band [*Appenzeller et al.*, 1998]. The ice core index also reveals that the NAO is an intermittent climate oscillation with no indication for dominant and persistent, multiannual periods evident [*Appenzeller et al.*, 1998]. We therefore suggest that the prominent period of 8.6-8.7 years which is identified by both spectral analysis and SSA of the entire Ras Umm Sidd coral time series can be also attributed to the NAO, but shifts to increased spectral power at a period of 7.6 years in the 20th century.

The most prominent oscillation in the Ras Umm Sidd coral record with a period of 70 years (Figure 5.3a) is most likely also associated with climate variability in the North Atlantic region. An oscillation with a period of 69-70 years was identified in instrumental global-mean temperature records (1850s-1992) with increased variability in the region of the North Atlantic and its bounding Northern Hemisphere continents, including northern Africa [*Schlesinger and Ramankutty*, 1994]. This oscillation was attributed to internal variability of the ocean-atmosphere system centered in the North Atlantic [*Schlesinger and Ramankutty*, 1994]. A 70-year oscillation was also identified as a prominent spectral peak in the tree-ring NAO index (1701-1980) [*Cook et al.*, 1998]. Multidecadal climate variability in the Nort Atlantic region has been widely noted elsewhere [*Mann et al.*, 1998]. Coupled ocean-atmosphere model simulations revealed 40- to 80-year oscillations associated with variations of the North Atlantic thermohaline circulation [*Delworth et al.*, 1993; *Delworth et al.*, 1997].

An important characteristic of the Ras Umm Sidd coral record is the dominance and persistance of the 70-year oscillation throughout the entire time series (1750-1995). This is in contrast to the tree-ring NAO index where the 70-year oscillation is largely restricted to the post-1850 interval [*Cook et al.*, 1998] and also to the ice core NAO index where significant variability on timescales of 80-90 years is observed from 1850 onward only [*Appenzeller et al.*, 1998]. Another important aspect is that a prominent cooling interval indicated by the mean annual Ras Umm Sidd coral record for the Middle East in the first half of the 19th century which can be also found in several Northern Hemisphere temperature reconstructions [*Mann et al.*, 1998; *Jones et al.*, 1998; *Overpeck et al.*, 1997] is related to the 70-year climate oscillation of North Atlantic origin (Figure 5.3a). This cooling interval is generally attributed to a pulse of large explosive volcanic eruptions but also to decreased solar irradiance during this time [*Mann et al.*, 1998; *Overpeck et al.*, 1997; *Lean et al.*, 1995].

The 5.7-year oscillation in the Ras Umm Sidd coral record is of considerable interest because it was identified as the most prominent period in the cospectrum of NAO and ENSO, using a winter NAO index derived from the pressure differences between Ponta Delgadas, Azores, and Akureyri, Iceland, and an index of ENSO derived from the winter pressure anomalies at Darwin, Australia, for the period 1900-1983 [*Rogers*, 1984]. The results of cross-spectral analysis between the Ras Umm Sidd coral $\delta^{18}O$ time series and the extended NINO3 index [*Kaplan et al.*, 1998; *Reynolds and Smith*, 1994] are shown in

Figure 5.4b. The extended NINO3 index is produced by optimal interpolation methods using present-day SST patterns to enhance the meager data available in the past [*Kaplan et al.*, 1998] and is updated from November 1981 by continuous direct observations [*Reynolds and Smith*, 1994]. Ras Umm Sidd coral $\delta^{18}O$ and NINO3 are coherent at periods of 5.7-5.8 and 2.0 years, where 56-70% of the variance is linearly correlated between these time series (Figure 5.4b). A coral $\delta^{18}O$ record from the Seychelles in the southwestern equatorial Indian Ocean (Figure 5.1) was shown to provide a proxy for the zonal Pacific-Indic ENSO teleconnection [*Charles et al.*, 1997]. Cross-spectral analysis between Ras Umm Sidd and Seychelles coral $\delta^{18}O$ indicates that the two time series are highly coherent at a period of 5.7 years (Figure 5.4c), where 75% of the variance is linearly correlated between these time series.

The results show that the prominent 5.7-year oscillation in the Ras Umm Sidd coral time series is linearly correlated not only to the NAO but also to the ENSO. A physical explanation for an ENSO signal in the Ras Umm Sidd coral record could be provided by the zonal Pacific-Indic teleconnection which controls the ENSO signal in the Seychelles coral record [*Charles et al.*, 1997]. Evidence that this is apparently not the case comes from a coral $\delta^{18}O$ record from the Dahlak Archipelago [*Klein et al.*, 1997] in the southern Red Sea (Figure 5.1). Cross-spectral analysis between the Ras Umm Sidd and the Dahlak record (not shown) reveals no significant coherencies in the 5- to 6-year frequency band. A lack of coherencies in this frequency band is also indicated by cross-spectral analysis between the Seychelles and the Dahlak coral record (not shown).

Our rationale are that if the zonal Pacific-Indic teleconnection would control the ENSO signals in both Seychelles (4.6°S) and Ras Umm Sidd (27.8°N) coral $\delta^{18}O$ this should also be the case for the Dahlak record (15.7°N) and all three coral records should reveal significant coherencies in the 5- to 6-year frequency band between each other, which is only the case for the Ras Umm Sidd and the Seychelles record. We therefore suggest that the correlation of the prominent 5.7-year oscillation in the Ras Umm Sidd coral time series with the ENSO results from an extratropical ENSO teleconnection via the North Pacific associated with variations in the latitudinal position of the subtropical westerly jet stream [*Philander*, 1990; *Hurrel*, 1996; *Price et al.*, 1998].

The concentration of significant but not persistant coherence between the NINO3 index [*Kaplan et al.*, 1998] and the NAO index [*Hurrel*, 1995] in the 5- to 6-year period band was recently reported for the interval of 1865-1995 applying multiresolution cross-spectral analysis [*Huang et al.*, 1998]. This relationship between ENSO and NAO was explained to be a result of changes in the atmospheric circulation over the Northern Hemisphere associated with variations in the Pacific-North American (PNA) teleconnection pattern [*Huang et al.*, 1998]. It was suggested that the ENSO modulates the NAO through the PNA pattern resulting in changes in the jet stream and strom track locations over the North Atlantic [*Huang et al.*, 1998]. However, there is also evidence that the winter NAO leads the changes in atmospheric conditions over the North Pacific

and western North America associated with the PNA pattern by three years during the period 1958-1997 [*Lin and Derome*, 1998].

The dominant role of the North Pacific (Figure 5.1) concerning the 5.7-year oscillation in the Ras Umm Sidd coral time series can be clearly seen in the results of cross-spectral analysis between the coral record and the North Pacific (NP) SST anomaly index [*Kaplan et al.*, 1998]. The two time series a coherent at a period of 5.7-5.8 years, where 92% of the variance is linearly correlated (Figure 5.4d). In summary, these results support our assumption that the prominent 5.7-year oscillation in the Ras Umm Sidd coral time series beside the NAO-related origin represents ENSO-NAO interactions via extratropical ENSO-North Pacific teleconnections.

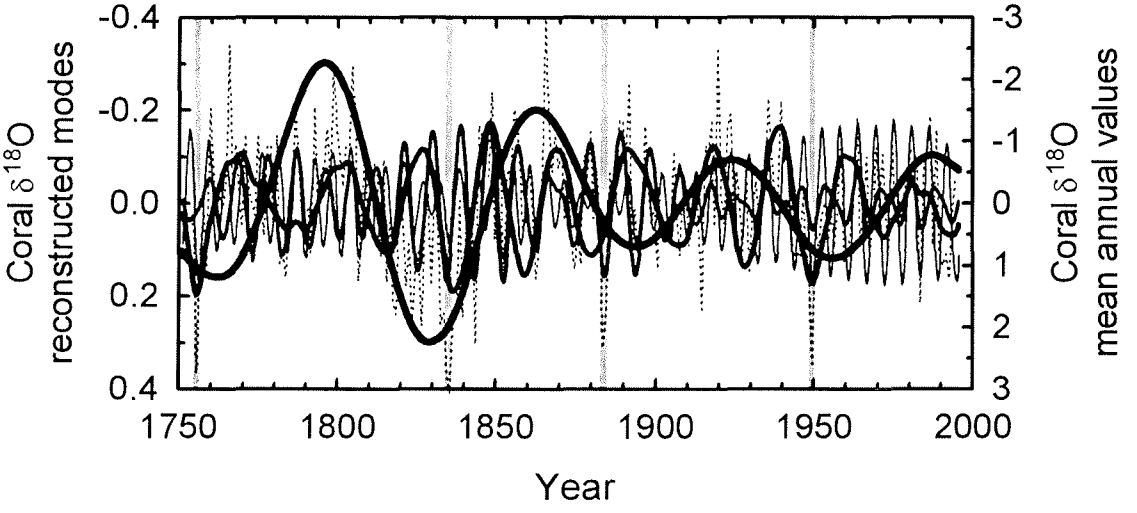

Figure 5.5. The four prominent oscillatory modes of the Ras Umm Sidd coral time series as reconstructed by singular spectrum analysis (SSA) are shown to reveal their interaction in the control of mean annual Middle East climate variability (see also Figure 5.3). Shading indicates extraordinarily cold years (1755, 1834-1835, 1883-1884, and 1949). Units are in ‰ relative to the Pee Dee belemnite (PDB) isotopic standard.

The frequency domain analysis of the Ras Umm Sidd coral $\delta^{18}O$ time series from the northernmost Red Sea reveals that both the NAO and the ENSO contributed significantly to the climate variability of the Middle East during the past ~250 years. The interaction between these two modes of the global climate system has an important control on Middle East temperature and aridity/rainfall variability on internannual to multidecadal timescales. This is emphasized by the interaction between the four prominent oscillations related to these modes in creating the extraordinarily cold years of 1755, 1834-1835, 1883-1884, and 1949 in the northern Red Sea and probably the entire Middle East, with the dominant role of the 70-year oscillation clearly evident (Figure 5.5). These years were most likely associated with increased aridity (high evaporation) and deep water formation in the northern Red Sea and increased rainfall in the eastern Mediterranean region [*Felis*

et al., to be submitted 1999]. However, the cold anomalies in 1755, 1835, and 1883-1884 where probably amplified by regional cooling resulting from the stratospheric aerosol input of co-occuring large explosive volcanic eruptions [*Felis et al.*, to be submitted 1999].

Frequency domain analysis of long $\delta^{18}O$ time series derived from fossil corals of the region will hopefully provide informations on the climate variability in the Middle East during the Mid-Holocene (6000-5000 years ago) and therefore on a possible influence of the Asian monsoon summer rainfall regime on these latitudes during these times.

5.5. Acknowledgments

We thank M. Fine (TAU) for drilling the core; M. Segl and her team (GeoB) for stable isotope analysis; A. H. Nawar (NIOF) for logistic support; the Government of Egypt and the Egyptian Environmental Affairs Agency (EEAA) for support and permission to sample in the Ras Mohammed National Park; C. Gervais for giving a length scale to the sampling profile; C. Price and M. N. Evans for discussions; and D. Paillard for providing the AnalySeries 1.1 software. This work is part of the Red Sea Program on Marine Sciences (RSP), funded by the BMBF (German Federal Ministry for Education, Science, Research, and Technology) through grant 03F0151A.

6. General conclusions

Coral stable isotope records in bimonthly resolution from two locations in the desert-enclosed northern Red Sea were used to reconstruct the climate and ocean variability of this subtropical region for the past nearly 250 years on the seasonal to multidecadal timescale. The study provides the first paleoclimatic record of this kind concerning resolution and length in the whole Middle East region. The study area is located near latitudes 28°-29°N at the northern rim of the African-Asian desert-belt with the winter-wet Mediterranean climate regime being in a distance of less than 300-500 km to the north.

- A 19-year (1974-1993) coral stable carbon isotope record ($\delta^{13}C$) from Eilat (Israel) at the northern end of the Gulf of Aqaba (the northeastern extension of the Red Sea proper) documents interannual events of extraordinarily large plankton blooms, indicated by anomalous ^{13}C depletions in the coral skeleton. These blooms are caused by deep vertical water mass mixing, convectively driven in colder winters, which results in increased supplies of nutrients to the surface waters.
- The deep vertical mixings can sometimes be driven by the cooling occuring throughout the Middle East after large tropical volcanic eruptions. There is evidence in the coral $\delta^{13}C$ record for an indirect volcanic signal of the eruptions of El Chichón (Mexico, 1982) and Mount Pinatubo (Philippines, 1991).
- Deep mixing induced $\delta^{13}C$ variations of the dissolved inorganic carbon in the surface waters can be neglected at this location. It is therefore suggested that the ^{13}C skeletal depletions can be best explained by changes in the coral's autotrophy-heterotrophy diet, through increased heterotrophic feeding on zooplankton during the

blooms. Increased feeding on ^{13}C-depleted zooplankton or increased heterotrophy at the expense of autotrophy can both result in a ^{13}C-depleted coral skeleton.

- The results of the Eilat coral record provide new insight into the controls of the $\delta^{13}C$ signal in the skeletons of massive corals and therefore address a long standing problem in coral-based paleoclimatic reconstructions. If the conclusions are substantiated, seasonal $\delta^{13}C$ records of corals which change from autotrophy under normal conditions to increased heterotrophy during bloom events may be used as indicators of ocean paleoproductivity at interannual resolution, available from no other source.
- A 245-year (1750-1995) coral oxygen isotope record ($\delta^{18}O$) from Ras Umm Sidd (Ras Mohammed National Park, Egypt) near the southern tip of the Sinai Peninsula in the northern Red Sea reveals new aspects on large-scale Middle East climate variability. The coral record, supported by instrumental and proxy records of climate, suggests that during colder periods on the interannual to interdecadal/multidecadal timescale the northern Red Sea region is more arid (higher evaporation) whereas the eastern Mediterranean region in the north is wetter. During warmer periods the northern Red Sea region is less arid (lower evaporation) whereas the eastern Mediterranean region is drier.
- This pattern is explained by variations in the latitudinal position of the subtropical westerly jet stream, the associated subtropical high-pressure belt, and therefore the descending branch of the northern Hadley cell with its subsiding air, as well as of the moisture bringing North Atlantic westerlies which are located in the north of this system. It is assumed that during a cold period the jet stream shifts southward with the location of the associated high-pressure belt over the northern Red Sea resulting in increased arid conditions in this region whereas the accompanied southward shift of the North Atlantic westerlies results in increased rainfall in the eastern Mediterranean region. During a warm period the jet stream is assumed to shift northward resulting in less arid conditions in the northern Red Sea whereas the location of the high-pressure belt over the eastern Mediterranean and the accompanied northward shift of the westerlies results in decreased rainfall in this region.
- Considering results of other paleostudies it could be possible that comparable processes may have also worked on the millennial timescale during the Holocene and on the timescales of Heinrich events and Dansgaard-Oeschger events during the last glacial period.
- The coral $\delta^{18}O$-based sea surface temperatures (SSTs) suggest that mean annual SSTs between 1751 and 1900 were ~0.3°C lower than the 20th century average.
- The northern Red Sea is probably the only site in the world oceans where water mass formation occurs and reef corals grow. The winter $\delta^{18}O$ values of the coral record can be used to detect episodic events of deep water formation of the Red Sea thermohaline circulation during anomalously arid and cold winters, which are sometimes associated with El Niño events and large volcanic eruptions.

- Spectral analysis of the coral time series reveals that both the North Atlantic Oscillation and the El Niño-Southern Oscillation phenomenon of tropical Pacific origin contributed significantly to the climate variability of the Middle East during the past 245 years on interannual to multidecadal timescales.
- The results suggest that interaction between extratropical and tropical modes of the global climate system has an important control on subtropical climate variability via atmospheric teleconnections, and that a prominent cooling interval in the first half of the 19th century evident in several Northern Hemisphere temperature reconstructions can be related to a 70-year climate oscillation of most probably North Atlantic origin, at least for the Middle East region.

7. Directions for future research

7.1. Centuries-long coral records of paleoclimate

The longest published coral stable isotope time series in seasonal resolution from New Caledonia in the southwest Pacific provides 335 years of record [*Quinn et al.*, 1998]. The longest coral time series in monthly resolution is from the Seychelles in the western equatorial Indian Ocean and provides 150 years of record [*Charles et al.*, 1997]. The at least seasonal-resolution coral time series published in the 1990s commonly provide 100-300 years of paleoclimatic record. It is also possible to generate coral stable isotope time series in near-weekly resolution, but this has only be done for short intervals of 6 to 12 years [*Gagan et al.*, 1994; *Gagan and Chivas*, 1995]. A recently published coral time series from the central equatorial Pacific provides a better-than-monthly resolution record for a 55-year interval [*Evans et al.*, 1998a]. The resolution of a coral time series is always a compromise between the given length of a record and the amount of stable isotope measurements possible for this study. For centuries-long coral-based reconstructions of large-scale ocean-atmosphere processes a bimonthly sampling resolution might be an optimal compromise as shown in this thesis or in a 200-year coral record from the southeastern Indian Ocean [*Kuhnert et al.*, 1999]. A bimonthly resolution also enables the refinement of the initial age model of a coral chronology which is usually based on density-band counting. The strong seasonal cycle in coral stable isotopes can be used to count annual layers in a coral rather than relying completely on a sporadically weak density banding [e.g., *Charles et al.*, 1997]. To the best of my experience at least 6 samples per year on average are necessary for effectively using the seasonal cycle in coral stable isotopes for the refinement of the age model of a coral chronology.

The published coral stable isotope records culminate between lengths of 100 and 300 years because most living massive coral colonies are not older than this. One goal for future coral-based paleoclimatc studies should be to search for older but still living colonies (which is already in progress) to provide well-dated seasonal resolution records for the past more than 500 years. A recent study from the Great Barrier Reef described a *Porites* record covering a period of 507 years where the annual variations in calcification could be related to SST variability [*Lough and Barnes*, 1997]. However, a stable isotope time series of such a record could provide seasonal or higher resolution paleoclimatic information which would also give better estimates of the mean annual values, for centuries. The challenge is to find these huge, old and still living coral colonies which is not easy because they are not widespread.

In the northern Red Sea a 2-week land-based survey at a total of 21 locations along the 180-km-long Sinai coast of the Gulf of Aqaba detected *Porites* colonies of 2- to 3-m-height (vertical diameter) at only 3 sites [*Felis and Pätzold*, 1996]. Considering the average growth rate for *Porites* corals of about 1 cm per year such colonies are probably growing since 200 to 300 years, which is comparable to the Ras Umm Sidd coral record described in this thesis. Larger and hopefully older, still living coral colonies can be possibly found along the fringing reefs of the Jordanian and Saudi Arabian coast of the Red Sea.

7.2. Methods

The dependence of coral $\delta^{18}O$ on both SST and the $\delta^{18}O$ of the seawater with the latter linked to variations in salinity raised up the need for an additional proxy either for salinity or for temperature. Measurement of the Sr/Ca ratio in corals by applying isotope dilution on a thermal ionization mass spectrometer (TIMS) [*Beck et al.*, 1992] was shown to provide a promising proxy for SST variability [*McCulloch et al.*, 1994; *Shen et al.*, 1996; *Alibert and McCulloch*, 1997; *Gagan et al.*, 1998], despite the reliability has also been called into question [*de Villiers et al.*, 1995] and still differences in the temperature calibrations between different studies exist [*Beck*, 1998]. However, this technique is expensive, laboratory-intensive, and time-consuming and therefore not adequate for the rapid generation of centuries-long coral Sr/Ca records in seasonal resolution. It is important to recall that the 245-year Ras Umm Sidd coral record in bimonthly resolution described in this thesis is based on more than 1500 stable isotope measurements. The longest published seasonal resolution coral Sr/Ca records only cover periods of 20 to 28 years [*Alibert and McCulloch*, 1997].

The combined use of coral Sr/Ca and $\delta^{18}O$ was shown to provide a powerful tool for reconstructing past SST and sea surface $\delta^{18}O$ changes simultaneously during short time intervals [*McCulloch et al.*, 1994; *Shen et al.*, 1996; *Gagan et al.*, 1998]. The use of both proxies in parallel can provide important information about past variations in SST and rainfall/evaporation and therefore on atmospheric moisture transport [*Gagan et al.*,

1998]. However, to reconstruct climate variability in seasonal resolution over several centuries there is the need for developing a faster technique for the measurement of Sr/Ca ratios in coral skeletons.

Much work is in progress for the more rapid determination of coral Sr/Ca ratios at high precision to allow the application of this technique to centuries-long time series. Recently, *Schrag* [1997] briefly presented such a procedure using a cheap (relative to TIMS) inductively coupled plasma-atomic emission spectrometer (ICP-AES multi collector). This procedure provided a much higher precision than the more common analysis on an ICP-MS quadrupole. Applying this procedure a centuries-long coral Sr/Ca record in seasonal resolution was generated (D. P. Schrag, personal communication, 1998) which, in combination with the coral $\delta^{18}O$ record, will provide a powerful tool for the reconstruction of past ocean-atmosphere variability. The generation of such long time series using coupled $\delta^{18}O$ and Sr/Ca measurements will become the goal of coral-based paleoclimatic research during the next years.

The promising application of Mg/Ca ratios measured by the simple, fast, and cheap technique of inductively coupled plasma-atomic emission spectrometry (ICP-AES) as a new proxy for coral-based SSTs [*Mitsuguchi et al.*, 1996] is possibly not so precise as reported earlier (T. Correge, personal communication, 1998). A new, fast and accurate analytical technique was recently introduced to measure Sr/Ca, Mg/Ca, U/Ca, and Ba/Ca on the same coral sample using an ICP-MS quadrupole [*Correge et al.*, 1997]. There is also much progress in the analysis of elemental ratios in corals in the solid state by microbeam methods such as ion microprobe [*Allison*, 1996; *Hart and Cohen*, 1996] or laser ablation ICP-MS (LA-ICP-MS) [*Sinclair et al.*, 1998]. However, there are still problems with the analytical precisions concerning the effective application in paleotemperature studies.

Coral cores for paleoclimatic studies of the past several hundred years are commonly collected from living colonies because the age model of the chronology can then be easily developed by counting the density bands or the seasonal cycles in geochemical parameters starting at the living top of the core. However, progress in TIMS U-Th dating may provide the opportunity to obtain well-dated coral records from already dead modern colonies. The precision of a recently reported TIMS U-Th date of 254±2 years from a Norwegian speleothem [*Lauritzen and Lundberg*, 1998] is encouraging. This age error is in the same range as these which are typically assigned to the bottom of 200- to 300-year-long coral cores collected from living colonies. Large, dead modern coral colonies probably provide an unique opportunity to extend seasonal resolution paleoclimatic records back over the entire millennium, by using well-dated cores from colonies which provide windows for different time periods of the record. This is a common procedure in dendroclimatology.

7.3. New sites for coral-based reconstructions of paleoclimate

Optimal sites for coral-based reconstructions of SST with respect to the global SST field were recently discussed in the work of *Evans et al.* [1998b]. As a further site for coral-based paleoclimatic studies in the Middle East Kuwait (~29°N) at the northwestern end of the Persian Gulf could be of considerable interest. This location is probably well-suited for verifying the paleoclimatic interpretation of the Ras Umm Sidd coral record described in this thesis and to extend its implication over the entire Middle East. A problem at this location could be the runoff resulting from the Euphrates-Tigris river system. However, this defect could be possibly exploited using a multiproxy approach to derive information about past rainfall variability in the source region of this river system which is located as far north as Asia Minor.

In a more global view a region of interest for coral-based paleoclimatic reconstructions is the tropical and subtropical Atlantic Ocean. The tropical Atlantic dipole, a decadal oscillation associated with relative changes in SST between the hemispheres, has a strong influence on the modulation of floods and droughts in northeast South America (Nordeste region of Brazil) and the Sahel region of Africa [*Chang et al.*, 1997]. Coral-based reconstructions of climate variability in the tropical Atlantic region over the past centuries would provide a better understanding of this oscillatory mode. Coral paleoclimatic work in this region already started recently [*Swart et al.*, 1998].

7.4. Paleoclimatic reconstructions from modern and fossil corals

The work of *Gagan et al.* [1998] successfully demonstrated the application of combined $\delta^{18}O$ and Sr/Ca measurements on modern and fossil corals to derive information about changes in temperature and surface-ocean water balance relative to the Mid-Holocene (~5000-6000 years B.P.) in the tropical western Pacific. Coral Sr/Ca records of different periods of time during the early Holocene were used to detect abrupt SST changes in this region [*Beck et al.*, 1997]. In the northern Red Sea region paleoclimatic work on Mid-Holocene corals is in progress [*Moustafa et al.*, submitted 1999]. The combined approach of using seasonal resolution paleoclimatic records derived from modern and fossil corals will provide information on possible changes in Middle East climate variability relative to the Mid-Holocene. The combination of the coral-derived paleoclimatic information with high-resolution marine sediment records from the Red Sea could be a focus for future studies. Work on such sediment records is already in progress in the eastern Mediterranean Sea [*Schilman et al.*, 1998]. A further region for such a combined study could be the tropical Atlantic Ocean, where also high-resolution marine sediment records exist [*Arz et al.*, 1998].

8. References

Ahmad, F., and S. A. R. Sultan, Surface heat fluxes and their comparison with the oceanic heat flow in the Red Sea, *Oceanol. Acta*, *12*, 33-36, 1989.

Alibert, C., and M. T. McCulloch, Strontium/calcium ratios in modern *Porites* corals from the Great Barrier Reef as a proxy for sea surface temperature: Calibration of the thermometer and monitoring of ENSO, *Paleoceanography*, *12*, 345-363, 1997.

Allison, N., Comparative determinations of trace and minor elements in coral aragonite by ion microprobe analysis, with preliminary results from Phuket, southern Thailand, *Geochim. Cosmochim. Acta*, *60*, 3457-3470, 1996.

Andrié, C., and L. Merlivat, Contribution des données isotopiques de deutérium, oxygène-18, hélium-3 et tritium, à l'étude de la circulation de la Mer Rouge, *Oceanol. Acta*, *12*, 165-174, 1989.

Appenzeller, C., T. F. Stocker, and M. Anklin, North Atlantic Oscillation dynamics recorded in Greenland ice cores, *Science*, *282*, 446-449, 1998.

Arz, H. W., J. Pätzold, and G. Wefer, Climatic changes during the last deglaciation recorded in sediment cores from the Northeast Brazilian continental margin, *Geo-Mar. Lett.*, in review, 1998.

Bacastow, R. B., C. D. Keeling, T. J. Lueker, M. Wahlen, and W. G. Mook, The ^{13}C Suess effect in the world surface oceans and its implication for oceanic uptake of CO_2: Analysis of observations at Bermuda, *Global Biogeochem. Cycles*, *10*, 335-346, 1996.

Baker, C. B., J. K. Eischeid, T. R. Karl, and H. F. Diaz, The quality control of long-term climatological data using objective data analysis, in *Preprints of AMS Ninth Conference on Applied Climatology, Dallas, TX, January 15-20, 1995*, 1994.

Barnes, D. J., and J. M. Lough, On the nature and causes of density banding in massive coral skeletons, *J. Exp. Mar. Biol. Ecol.*, *167*, 91-108, 1993.

Barnes, D. J., R. B. Taylor, and J. M. Lough, On the inclusion of trace materials into massive coral skeletons. Part II: Distortions in skeletal records of annual climate cycles due to growth processes, *J. Exp. Mar. Biol. Ecol.*, *194*, 251-275, 1995.

Barnston, A. G., and R. E. Livezey, Classification, seasonality and persistence of low-frequency atmospheric circulation patterns, *Mon. Weather Rev.*, *115*, 1083-1126, 1987.

Barry, R. G., and R. J. Chorley, *Atmosphere, weather, and climate*, 7th ed., 409 pp., Routledge, London, 1998.

Beck, W., Warmer and wetter 6000 years ago?, *Science*, *279*, 1003-1004, 1998.

Beck, J. W., R. L. Edwards, E. Ito, F. W. Taylor, J. Récy, F. Rougerie, P. Joannot, and C Henin, Sea-surface temperature from coral skeletal strontium/calcium ratios, *Science*, *257*, 644-647, 1992.

Beck, J. W., J. Récy, F. Taylor, R. L. Edwards, and G. Cabioch, Abrupt changes in early Holocene tropical sea surface temperature derived from coral records, *Nature*, *385*, 705-707, 1997.

Begin, Z. B., W. Broecker, B. Buchbinder, Y. Druckman, A. Kaufman, M. Magaritz, and D. Neev, Dead Sea and Lake Lisan levels in the last 30,000 years, *Rep. Geol. Surv. Israel*, *29*, 1-17, 1985.

Blackman, R. B., and J. W. Tukey, *The measurement of power spectra from the point of view of communication engineering*, 190 pp., Dover Publications, New York, 1958.

Bottomley, M., C. K. Folland, J. Hsiung, R. E. Newell, and D. E. Parker, *Global Ocean Surface Temperature Atlas (GOSTA)*, 20 + iv pp. and 313 plates, Joint Meteorol. Off./Mass. Inst. of Technol. Proj., supported by U.S. Off. of Nav. Res., funded by UK Depts. of Energy and Environment, Her Majesty's Stationary Office, London, 1990.

Briffa, K. R., P. D. Jones, F. H. Schweingruber, and T. J. Osborn, Influence of volcanic eruptions on Northern Hemisphere summer temperature over the past 600 years, *Nature*, *393*, 450-455, 1998.

Buckle, C., *Weather and climate in Africa*, 1st ed., 312 pp., Longman, Essex, 1996.

Buddemeier, R. W., and R. A. Kinzie, Coral growth, *Oceanogr. Mar. Biol. Ann. Rev.*, *14*, 183-225, 1976.

Cane, M. A., A role for the tropical Pacific, *Science*, *282*, 59-61, 1998.

Carriquiry, J. D., M. J. Risk, and H. P. Schwarcz, Stable isotope geochemistry of corals from Costa Rica as a proxy indicator of the El Niño/Southern Oscillation (ENSO), *Geochim. Cosmochim. Acta*, *58*, 335-351, 1994.

Cember, R. P., On the sources, formation, and circulation of Red Sea deep water, *J. Geophys. Res.*, *93*, 8175-8191, 1988.

Chang, P., L. Ji, and H. Li, A decadal climate variation in the tropical Atlantic Ocean from thermodynamic air-sea interactions, *Nature*, *385*, 516-518, 1997.

Charles, C. D., D. E. Hunter, and R. G. Fairbanks, Interaction between the ENSO and the Asian monsoon in a coral record of tropical climate, *Science*, *277*, 925-928, 1997.

Clifford, M., C. Horton, and J. Schmitz, An oceanographic nowcast/forecast system for the Red Sea, *J. Geophys. Res.*, *102*, 25101-25122, 1997.

Cohen, A. L., and S. R. Hart, The effect of colony topography on climate signals in coral skeleton, *Geochim. Cosmochim. Acta*, *61*, 3905-3912, 1997.

Cole, J. E., R. G. Fairbanks, and G. T. Shen, Recent variability in the Southern Oscillation: Isotopic results from a Tarawa Atoll coral, *Science*, *260*, 1790-1793, 1993.

Cook, E. R., R. D. D'Arrigo, and K. R. Briffa, A reconstruction of the North Atlantic Oscillation using tree-ring chronologies from North America and Europe, *Holocene*, *8*, 9-17, 1998.

Correge, T., G. Cabioch, T. M. Quinn, J. Recy, and F. W. Taylor, Late Quaternary tropical sea surface temperature reconstruction from multi-tracer analyses of massive corals from the western Pacific (abstract), *Eos Trans. AGU*, *78*(46), F49, 1997.

Craig, H., Isotopic composition and origin of the Red Sea and Salton Sea geothermal brines, *Science*, *154*, 1544-1548, 1966.

Crowley, T. J., and K.-Y. Kim, Comparison of proxy records of climate change and solar forcing, *Geophys. Res. Lett.*, *23*, 359-362, 1996.

Crowley, T. J., T. M. Quinn, F. W. Taylor, C. Henin, and P. Joannot, Evidence for a volcanic cooling signal in a 335-year coral record from New Caledonia, *Paleoceanography*, *12*, 633-639, 1997.

da Silva, A., A. C. Young, and S. Levitus, Atlas of Surface Marine Data 1994, Volume 1: Algorithms and Procedures, *NOAA Atlas NESDIS 6*, U.S. Department of Commerce, Washington, D.C., 1994.

Delworth, T., S. Manabe, and R. J. Stouffer, Interdecadal variability of the thermohaline circulation in a coupled ocean-atmosphere model, *J. Clim.*, *6*, 1993-2011, 1993.

Delworth, T. L., S. Manabe, and R. J. Stouffer, Multidecadal climate variability in the Greenland Sea and surrounding regions: A coupled model simulation, *Geophys. Res. Lett.*, *24*, 257-260, 1997.

Dettinger, M. D., M. Ghil, C. M. Strong, W. Weibel, and P. Yiou, Software expedites singular-spectrum analysis of noisy time series, *Eos Trans. AGU*, *76*(2), 12, 14, 21, 1995.

de Villiers, S., B. K. Nelson, and A. R. Chivas, Biological controls on coral Sr/Ca and $\delta^{18}O$ reconstructions of sea surface temperatures, *Science*, *269*, 1247-1249, 1995.

Diaz, H. F., and G. N. Kiladis, Atmospheric teleconnections associated with the extreme phases of the Southern Oscillation, in *El Niño: Historical and paleoclimatic aspects of the Southern Oscillation*, edited by H. F. Diaz and V. Markgraf, pp. 7-28, Cambridge Univ. Press, Cambridge, 1992.

Druffel, E. R. M., and S. Griffin, Large variations of surface ocean radiocarbon: Evidence of circulation changes in the southwestern Pacific, *J. Geophys. Res.*, *98*, 20249-20259, 1993.

Dunbar, R. B., and J. E. Cole, *Coral records of ocean-atmosphere variability*, NOAA Climate and Global Change Program, *Special Report No. 10*, 38 pp., Boulder, CO, 1993.

Dunbar, R. B., G. M. Wellington, M. W. Colgan, and P. W. Glynn, Eastern Pacific sea surface temperature since 1600 A.D.: The $\delta^{18}O$ record of climate variability in Galápagos corals, *Paleoceanography*, *9*, 291-315, 1994.

Echelman, T., and L. Fishelson, Surface zooplankton dynamics and community structure in the Gulf of Aqaba (Eilat), Red Sea, *Mar. Biol.*, *107*, 179-190, 1990.

Epstein, S., R. Buchsbaum, H. A. Lowenstam, and H. C. Urey, Revised carbonate-water isotopic temperature scale, *Geol. Soc. Am. Bull.*, *64*, 1315-1326, 1953.

Eshel, G., Coupling of deep water formation and the general circulation: A case study of the Red Sea, Ph.D. thesis, Columbia Univ., New York, 127 pp., 1996.

Eshel, G., and N. H. Naik, Climatological coastal jet collision, intermediate water formation, and the general circulation of the Red Sea, *J. Phys. Oceanogr.*, *27*, 1233-1257, 1997.

Eshel, G., M. A. Cane, and M. B. Blumenthal, Modes of subsurface, intermediate, and deep water renewal in the Red Sea, *J. Geophys. Res.*, *99*, 15941-15952, 1994.

Eshel, G., D. P. Schrag, and B. F. Farrel, Troposphere-planetary boundary layer interactions and the evolution of ocean surface density: Lessons from Red Sea corals, submitted to *J. Clim.*, 1998.

Evans, M. N., R. G. Fairbanks, and J. L. Rubenstone, A proxy index of ENSO teleconnections, *Nature*, *394*, 732-733, 1998a.

Evans, M. N., A. Kaplan, and M. A. Cane, Optimal sites for coral-based reconstruction of global sea surface temperature, *Paleoceanography*, 13, 502-516, 1998b.

Evans, M. N., A. Kaplan, and M. A. Cane, Cross-validation of a sparse network of coral data and sea surface temperatures: Potential for coral-based SST field reconstructions, submitted to *Paleoceanography*, 1998.

Fairbanks, R. G., and R. E. Dodge, Annual periodicity of the $^{18}O/^{16}O$ and $^{13}C/^{12}C$ ratios in the coral *Montastrea annularis*, *Geochim. Cosmochim. Acta*, *43*, 1009-1020, 1979.

Felis, T., and J. Pätzold, Survey for large *Porites* colonies along the Sinai coast of the Gulf of Aqaba, unpublished report, 55 pp., Fachbereich Geowissenschaften (Meeresgeologie), Universität Bremen, Bremen, Germany, 1996.

Felis, T., J. Pätzold, G. Wefer, M. Fine, Y. Loya, and A. H. Nawar, First results of a coral-based history of recent climate in the northern Red Sea, *Zbl. Geol. Paläont. Teil I, 1997/1-2*, 197-207, 1998a.

Felis, T., J. Pätzold, Y. Loya, and G. Wefer, Vertical water mass mixing and plankton blooms recorded in skeletal stable carbon isotopes of a Red Sea coral, *J. Geophys. Res.*, *103*, 30731-30739, 1998b.

Felis, T., J. Pätzold, Y. Loya, M. Fine, A. H. Nawar, and G. Wefer, A coral oxygen isotope record of temperature, aridity, and deep water formation from the northern Red Sea since the year 1750, to be submitted 1999.

Gagan, M. K., and A. R. Chivas, Oxygen isotopes in western Australian coral reveal Pinatubo aerosol-induced cooling in the Western Pacific Warm Pool, *Geophys. Res. Lett.*, *22*, 1069-1072, 1995.

Gagan, M. K., A. R. Chivas, and P. J. Isdale, High-resolution isotopic records from corals using ocean temperature and mass-spawning chronometers, *Earth Planet. Sci. Lett.*, *121*, 549-558, 1994.

Gagan, M. K., A. R. Chivas, and P. J. Isdale, Timing coral-based climatic histories using ^{13}C enrichments driven by synchronized spawning, *Geology*, *24*, 1009-1012, 1996.

Gagan, M. K., L. K. Ayliffe, D. Hopley, J. A. Cali, G. E. Mortimer, J. Chappell, M. T. McCulloch, and M. J. Head, Temperature and surface-ocean water balance of the Mid-Holocene tropical western Pacific, *Science*, *279*, 1014-1018, 1998.

Ganssen, G., and D. Kroon, Evidence for Red Sea surface circulation from oxygen isotopes of modern surface waters and planctonic foraminiferal tests, *Paleoceanography*, *6*, 73-82, 1991.

Geiselhart, S., C. Hemleben, D. Meischner, and M. Segl, Late Quaternary paleoceanographic and paleoclimatologic history of the Red Sea during the past 380,000 years, in *Abstracts 6th International Conference on Paleoceanography, Lisbon*, p. 113, Instituto Geológico e Mineiro, Lisbon, Portugal, 1998.

Genin, A., B. Lazar, and S. Brenner, Vertical mixing and coral death in the Red Sea following the eruption of Mount Pinatubo, *Nature*, *377*, 507-510, 1995.

Ghil, M., and R. Vautard, Interdecadal oscillations and the warming trend in global temperature time series, *Nature*, *350*, 324-327, 1991.

Goodfriend, G. A., and M. Magaritz, Palaeosols and late Pleistocene rainfall fluctuations in the Negev Desert, *Nature* , *332*, 144-146, 1988.

Graf, H.-F., I. Kirchner, A. Robock, and I. Schult, Pinatubo eruption winter climate effects: Model versus observations, *Clim. Dyn.*, *9*, 81-93, 1993.

Grossman, E. L., and T.-L. Ku, Oxygen and carbon isotope fractionation in biogenic aragonite: temperature effects, *Chem. Geol.*, *59*, 59-74, 1986.

Gvirtzman, G., Fluctuations of sea level during the past 400 000 years: The record of Sinai, Egypt (northern Red Sea), *Coral Reefs, 13*, 203-214, 1994.

Gvirtzman, G., and B. Buchbinder, Recent and Pleistocene coral reefs and coastal sediments of the Gulf of Elat, in *Tenth International Congress on Sedimentology, Jerusalem, Excursion Guidebook, Part II*, pp. 161-191, International Association of Sedimentology, Jerusalem, Israel, 1978.

Gvirtzman. G., J. Kronfeld, and B. Buchbinder, Dated coral reefs of southern Sinai (Red Sea) and their implication to late Quaternary sea levels, *Mar. Geol.*, *108*, 29-37, 1992.

Hart, S. R., and A. L. Cohen, An ion probe study of annual cycles of Sr/Ca and other trace elements in corals, *Geochim. Cosmochim. Acta*, *60*, 3075-3084, 1996.

Heiss, G. A., Coral reefs in the Red Sea: Growth, production, and stable isotopes, *GEOMAR Rep. 32*, 141 pp., GEOMAR, Kiel, Germany, 1994.

Huang, J., K. Higuchi, and A. Shabbar, The relationship between the North Atlantic Oscillation and the El Niño-Southern Oscillation, *Geophys. Res. Lett.*, *25*, 2707-2710, 1998.

Hurrel, J. W., Decadal trends in the North Atlantic Oscillation: Regional temperatures and precipitation, *Science*, *269*, 676-679, 1995.

Hurrel, J. W., Influence of variations in extratropical wintertime teleconnections on Northern Hemisphere temperature, *Geophys. Res. Lett.*, *23*, 665-668, 1996.

Hurrel, J. W., and H. van Loon, Decadal variations in climate associated with the North Atlantic Oscillation, *Clim. Change*, *36*, 301-326, 1997.

Jenkins, G. M., and D. G. Watts, *Spectral analysis and its applications*, 525 pp., Holden-Day, Oakland, 1968.

Jones, P. D., K. R. Briffa, T. Barnett, and S. F. B. Tett, High-resolution paleoclimatic records for the last millennium: interpretation, integration and comparison with General Circulation Model control-run temperatures, *Holocene*, *8*, 455-471, 1998.

Ji, J., N. Petit-Maire, and Z. Yan, The last 1000 years: Climatic change in arid Asia and Africa, *Global Planet. Change*, *7*, 203-210, 1993.

Kaiser, J., Partnering of the Red Sea lets scientists bond, *Science*, *279*, 1448, 1998.

Kaplan, A., M. Cane, Y. Kushnir, A. Clement, M. Blumenthal, and B. Rajagopalan, Analyses of global sea surface temperature 1856-1991, *J. Geophys. Res.*, *103*, 18567-18589, 1998.

Kirchner, I., and H.-F. Graf, Volcanos and El Niño: Signal seperation in Northern Hemisphere winter, *Clim. Dyn.*, *11*, 341-358, 1995.

Klein, R., J. Pätzold, G. Wefer, and Y. Loya, Seasonal variations in the stable isotopic composition and the skeletal density pattern of the coral *Porites lobata* (Gulf of Eilat, Red Sea), *Mar. Biol.*, *112*, 259-263, 1992.

Klein, R., J. Pätzold, G. Wefer, and Y. Loya, Depth-related timing of density band formation in *Porites* spp. corals from the Red Sea inferred from X-ray chronology and stable isotope composition, *Mar. Ecol. Prog. Ser.*, *97*, 99-104, 1993.

Klein, R., A. W. Tudhope, C. P. Chilcott, J. Pätzold, Z. Abdulkarim, M. Fine, A. E. Fallick, and Y. Loya, Evaluating southern Red Sea corals as a proxy record for the Asian monsoon, *Earth Planet. Sci. Lett.*, *148*, 381-394, 1997.

Klinker, J., Z. Reiss, C. Kropach, I. Levanon, H. Harpaz, E. Halicz, and G. Assaf, Observations on the circulation pattern in the Gulf of Elat ('Aqaba), Red Sea, *Isr. J. Earth Sci.*, *25*, 85-103, 1976.

Knutson, D. W., R. W. Buddemeier, and S. V. Smith, Coral chronometers: Seasonal growth bands in reef corals, *Science*, *177*, 270-272, 1972.

Kuhnert, H., J. Pätzold, B. G. Hatcher, K.-H. Wyrwoll, A. Eisenhauer, L. B. Collins, Z. R. Zhu, and G. Wefer, A 200-year coral stable isotope record from a high-latitude reef off Western Australia, *Coral Reefs*, in press 1998/1999.

Lauritzen, S.-E., and J. Lundberg, Rapid temperature variations and volcanic events during the Holocene from a Norwegian speleothem record, in *Abstracts 1st IGBP PAGES Open Science Meeting, London*, p. 88, PAGES International Project Office, Bern, Switzerland, 1998.

Lautenschlager, M., and K. Herterich, Atmospheric response to ice age conditions: Climatology near the Earth's surface, *J. Geophys. Res.*, *95*, 22547-22557, 1990.

Lean, J., J. Beer, and R. Bradley, Reconstruction of solar irradiance since 1610: Implications for climate change, *Geophys. Res. Lett.*, *22*, 3195-3198, 1995.

Levitus, S., and T. Boyer, World Ocean Atlas 1994, Volume 4: Temperature, *NOAA Atlas NESDIS 4*, U.S. Department of Commerce, Washington, D.C., 1994.

Levitus, S., Burgett, R., and T. Boyer, World Ocean Atlas 1994, Volume 3: Salinity, *NOAA Atlas NESDIS 3*, U.S. Department of Commerce, Washington, D.C., 1994.

Lewis, J. B., and W. S. Price, Feeding mechanisms and feeding strategies of Atlantic reef corals, *J. Zool.*, *176*, 527-544, 1975.

Lin, H., and J. Derome, A three-year lagged correlation between the North Atlantic Oscillation and winter conditions over the North Pacific and North America, *Geophys. Res. Lett.*, *25*, 2829-2832, 1998.

Lindell, D., and A. F. Post, Ultraphytoplankton succession is triggered by deep winter mixing in the Gulf of Aqaba (Eilat), Red Sea, *Limnol. Oceanogr.*, *40*, 1130-1141, 1995.

Linsley, B. K., R. B. Dunbar, G. M. Wellington, and D. A. Mucciarone, A coral-based reconstruction of Intertropical Convergence Zone variability over Central America since 1707, *J. Geophys. Res.*, *99*, 9977-9994, 1994.

Liphschitz, N., Middle East tree rings, data accessed via Internet from World Data Center-A for Paleoclimatology, NOAA/NGDC, Boulder CO, USA (http://www.ngdc.noaa.gov/paleo/paleo.html), 1998.

Lipp, J., P. Trimborn, T. Edwards, Y. Waisel, and D. Yakir, Climatic effects on the $\delta^{18}O$ and $\delta^{13}C$ of cellulose in the desert tree *Tamarix jordanis*, *Geochim. Cosmochim. Acta*, *60*, 3305-3309, 1996.

Lough, J. M., and D. J. Barnes, Several centuries of variation in skeletal extension, density and calcification in massive *Porites* colonies from the Great Barrier Reef: A proxy for seawater temperature and a background of variability against which to identify unnatural change, *J. Exp. Mar. Biol. Ecol.*, *211*, 29-67, 1997.

Mann, M. E., R. S. Bradley, and M. K. Hughes, Global-scale temperature patterns and climate forcing over the past six centuries, *Nature*, *392*, 779-787, 1998.

McConnaughey, T., ^{13}C and ^{18}O isotopic disequilibrium in biological carbonates: I. Patterns, *Geochim. Cosmochim. Acta*, *53*, 151-162, 1989a.

McConnaughey, T., ^{13}C and ^{18}O isotopic disequilibrium in biological carbonates: II. *In vitro* simulation of kinetic isotope effects, *Geochim. Cosmochim. Acta*, *53*, 163-171, 1989b.

McConnaughey, T. A., J. Burdett, J. F. Whelan, and C. K. Paull, Carbon isotopes in biological carbonates: Respiration and photosynthesis, *Geochim. Cosmochim. Acta*, *61*, 611-622, 1997.

McCulloch, M. T., M. K. Gagan, G. E. Mortimer, A. R. Chivas, and P. J. Isdale, A high-resolution Sr/Ca and $\delta^{18}O$ coral record from the Great Barrier Reef, Australia, and the 1982-1983 El Niño, *Geochim. Cosmochim. Acta*, *58*, 2747-2754, 1994.

Mitsuguchi, T., E. Matsumoto, O. Abe, T. Uchida, and P. J. Isdale, Mg/Ca thermometry in coral skeletons, *Science*, *274*, 961-963, 1996.

Morcos, S. A., Physical and chemical oceanography of the Red Sea, *Oceanogr. Mar. Biol. Ann. Rev.*, *8*, 73-202, 1970.

Moulin, C., C. E. Lambert, F. Dulac, and U. Dayan, Control of atmospheric export of dust from North Africa by the North Atlantic Oscillation, *Nature*, *387*, 691-694, 1997.

Moustafa, Y. A., J. Pätzold, Y. Loya, and G. Wefer, Mid-Holocene stable isotope record of fossil corals from the northern Red Sea, submitted to *Geol. Rundsch.*, 1999.

Muscatine, L., J. W. Porter, and I. R. Kaplan, Resource partitioning by reef corals as determined from stable isotope composition, *Mar. Biol.*, *100*, 185-193, 1989.

Nozaki, Y., D. M. Rye, K. K. Turekian, and R. E. Dodge, A 200 year record of carbon-13 and carbon-14 variations in a Bermuda coral, *Geophys. Res. Lett.*, *5*, 825-828, 1978.

Ormond, R., O. Hassan, D. Medio, M. Pearson, and M. Salem, Effectiveness of coral protection programmes in the Ras Mohammed National Park, Egyptian Red Sea, in *Proc. 8th Int. Coral Reef Sym., Panama*, edited by H. A. Lessios and I. G. Macintyre, pp. 1931-1936, Smithsonian Tropical Research Institute, Balboa, Panama, 1997.

Overpeck, J., K. Hughen, D. Hardy, R. Bradley, R. Case, M. Douglas, B. Finney, K. Gajewski, G. Jacoby, A. Jennings, S. Lamoureux, A. Lasca, G. MacDonald, J. Moore, M. Retelle, S. Smith, A. Wolfe, and G. Zielinski, Arctic environmental change of the last four centuries, *Science*, *278*, 1251-1256, 1997.

Paillard, D., L. Labeyrie, and P. Yiou, Macintosh Program performs time-series analysis, *Eos Trans. AGU*, *77*, 379, 1996.

Paldor, N., and D. A. Anati, Seasonal variations of temperature and salinity in the Gulf of Elat (Aqaba), *Deep-Sea Res.*, *26*, 661-672, 1979.

Parker, D. E., P. D. Jones, C. K. Folland, and A. Bevan, Interdecadal changes of surface temperature since the late nineteenth century, *J. Geophys. Res.*, *99*, 14373-14399, 1994.

Pätzold, J., Growth rhythms recorded in stable isotopes and density bands in the reef coral *Porites lobata* (Cebu, Philippines), *Coral Reefs*, *3*, 87-90, 1984.

Pätzold, J., Temperatur- und CO_2-Änderungen im tropischen Oberflächenwasser der Philippinen während der letzten 120 Jahre: Speicherung in stabilen Isotopen hermatyper Korallen, *Berichte Geol.-Paläont. Inst. Univ. Kiel 12*, 92 pp., Univ. Kiel, Kiel, Germany, 1986.

Pätzold, J., Coral proxy records from the Bermudas, *in Abstracts American Society of Limnology and Oceanography (ASLO) & Phycological Society of America (PSA) 1994 Joint Meeting, June 12-16, Miami*, a-57, 1994.

Pätzold, J., and G. Wefer, Bermuda coral reef record of the last 1000 years, in *Abstracts 4th International Conference on Paleoceanography, Kiel*, p. 224-225, Geol.-Paläont. Inst. Univ., Kiel, Germany, 1992.

Pearse, V. B., Incorporation of metabolic CO_2 into coral skeleton, *Nature*, *228*, 383-383, 1970.

Philander, S. G., *El Niño, La Niña, and the Southern Oscillation*, 293 pp., Academic Press, San Diego, 1990.

Prentice, I. C., J. Guiot, and S. P. Harrison, Mediterranean vegetation, lake levels and paleoclimate at the Last Glacial Maximum, *Nature*, *360*, 658-660, 1992.

Price, C., L. Stone, A. Huppert, B. Rajagopalan, and P. Alpert, A possible link between El Niño and precipitation in Israel, *Geophys. Res. Lett.*, *25*, 3963-3966, 1998.

Privett, D. W., Monthly chart of evaporation from the North Indian Ocean, including the Red Sea and the Persian Gulf, *Q. J. R. Meteorol. Soc.*, *85*, 424-428, 1959.

Qin, B., and G. Yu, Implications of lake level variations at 6 ka and 18 ka in mainland Asia, *Global Planet. Change*, *18*, 59-72, 1998.

Quinn, T. M., F. W. Taylor, and T. J. Crowley, A 173 year stable isotope record from a tropical South Pacific coral, *Quat. Sci. Rev.*, *12*, 407-418, 1993.

Quinn, T. M., T. J. Crowley, and F. W. Taylor, New stable isotope results from a 173-year coral from Espiritu Santo, Vanuatu, *Geophys. Res. Lett.*, *23*, 3413-3416, 1996.

Quinn, T. M., T. J. Crowley, F. W. Taylor, C. Henin, P. Joannot, and Y. Join, A multicentury stable isotope record from a New Caledonia coral: Interannual and

decadal sea surface temperature variability in the southwest Pacific since 1657 A.D., *Paleoceanography*, *13*, 412-426, 1998.

Quinn, W. H., A study of Southern Oscillation-related climatic activity for A.D. 622-1900 incorporating Nile River flood data, in *El Niño: Historical and paleoclimatic aspects of the Southern Oscillation*, edited by H. F. Diaz and V. Markgraf, pp. 119-149, Cambridge Univ. Press, Cambridge, 1992.

Reiss., Z., and L. Hottinger, *The Gulf of Aqaba. Ecological Micropaleontology*, 345 pp., Springer-Verlag, Berlin, 1984.

Reiss, Z., C. Kropach, I. Levanon, J. Klinker, H. Harpaz, Y. Shapiro, and Z. Ben-Avraham, DCPE - Data Collecting Program in the Gulf of Elat, Report No. 2, in *Fifth Report of the H. Steinitz Marine Biology Laboratory, Elat*, edited by Z. Reiss and I. Paperna, pp. 22-68, Hebrew Univ. of Jerusalem, Jerusalem, 1976.

Reiss, Z., I. Levanon, G. Raz, H. Harpaz, Z. Ben-Avraham, and E. Padan, DCPE - Data Collecting Program in the Gulf of Elat, Report No. 3, in *Sixth Report of the H. Steinitz Marine Biology Laboratory, Elat*, edited by M. Shilo and I. Paperna, pp. 31-54, Hebrew Univ. of Jerusalem, Jerusalem, 1977.

Reynolds, R. W., and T. M. Smith, Improved global sea surface temperature analyses, *J. Clim.*, *7*, 929-948, 1994.

Rind, D., Latitudinal temperature gradients and climate change, *J. Geophys. Res.*, *103*, 5943-5971, 1998.

Robock, A., and J. Mao, Winter warming from large volcanic eruptions, *Geophys. Res. Lett.*, *19*, 2405-2408, 1992.

Rogers, J. C., The association between the North Atlantic Oscillation and the Southern Oscillation in the Northern Hemisphere, *Mon. Weather Rev.*, *112*, 1999-2015, 1984.

Rogers, J. C., and H. van Loon, The seasaw in winter temperatures between Greenland and Northern Europe: Part II: Some oceanic and atmospheric effects in middle and high latitudes, *Mon. Weather Rev.*, *107*, 509-519, 1979.

Rosenan, N., One hundred years of rainfall in Jerusalem. A homotopic series of annual amounts, *Isr. Expl. J.*, *5*, 137-153, 1955.

Savitzky, A., and J. E. Golay, Smoothing and differentiation of data by simplified least squares procedure, *Anal. Chem.*, *36*, 1627-1639, 1964.

Schilman, B., A. Almogi-Labin, L. Labeyrie, M. Patern, and B. Luz, Eastern Mediterranean paleoceanography of the last 3500 years, in *Abstracts 6th International Conference on Paleoceanography, Lisbon*, p. 203, Instituto Geológico e Mineiro, Lisbon, Portugal, 1998.

Schlesinger, M. E., and N. Ramankutty, An oscillation in the global climate system of period 65-70 years, *Nature*, *367*, 723-726, 1994.

Schrag, D. P., Temperature and salinity history of the northern Red Sea from high-resolution elemental and stable isotope records (abstract), *Eos Trans. AGU*, *78* (46), F387, 1997.

Schrag, D. P., G. Eshel, and M. D. Moore, Tropics-outer tropics interactions: Lessons from Red Sea corals I (abstract), *Eos Trans. AGU*, *78(17)*, S190, 1997.

Schramm, A., S. L. Goldstein, and M. Stein, Climate change in the Middle East during the last glacial period and relationship to the marine and ice records (abstract), *Eos Trans. AGU, 78*(46), F354, 1997.

Sebens, K. P., K. S. Vandersall, L. A. Savina, and K. R. Graham, Zooplankton capture by two scleractinian corals, *Madracis mirabilis* and *Montastrea cavernosa*, in a field enclosure, *Mar. Biol., 127*, 303-317, 1996.

Shemesh, A., B. Luz, and J. Erez, Carbon isotopes, dissolved oxygen, and the carbonate system in the northern Gulf of Aqaba (Elat), *Isr. J. Earth Sci., 43*, 145-155, 1994.

Shen, C.-C., T. Lee, C.-Y. Chen, C.-H. Wang, C.-F. Dai, and L.-A. Li, The calibration of *D*[Sr/Ca] versus sea surface temperature relationship for *Porites* corals, *Geochim. Cosmochim. Acta, 60*, 3849-3858, 1996.

Shen, G. T., J. E. Cole, D. W. Lea, L. J. Linn, T. A. McConnaughey, and R. G. Fairbanks, Surface ocean variability at Galapagos from 1936-1982: Calibration of geochemical tracers in corals, *Paleoceanography, 7*, 563-588, 1992.

Sinclair, D. J., L. P. J. Kinsley, and M. T. McCulloch, High resolution analysis of trace elements in corals by laser ablation ICP-MS, *Geochim. Cosmochim. Acta, 62*, 1889-1901, 1998.

Slutz, R. J., S. J. Lubker, J. D. Hiscox, S. D. Woodruff, R. L. Jenne, D. H. Joseph, P. M. Steurer, and J. D. Elms, *Comprehensive Ocean-Atmosphere Data Set. Release 1*, 268 pp., NOAA Environmental Research Laboratories, Climate Research Program, Boulder, CO, 1985.

Spero, H. J., J. Bijma, D. W. Lea, and B. E. Bemis, Effect of seawater carbonate concentration on foraminiferal carbon and oxygen isotopes, *Nature, 390*, 497-500, 1997.

Stein, M., S. L. Goldstein, A. Schramm, A. Katz, and A. Starinsky, Lake Lisan sediments (paleo-Dead Sea) as monitors of the last glacial history, in *Abstracts 1st IGBP PAGES Open Science Meeting, London*, p. 121, PAGES International Project Office, Bern, Switzerland, 1998.

Stocker, T. F., The seasaw effect, *Science, 282*, 61-62, 1998.

Swart, P. K., Carbon and oxygen isotope fractionation in scleractinian corals: a review, *Earth-Sci. Rev., 19*, 51-80, 1983.

Swart, P. K., J. J. Leder, A. M. Szmant, and R. E. Dodge, The origin of variations in the isotopic record of scleractinian corals: II. Carbon, *Geochim. Cosmochim. Acta, 60*, 2871-2885, 1996a.

Swart, P. K., R. E. Dodge, and H. J. Hudson, A 240-year stable oxygen and carbon isotopic record in a coral from South Florida: Implications for the prediction of precipitation in southern Florida, *Palaios, 11*, 362-375, 1996b.

Swart, P. K., G. F. Healy, R. E. Dodge, P. Kramer, J. H. Hudson, R. B. Halley, M. B. Robblee, The stable oxygen and carbon isotopic record from a coral growing in Florida Bay: A 160 year record of climatic and anthropogenic influence, *Palaeogeogr. Palaeoclimatol. Palaeoecol., 123*, 219-237, 1996c.

Swart, P. K., K. S. White, D. Enfield, R. E. Dodge, and P. Milne, Stable oxygen isotopic composition of corals from the Gulf of Guinea as indicators of periods of extreme precipitation conditions in the sub-Sahara, *J. Geophys. Res.*, *103*, 27885-27892, 1998.

Taylor, R. B., D. J. Barnes, and J. M. Lough, On the inclusion of trace materials into massive coral skeletons. 1. Materials occuring in the environment in short pulses, *J. Exp. Mar. Biol. Ecol.*, *185*, 255-278, 1995.

van Loon, H., and J. C. Rogers, The seaswaw in winter temperatures between Greenland and Northern Europe: Part I: General Description, *Mon. Weather Rev.*, *106*, 296-310, 1978.

Vautard, R., and M. Ghil, Singular Spectrum Analysis in nonlinear dynamics, with applications to paleoclimatic time series, *Physica D*, *35*, 395-424, 1989.

Vautard, R., P. Yiou, and M. Ghil, Singular-spectrum analysis: A toolkit for short, noisy chaotic signals, *Physica D*, *58*, 95-126, 1992.

Walther, J., Die Korallenriffe der Sinaihalbinsel: Geologische und biologische Beobachtungen, *Abhandlungen der mathematisch-physischen Classe der Königl. Sächsischen Gesellschaft der Wissenschaften*, *14 (10)*, 439-505, 1888.

Wefer, G., and W. H. Berger, Isotope paleontology: Growth and composition of extant calcareous species, *Mar. Geol.*, *100*, 207-248, 1991.

Wellington, G. M., and R. B. Dunbar, Stable isotopic signature of El Niño-Southern Oscillation events in eastern tropical Pacific reef corals, *Coral Reefs*, *14*, 5-25, 1995.

Woelk, S., and D. Quadfasel, Renewal of deep water in the Red Sea during 1982-1987, *J. Geophys. Res.*, *101*, 18155-18165, 1996.

Wolf-Vecht, A., N. Paldor, and S. Brenner, Hydrographic indications of advection/convection effects in the Gulf of Elat, *Deep-Sea Res.*, *39*, 1393-1401, 1992.

Woodruff, S. D., S. J. Lubker, K. Wolter, S. J. Worley, and J. D. Elms, *Comprehensive Ocean-Atmosphere Data Set (COADS)*, *Release 1a: 1980-1992*, Earth System Monitor, Vol. 4, No. 1, NOAA, 1993.

Yakir, D., A. Issar, J. Gat, E. Adar, P. Trimborn, and J. Lipp, ^{13}C and ^{18}O of wood from the Roman siege rampart in Masada, Israel (AD 70-73): Evidence for a less arid climate for the region, *Geochim. Cosmochim. Acta*, *58*, 3535-3539, 1994.

Yakir, D., S. Lev-Yadun, and A. Zangvil, El Niño and tree growth near Jerusalem over the last 20 years, *Global Change Biology*, *2*, 97-101, 1996.

Yiou, P., M. Ghil, J. Jouzel, D. Paillard, R. Vautard, Nonlinear variability of the climate system from singular and power spectra of Late Quaternary records, *Clim. Dyn.*, *9*, 371-389, 1994.

Appendix: Data tables

Coral core EILAT-1 (*Porites* sp.) - Stable isotope data

Core depth [cm]	Age [years]	$\delta^{18}O$ [‰ PDB]	$\delta^{13}C$ [‰ PDB]
15.725		-3.12	-0.97
15.650		-3.31	-1.24
15.550		-3.18	-1.51
15.450		-2.91	-1.31
15.300	1974.208	-2.59	-1.54
15.150	1974.358	-2.89	-1.33
15.050	1974.458	-3.03	-0.94
14.950	1974.558	-3.22	-0.91
14.875	1974.633	-3.47	-1.23
14.750	1974.758	-3.36	-1.09
14.675	1974.833	-3.32	-1.43
14.575	1974.933	-3.21	-1.51
14.475	1975.033	-3.05	-1.49
14.400	1975.108	-2.83	-1.78
14.300	1975.208	-2.69	-1.99
14.025	1975.498	-2.74	-0.72
13.875	1975.656	-3.27	-1.17
13.750	1975.787	-3.21	-1.28
13.650	1975.893	-3.26	-1.15
13.550	1975.998	-2.86	-1.49
13.450	1976.103	-2.73	-1.76
13.350	1976.208	-2.56	-2.52
13.250	1976.319	-2.61	-1.74
13.150	1976.431	-2.87	-1.02
13.075	1976.514	-3.03	-0.76
12.975	1976.625	-3.22	-1.16
12.875	1976.736	-3.18	-1.17
12.775	1976.847	-3.13	-1.23
12.675	1976.958	-3.12	-1.46
12.550	1977.097	-2.71	-1.22
12.450	1977.208	-2.66	-1.03
12.250	1977.382	-2.68	-1.47
12.125	1977.491	-2.82	-1.21
12.075	1977.534	-2.88	-1.43
11.950	1977.643	-3.21	-1.30
11.850	1977.730	-3.33	-1.29
11.775	1977.795	-3.31	-1.39
11.650	1977.904	-3.24	-1.23
11.525	1978.013	-3.03	-1.93
11.425	1978.100	-2.80	-1.70
11.300	1978.208	-2.64	-2.42
11.225	1978.299	-2.69	-2.60
11.125	1978.420	-3.04	-2.05
11.025	1978.542	-3.18	-1.27
10.950	1978.633	-3.23	-0.79
10.875	1978.723	-3.13	-0.49
10.775	1978.845	-3.20	-0.98
10.700	1978.936	-3.13	-0.99
10.575	1979.087	-2.87	-1.79
10.475	1979.208	-2.63	-2.23
10.375	1979.306	-2.64	-2.15
10.275	1979.403	-3.03	-1.10
10.200	1979.477	-3.06	-0.90
10.100	1979.574	-3.16	-0.89
10.025	1979.647	-3.38	-1.66
9.925	1979.745	-3.32	-1.58
9.825	1979.842	-3.13	-1.91
9.725	1979.940	-3.17	-1.86
9.650	1980.013	-3.20	-2.19
9.525	1980.135	-2.71	-2.42
9.450	1980.208	-2.62	-2.49
9.350	1980.316	-2.77	-2.06
9.250	1980.425	-2.99	-1.84
9.150	1980.533	-3.25	-2.21
9.075	1980.614	-3.18	-1.94
9.000	1980.695	-3.30	-1.94
8.875	1980.830	-3.16	-2.24
8.750	1980.965	-3.11	-2.41
8.625	1981.100	-2.89	-2.43
8.525	1981.208	-2.80	-2.18
8.425	1981.337	-2.84	-1.62
8.325	1981.466	-3.21	-1.61
8.225	1981.595	-3.47	-2.34
8.125	1981.724	-3.27	-1.97
8.025	1981.853	-3.20	-2.04
7.950	1981.950	-2.99	-2.18
7.850	1982.079	-2.83	-2.37
7.750	1982.208	-2.69	-2.54
7.650	1982.337	-2.92	-1.82
7.550	1982.466	-3.16	-1.20
7.450	1982.595	-3.45	-2.15
7.375	1982.692	-3.50	-1.74
7.275	1982.821	-3.42	-1.90
7.175	1982.950	-2.96	-2.28
7.075	1983.079	-2.69	-2.61
6.975	1983.208	-2.66	-2.89
6.875	1983.408	-3.22	-1.13
6.775	1983.608	-3.39	-1.23
6.675	1983.808	-3.18	-1.45
6.575	1984.008	-2.65	-1.27
6.475	1984.208	-2.37	-1.01
6.350	1984.340	-2.52	-0.83
6.250	1984.445	-2.94	-0.98
6.150	1984.550	-3.26	-1.32
6.075	1984.629	-3.33	-1.45
5.950	1984.761	-3.30	-1.67
5.850	1984.866	-3.17	-1.97
5.750	1984.971	-2.81	-2.06
5.625	1985.103	-2.64	-1.72
5.525	1985.208	-2.62	-1.39
5.425	1985.337	-3.05	-1.50
5.325	1985.466	-3.25	-1.59
5.225	1985.595	-3.07	-0.87
5.125	1985.724	-3.13	-1.77
5.000	1985.886	-2.89	-2.14
4.875	1986.047	-2.84	-2.07
4.750	1986.208	-2.75	-2.01
4.650	1986.323	-2.94	-1.73
4.525	1986.465	-3.23	-2.25
4.425	1986.580	-3.43	-2.70
4.300	1986.723	-3.58	-2.10
4.225	1986.808	-3.44	-1.90
4.100	1986.951	-3.06	-2.10
3.975	1987.094	-2.74	-2.48
3.875	1987.208	-2.60	-2.22
3.775	1987.390	-3.06	-1.10
3.675	1987.572	-3.38	-1.67
3.575	1987.754	-3.44	-2.24
3.500	1987.890	-3.20	-2.15
3.400	1988.072	-2.94	-2.16
3.325	1988.208	-2.75	-2.20
3.200	1988.381	-2.88	-1.75
3.075	1988.553	-3.38	-1.67
2.975	1988.691	-3.59	-1.68
2.875	1988.829	-3.54	-1.59
2.800	1988.932	-3.08	-1.36
2.700	1989.070	-2.81	-1.94
2.600	1989.208	-2.56	-2.79
2.500	1989.337	-2.97	-0.99
2.375	1989.499	-3.03	-1.22
2.275	1989.628	-3.34	-1.27
2.150	1989.789	-3.30	-1.57
2.050	1989.918	-2.97	-1.91
1.950	1990.047	-2.75	-1.54
1.825	1990.208	-2.67	-1.14
1.700	1990.381	-3.45	-1.86
1.575	1990.553	-3.40	-1.66
1.450	1990.726	-3.27	-2.09
1.325	1990.898	-3.10	-2.09
1.225	1991.036	-2.86	-2.12
1.100	1991.208	-2.85	-2.00
1.000	1991.375	-3.12	-1.66

Coral core EILAT-1 (*Porites* sp.) - Stable isotope data

Core depth [cm]	Age [years]	$\delta^{18}O$ [‰ PDB]	$\delta^{13}C$ [‰ PDB]
0.875	1991.583	-3.38	-1.64
0.775	1991.750	-3.27	-1.53
0.675	1991.917	-3.04	-1.47
0.600	1992.042	-2.82	-2.67
0.500	1992.208	-2.37	-2.71
0.400	1992.431	-3.36	-1.12
0.300	1992.653	-3.32	-1.78
0.175	1992.931	-3.04	-2.26
0.050	1993.208	-2.59	-2.90

Coral core EILAT-1 (*Porites* sp.) - Annual coral growth rate

Year	Growth rate [cm/year]
1974	1.000
1975	0.950
1976	0.900
1977	1.150
1978	0.825
1979	1.025
1980	0.925
1981	0.775
1982	0.775
1983	0.500
1984	0.950
1985	0.775
1986	0.875
1987	0.550
1988	0.725
1989	0.775
1990	0.725
1991	0.600
1992	0.450

Coral core RUS-95 (*Porites* sp.) - Stable isotope data

Core depth [cm]	Age [years]	$\delta^{18}O$ [‰ PDB]	Core depth [cm]	Age [years]	$\delta^{18}O$ [‰ PDB]	Core depth [cm]	Age [years]	$\delta^{18}O$ [‰ PDB]
241.350		-3.45	231.325	1762.222	-2.92	221.250	1775.125	-2.88
241.250		-3.25	231.225	1762.351	-2.90	221.075	1775.309	-3.12
241.050	1750.925	-2.82	231.100	1762.512	-3.34	220.875	1775.520	-3.67
240.850	1751.125	-2.78	231.000	1762.641	-3.93	220.775	1775.625	-3.86
240.750	1751.225	-3.01	230.900	1762.770	-3.58	220.700	1775.704	-3.51
240.650	1751.325	-3.02	230.800	1762.899	-3.45	220.500	1775.914	-3.17
240.550	1751.425	-3.44	230.700	1763.028	-3.17	220.300	1776.125	-2.82
240.475	1751.500	-3.75	230.625	1763.125	-2.65	220.100	1776.341	-3.10
240.275	1751.700	-3.42	230.500	1763.403	-3.43	220.000	1776.449	-3.42
240.100	1751.875	-3.16	230.375	1763.681	-3.47	219.925	1776.530	-3.40
239.850	1752.125	-2.72	230.275	1763.903	-3.44	219.825	1776.639	-3.63
239.775	1752.232	-3.00	230.175	1764.125	-2.79	219.725	1776.747	-3.37
239.675	1752.375	-3.18	230.100	1764.261	-3.78	219.550	1776.936	-3.39
239.575	1752.518	-3.28	230.000	1764.443	-3.39	219.375	1777.125	-2.96
239.475	1752.661	-3.77	229.800	1764.807	-3.25	219.200	1777.292	-3.69
239.375	1752.804	-3.58	229.625	1765.125	-3.12	219.125	1777.363	-3.47
239.150	1753.125	-2.88	229.450	1765.337	-3.54	218.850	1777.625	-3.60
238.950	1753.320	-3.03	229.350	1765.458	-3.67	218.675	1777.792	-3.41
238.875	1753.393	-3.51	229.250	1765.580	-3.85	218.500	1777.958	-3.15
238.775	1753.491	-3.57	229.150	1765.701	-3.77	218.325	1778.125	-3.11
238.675	1753.588	-3.59	228.950	1765.943	-3.48	218.150	1778.394	-3.31
238.575	1753.686	-3.15	228.875	1766.034	-3.37	217.975	1778.663	-3.55
238.375	1753.881	-3.22	228.800	1766.125	-2.87	217.900	1778.779	-3.75
238.125	1754.125	-3.02	228.700	1766.243	-3.19	217.825	1778.894	-3.54
238.025	1754.246	-3.45	228.525	1766.449	-3.44	217.675	1779.125	-2.97
237.925	1754.367	-3.44	228.325	1766.684	-3.63	217.475	1779.354	-3.21
237.825	1754.489	-3.71	228.150	1766.890	-3.18	217.400	1779.439	-3.44
237.700	1754.640	-3.17	227.950	1767.125	-2.86	217.325	1779.525	-3.58
237.475	1754.913	-2.89	227.875	1767.211	-3.04	217.150	1779.725	-3.42
237.300	1755.125	-2.86	227.775	1767.325	-3.21	216.975	1779.925	-3.02
237.225	1755.240	-3.09	227.675	1767.439	-3.36	216.800	1780.125	-2.79
237.100	1755.433	-3.23	227.600	1767.525	-3.89	216.600	1780.336	-3.47
237.000	1755.587	-3.52	227.425	1767.725	-3.66	216.400	1780.546	-3.69
236.875	1755.779	-2.57	227.250	1767.925	-3.45	216.200	1780.757	-3.55
236.650	1756.125	-2.47	227.075	1768.125	-2.99	216.125	1780.836	-3.55
236.425	1756.321	-3.26	227.000	1768.240	-3.17	216.050	1780.914	-3.69
236.325	1756.408	-3.48	226.900	1768.394	-3.05	215.850	1781.125	-2.81
236.175	1756.538	-3.41	226.800	1768.548	-3.37	215.650	1781.279	-2.86
236.075	1756.625	-3.65	226.725	1768.663	-3.71	215.475	1781.413	-3.50
235.950	1756.734	-3.38	226.625	1768.817	-3.58	215.275	1781.567	-3.36
235.700	1756.951	-3.14	226.425	1769.125	-2.84	215.200	1781.625	-3.86
235.500	1757.125	-2.90	226.325	1769.258	-3.01	215.100	1781.702	-3.40
235.300	1757.354	-2.98	226.225	1769.392	-2.96	214.925	1781.837	-3.13
235.200	1757.468	-3.14	226.125	1769.525	-3.69	214.750	1781.971	-2.98
235.075	1757.611	-3.41	226.050	1769.625	-3.49	214.550	1782.125	-2.89
234.950	1757.754	-3.76	225.850	1769.892	-3.45	214.475	1782.211	-3.19
234.850	1757.868	-3.74	225.675	1770.125	-3.08	214.400	1782.296	-3.18
234.625	1758.125	-2.76	225.600	1770.245	-3.15	214.225	1782.496	-3.49
234.450	1758.314	-3.05	225.500	1770.405	-3.38	214.125	1782.611	-3.76
234.400	1758.368	-3.27	225.425	1770.525	-3.99	214.050	1782.696	-3.40
234.325	1758.449	-3.44	225.325	1770.685	-3.58	213.875	1782.896	-2.92
234.250	1758.530	-3.49	225.125	1771.005	-3.18	213.675	1783.125	-2.70
234.175	1758.611	-3.43	225.050	1771.125	-3.11	213.500	1783.262	-2.96
234.075	1758.720	-3.41	224.950	1771.292	-3.28	213.300	1783.419	-3.02
233.900	1758.909	-2.99	224.850	1771.458	-3.80	213.150	1783.537	-3.59
233.700	1759.125	-2.96	224.650	1771.792	-3.18	212.950	1783.694	-3.55
233.625	1759.211	-3.28	224.450	1772.125	-2.86	212.750	1783.850	-3.51
233.475	1759.382	-3.31	224.275	1772.300	-3.51	212.550	1784.007	-2.89
233.400	1759.468	-3.62	224.175	1772.400	-3.41	212.475	1784.066	-2.92
233.325	1759.554	-4.05	224.075	1772.500	-3.78	212.400	1784.125	-2.87
233.225	1759.668	-3.74	223.875	1772.700	-3.45	212.225	1784.271	-3.21
233.025	1759.896	-3.37	223.650	1772.925	-3.05	212.125	1784.354	-3.25
232.825	1760.125	-2.60	223.450	1773.125	-2.86	212.050	1784.417	-3.34
232.750	1760.222	-3.25	223.225	1773.313	-3.03	211.875	1784.563	-3.66
232.650	1760.351	-3.56	223.125	1773.396	-3.38	211.700	1784.708	-3.57
232.575	1760.448	-3.86	223.025	1773.479	-3.48	211.525	1784.854	-3.51
232.475	1760.577	-3.69	222.850	1773.625	-3.69	211.375	1784.979	-3.12
232.275	1760.835	-3.26	222.650	1773.792	-3.35	211.200	1785.125	-2.99
232.050	1761.125	-2.83	222.450	1773.958	-3.22	211.025	1785.271	-3.31
231.825	1761.471	-3.14	222.250	1774.125	-2.87	210.850	1785.417	-3.45
231.725	1761.625	-3.39	222.075	1774.300	-3.30	210.700	1785.542	-3.93
231.650	1761.740	-3.46	221.975	1774.400	-3.34	210.550	1785.667	-3.73
231.550	1761.894	-3.81	221.875	1774.500	-3.84	210.375	1785.813	-3.16
231.475	1762.010	-3.54	221.675	1774.700	-3.81	210.175	1785.979	-3.14
231.400	1762.125	-2.77	221.500	1774.875	-3.41	210.000	1786.125	-2.97

Coral core RUS-95 (*Porites* sp.) - Stable isotope data

Core depth [cm]	Age [years]	$\delta^{18}O$ [‰ PDB]	Core depth [cm]	Age [years]	$\delta^{18}O$ [‰ PDB]	Core depth [cm]	Age [years]	$\delta^{18}O$ [‰ PDB]
209.825	1786.250	-3.34	197.775	1796.920	-3.49	186.000	1809.934	-3.37
209.625	1786.393	-3.35	197.575	1797.125	-2.80	185.775	1810.125	-2.90
209.450	1786.518	-3.76	197.350	1797.325	-3.12	185.625	1810.271	-3.34
209.250	1786.661	-3.73	197.225	1797.436	-3.59	185.500	1810.393	-3.39
209.075	1786.786	-3.74	197.150	1797.503	-3.58	185.375	1810.515	-3.69
208.900	1786.911	-3.40	196.925	1797.703	-3.67	185.175	1810.710	-3.62
208.700	1787.054	-3.15	196.700	1797.903	-3.43	184.950	1810.930	-3.14
208.600	1787.125	-2.94	196.450	1798.125	-2.75	184.750	1811.125	-3.01
208.525	1787.198	-3.06	196.350	1798.254	-3.46	184.650	1811.268	-3.31
208.325	1787.393	-3.64	196.225	1798.415	-3.80	184.525	1811.446	-3.44
208.125	1787.588	-3.65	196.100	1798.577	-3.96	184.400	1811.625	-3.89
207.975	1787.735	-3.38	195.925	1798.802	-3.82	184.275	1811.804	-3.51
207.775	1787.930	-3.29	195.800	1798.964	-3.16	184.050	1812.125	-2.84
207.575	1788.125	-2.98	195.675	1799.125	-2.96	183.875	1812.337	-3.32
207.400	1788.281	-3.27	195.600	1799.261	-3.76	183.775	1812.458	-3.40
207.225	1788.436	-3.35	195.500	1799.443	-3.70	183.675	1812.580	-3.92
207.150	1788.503	-3.65	195.325	1799.761	-3.40	183.550	1812.731	-3.71
207.050	1788.592	-3.51	195.125	1800.125	-3.04	183.425	1812.883	-3.36
206.875	1788.747	-3.48	194.925	1800.307	-3.34	183.225	1813.125	-2.67
206.650	1788.947	-3.09	194.850	1800.375	-3.58	183.000	1813.415	-3.37
206.450	1789.125	-2.67	194.750	1800.466	-3.67	182.800	1813.673	-3.50
206.250	1789.285	-3.21	194.650	1800.557	-3.79	182.725	1813.770	-3.60
206.050	1789.445	-3.67	194.450	1800.739	-3.50	182.625	1813.899	-3.34
205.950	1789.525	-3.90	194.225	1800.943	-3.18	182.450	1814.125	-3.04
205.875	1789.585	-3.78	194.025	1801.125	-3.17	182.275	1814.366	-3.28
205.650	1789.765	-3.48	193.925	1801.236	-3.23	182.200	1814.470	-3.39
205.425	1789.945	-2.92	193.825	1801.347	-3.69	182.125	1814.573	-3.95
205.200	1790.125	-2.71	193.725	1801.458	-3.94	182.025	1814.711	-3.60
205.075	1790.241	-3.39	193.525	1801.681	-3.27	181.925	1814.849	-3.52
205.000	1790.311	-3.09	193.325	1801.903	-3.06	181.725	1815.125	-2.86
204.900	1790.404	-3.66	193.125	1802.125	-2.95	181.525	1815.311	-3.01
204.800	1790.497	-3.58	192.925	1802.383	-3.55	181.425	1815.404	-3.39
204.600	1790.683	-3.54	192.750	1802.609	-3.68	181.300	1815.520	-3.40
204.350	1790.916	-3.06	192.625	1802.770	-3.65	181.200	1815.613	-3.45
204.125	1791.125	-2.51	192.550	1802.867	-3.47	181.025	1815.776	-3.35
204.000	1791.216	-3.22	192.350	1803.125	-3.04	180.850	1815.939	-3.10
203.875	1791.307	-3.14	192.150	1803.292	-3.06	180.650	1816.125	-2.99
203.750	1791.398	-3.42	192.050	1803.375	-3.49	180.525	1816.281	-3.21
203.650	1791.470	-3.58	191.950	1803.458	-3.48	180.425	1816.406	-3.51
203.550	1791.543	-3.50	191.750	1803.625	-3.78	180.300	1816.563	-3.71
203.475	1791.598	-3.55	191.575	1803.771	-3.76	180.050	1816.875	-3.18
203.300	1791.725	-3.60	191.350	1803.958	-3.33	179.850	1817.125	-2.49
203.125	1791.852	-3.10	191.150	1804.125	-3.22	179.725	1817.268	-2.82
202.925	1791.998	-3.00	190.925	1804.406	-3.57	179.600	1817.411	-3.28
202.750	1792.125	-2.82	190.825	1804.531	-3.87	179.475	1817.554	-3.41
202.675	1792.190	-3.40	190.725	1804.656	-3.85	179.350	1817.696	-3.57
202.575	1792.277	-3.20	190.525	1804.906	-3.49	179.150	1817.925	-3.43
202.400	1792.429	-3.87	190.350	1805.125	-3.30	178.975	1818.125	-2.80
202.225	1792.582	-4.01	190.150	1805.330	-3.31	178.775	1818.315	-2.99
202.000	1792.777	-3.56	190.075	1805.407	-3.39	178.700	1818.387	-3.55
201.775	1792.973	-3.08	189.975	1805.510	-3.48	178.625	1818.458	-3.48
201.600	1793.125	-2.69	189.875	1805.612	-3.85	178.425	1818.649	-3.47
201.400	1793.330	-3.35	189.775	1805.715	-3.74	178.225	1818.839	-2.95
201.200	1793.535	-3.53	189.575	1805.920	-3.21	178.025	1819.030	-2.89
201.100	1793.638	-4.02	189.475	1806.022	-2.84	177.925	1819.125	-2.68
201.000	1793.740	-3.42	189.375	1806.125	-2.68	177.825	1819.263	-3.36
200.800	1793.946	-3.27	189.175	1806.392	-3.43	177.750	1819.366	-3.78
200.625	1794.125	-2.80	189.075	1806.525	-3.67	177.625	1819.539	-3.76
200.450	1794.325	-2.94	188.975	1806.658	-3.52	177.425	1819.815	-3.29
200.375	1794.411	-3.48	188.800	1806.892	-3.03	177.200	1820.125	-2.85
200.275	1794.525	-3.26	188.625	1807.125	-2.94	177.100	1820.246	-3.33
200.200	1794.611	-4.07	188.525	1807.233	-3.21	176.975	1820.398	-3.45
200.125	1794.696	-3.61	188.450	1807.314	-3.23	176.875	1820.519	-3.61
199.925	1794.925	-3.47	188.275	1807.503	-3.84	176.775	1820.640	-3.70
199.750	1795.125	-2.90	188.100	1807.693	-3.54	176.575	1820.883	-3.19
199.550	1795.292	-3.00	187.900	1807.909	-3.00	176.375	1821.125	-2.70
199.450	1795.375	-3.52	187.700	1808.125	-2.91	176.275	1821.243	-2.85
199.350	1795.458	-3.47	187.475	1808.425	-3.59	176.175	1821.360	-3.42
199.150	1795.625	-3.90	187.300	1808.658	-3.71	176.050	1821.507	-3.60
198.975	1795.771	-3.46	187.225	1808.758	-3.79	175.975	1821.596	-3.67
198.775	1795.938	-3.49	187.125	1808.892	-3.49	175.725	1821.890	-3.09
198.550	1796.125	-2.82	186.950	1809.125	-3.09	175.525	1822.125	-2.73
198.375	1796.304	-3.39	186.675	1809.359	-3.17	175.425	1822.279	-3.14
198.175	1796.510	-3.70	186.425	1809.572	-3.26	175.325	1822.433	-3.61
198.075	1796.612	-3.88	186.300	1809.678	-3.69	175.175	1822.663	-3.50
198.000	1796.689	-3.62	186.225	1809.742	-3.57	175.100	1822.779	-3.49

Coral core RUS-95 (*Porites* sp.) - Stable isotope data

Core depth [cm]	Age [years]	$\delta^{18}O$ [‰ PDB]	Core depth [cm]	Age [years]	$\delta^{18}O$ [‰ PDB]	Core depth [cm]	Age [years]	$\delta^{18}O$ [‰ PDB]
175.000	1822.933	-3.21	161.925	1836.366	-3.11	148.950	1850.569	-3.76
174.875	1823.125	-2.79	161.800	1836.458	-3.18	148.800	1850.792	-3.56
174.750	1823.260	-2.88	161.575	1836.625	-3.63	148.575	1851.125	-2.86
174.625	1823.395	-3.33	161.350	1836.792	-3.56	148.375	1851.392	-3.42
174.500	1823.530	-3.61	161.125	1836.958	-2.89	148.250	1851.558	-3.93
174.375	1823.666	-3.41	160.900	1837.125	-2.60	148.150	1851.692	-3.67
174.150	1823.909	-2.95	160.700	1837.295	-3.28	147.925	1851.992	-3.30
173.950	1824.125	-2.82	160.600	1837.380	-3.49	147.825	1852.125	-2.75
173.850	1824.292	-3.39	160.500	1837.465	-3.60	147.700	1852.325	-2.96
173.750	1824.458	-3.61	160.275	1837.657	-3.41	147.500	1852.645	-3.87
173.550	1824.792	-3.25	160.050	1837.848	-3.08	147.400	1852.805	-3.47
173.350	1825.125	-2.71	159.825	1838.040	-3.04	147.300	1852.965	-3.24
173.225	1825.304	-3.53	159.725	1838.125	-2.95	147.200	1853.125	-2.89
173.100	1825.482	-3.45	159.625	1838.239	-3.23	146.975	1853.316	-3.51
172.875	1825.804	-3.44	159.375	1838.525	-3.74	146.825	1853.444	-3.57
172.650	1826.125	-2.63	159.200	1838.725	-3.56	146.725	1853.529	-4.00
172.425	1826.500	-3.16	158.950	1839.011	-3.05	146.575	1853.657	-3.66
172.250	1826.792	-3.56	158.850	1839.125	-2.62	146.350	1853.848	-3.43
172.150	1826.958	-3.53	158.725	1839.250	-2.74	146.250	1853.934	-3.40
172.050	1827.125	-2.75	158.525	1839.450	-3.39	146.125	1854.040	-3.06
171.925	1827.247	-2.81	158.275	1839.700	-3.72	146.025	1854.125	-2.94
171.725	1827.442	-3.31	158.050	1839.925	-3.10	145.900	1854.236	-3.13
171.625	1827.540	-3.53	157.850	1840.125	-2.76	145.775	1854.347	-3.72
171.425	1827.735	-3.79	157.650	1840.375	-3.36	145.675	1854.436	-3.60
171.225	1827.930	-3.51	157.550	1840.500	-3.67	145.575	1854.525	-3.80
171.025	1828.125	-2.92	157.450	1840.625	-3.71	145.425	1854.658	-3.58
170.825	1828.325	-3.02	157.250	1840.875	-3.44	145.275	1854.792	-3.65
170.625	1828.525	-3.69	157.050	1841.125	-2.76	145.175	1854.881	-3.45
170.450	1828.700	-4.01	156.800	1841.363	-3.19	145.050	1854.992	-3.19
170.350	1828.800	-3.64	156.675	1841.482	-3.52	144.900	1855.125	-3.02
170.250	1828.900	-3.28	156.550	1841.601	-3.78	144.800	1855.233	-3.10
170.025	1829.125	-2.85	156.350	1841.792	-3.30	144.700	1855.341	-3.46
169.775	1829.292	-2.97	156.100	1842.030	-2.90	144.600	1855.449	-3.63
169.675	1829.358	-2.95	156.000	1842.125	-2.77	144.400	1855.666	-3.93
169.550	1829.442	-3.28	155.900	1842.263	-3.12	144.175	1855.909	-3.77
169.350	1829.575	-3.86	155.700	1842.539	-3.62	143.975	1856.125	-3.14
169.100	1829.742	-3.41	155.600	1842.677	-3.57	143.775	1856.336	-3.36
168.900	1829.875	-3.07	155.475	1842.849	-3.65	143.675	1856.441	-3.26
168.700	1830.008	-3.01	155.275	1843.125	-2.96	143.575	1856.546	-3.57
168.525	1830.125	-2.90	155.025	1843.395	-3.05	143.450	1856.678	-4.05
168.325	1830.307	-3.18	154.775	1843.666	-3.40	143.250	1856.888	-3.72
168.175	1830.443	-3.50	154.525	1843.936	-3.08	143.025	1857.125	-3.14
168.050	1830.557	-3.80	154.350	1844.125	-2.71	142.825	1857.354	-3.46
167.825	1830.761	-3.40	154.225	1844.250	-3.28	142.750	1857.439	-3.41
167.650	1830.920	-3.55	154.100	1844.375	-3.77	142.650	1857.554	-3.64
167.425	1831.125	-2.88	154.000	1844.475	-3.72	142.550	1857.668	-3.91
167.300	1831.260	-3.04	153.800	1844.675	-4.09	142.475	1857.754	-3.69
167.200	1831.368	-3.40	153.600	1844.875	-3.41	142.350	1857.896	-3.34
167.075	1831.503	-3.54	153.350	1845.125	-3.38	142.275	1857.982	-3.05
166.950	1831.639	-3.80	153.225	1845.304	-3.50	142.150	1858.125	-2.79
166.725	1831.882	-3.27	153.100	1845.482	-3.77	142.075	1858.250	-3.23
166.500	1832.125	-2.79	152.850	1845.839	-3.36	141.975	1858.417	-3.34
166.300	1832.341	-2.90	152.650	1846.125	-2.91	141.875	1858.583	-3.46
166.050	1832.611	-3.44	152.450	1846.375	-3.20	141.775	1858.750	-3.59
165.975	1832.693	-3.37	152.375	1846.469	-3.88	141.650	1858.958	-3.45
165.900	1832.774	-3.55	152.275	1846.594	-3.70	141.550	1859.125	-3.10
165.625	1833.071	-3.04	152.050	1846.875	-3.62	141.350	1859.285	-3.23
165.375	1833.125	-2.85	151.950	1847.000	-3.76	141.150	1859.445	-3.48
165.125	1833.611	-3.37	151.850	1847.125	-2.73	140.950	1859.605	-3.74
165.000	1833.747	-3.43	151.675	1847.296	-3.27	140.725	1859.785	-3.49
164.900	1833.855	-3.36	151.475	1847.491	-3.42	140.500	1859.965	-3.29
164.625	1834.125	-2.51	151.275	1847.686	-3.60	140.300	1860.125	-2.96
164.500	1834.229	-2.57	151.050	1847.905	-3.84	140.125	1860.296	-3.51
164.400	1834.313	-3.63	150.825	1848.125	-3.17	139.925	1860.491	-3.77
164.150	1834.521	-3.22	150.700	1848.304	-3.60	139.725	1860.686	-3.67
163.925	1834.708	-3.27	150.600	1848.446	-3.70	139.525	1860.881	-3.39
163.675	1834.917	-3.10	150.375	1848.768	-3.78	139.275	1861.125	-2.79
163.425	1835.125	-2.68	150.125	1849.125	-2.90	139.175	1861.223	-3.05
163.325	1835.210	-2.71	150.025	1849.239	-2.93	139.075	1861.320	-3.21
163.125	1835.380	-2.85	149.900	1849.382	-3.28	138.875	1861.515	-3.73
162.875	1835.593	-3.12	149.775	1849.525	-3.68	138.675	1861.710	-3.69
162.725	1835.721	-3.28	149.650	1849.668	-3.49	138.475	1861.905	-3.45
162.625	1835.806	-3.52	149.475	1849.868	-3.62	138.250	1862.125	-2.96
162.375	1836.019	-3.29	149.350	1850.011	-3.15	138.150	1862.225	-3.31
162.250	1836.125	-2.54	149.250	1850.125	-2.97	138.050	1862.325	-3.55
162.150	1836.199	-2.73	149.050	1850.421	-3.76	137.850	1862.525	-3.75

Coral core RUS-95 (*Porites* sp.) - Stable isotope data

Core depth [cm]	Age [years]	$\delta^{18}O$ [‰ PDB]	Core depth [cm]	Age [years]	$\delta^{18}O$ [‰ PDB]	Core depth [cm]	Age [years]	$\delta^{18}O$ [‰ PDB]
137.650	1862.725	-3.36	125.050	1873.125	-2.82	111.575	1886.125	-3.07
137.450	1862.925	-2.61	124.950	1873.214	-3.11	111.350	1886.292	-3.18
137.250	1863.125	-2.59	124.750	1873.392	-3.52	111.250	1886.366	-3.09
137.000	1863.260	-3.34	124.650	1873.481	-3.75	111.150	1886.440	-3.41
136.775	1863.382	-3.66	124.550	1873.569	-3.76	111.050	1886.514	-3.38
136.500	1863.530	-3.76	124.350	1873.747	-3.56	110.900	1886.625	-3.82
136.250	1863.666	-3.49	124.150	1873.925	-3.08	110.650	1886.810	-3.87
136.025	1863.787	-3.52	123.925	1874.125	-2.66	110.425	1886.977	-3.23
135.800	1863.909	-3.23	123.700	1874.305	-3.33	110.225	1887.125	-2.98
135.700	1863.963	-3.13	123.500	1874.465	-3.73	110.025	1887.232	-3.17
135.600	1864.017	-3.03	123.300	1874.625	-3.45	109.925	1887.285	-3.19
135.400	1864.125	-3.03	123.100	1874.785	-3.49	109.825	1887.338	-3.39
135.100	1864.304	-3.23	122.900	1874.945	-3.26	109.625	1887.445	-3.51
134.925	1864.409	-3.45	122.675	1875.125	-2.99	109.400	1887.565	-3.78
134.750	1864.513	-3.76	122.500	1875.366	-3.93	109.200	1887.672	-3.81
134.550	1864.632	-3.74	122.325	1875.608	-3.32	108.975	1887.792	-3.78
134.350	1864.752	-3.87	122.125	1875.884	-3.25	108.750	1887.912	-3.23
134.150	1864.871	-3.38	121.950	1876.125	-2.75	108.550	1888.018	-3.18
133.950	1864.991	-3.29	121.750	1876.265	-3.11	108.350	1888.125	-3.12
133.825	1865.065	-3.29	121.550	1876.406	-3.49	108.150	1888.282	-3.51
133.725	1865.125	-3.28	121.375	1876.529	-3.66	107.925	1888.458	-3.83
133.525	1865.367	-3.96	121.175	1876.669	-3.70	107.725	1888.615	-3.86
133.425	1865.489	-4.19	120.950	1876.827	-3.41	107.475	1888.811	-3.77
133.300	1865.640	-3.73	120.725	1876.985	-3.07	107.300	1888.949	-3.28
133.100	1865.883	-3.70	120.625	1877.055	-3.09	107.075	1889.125	-3.16
132.900	1866.125	-3.02	120.525	1877.125	-3.00	107.000	1889.192	-3.52
132.700	1866.288	-3.54	120.325	1877.360	-3.73	106.900	1889.281	-3.65
132.500	1866.452	-3.58	120.125	1877.596	-3.93	106.650	1889.503	-3.84
132.300	1866.615	-3.88	119.900	1877.860	-3.31	106.400	1889.725	-3.60
132.100	1866.778	-3.72	119.675	1878.125	-2.86	106.175	1889.925	-3.45
131.925	1866.921	-3.52	119.500	1878.304	-3.51	105.950	1890.125	-2.95
131.675	1867.125	-3.04	119.400	1878.407	-3.63	105.775	1890.262	-3.30
131.575	1867.207	-3.39	119.300	1878.510	-4.01	105.550	1890.439	-3.76
131.475	1867.288	-3.53	119.100	1878.715	-3.72	105.475	1890.498	-3.89
131.300	1867.431	-3.87	118.900	1878.920	-3.22	105.350	1890.596	-3.95
131.200	1867.513	-3.85	118.700	1879.125	-3.02	105.100	1890.792	-3.70
131.075	1867.615	-3.67	118.625	1879.196	-3.37	104.875	1890.968	-3.11
130.850	1867.798	-3.25	118.500	1879.315	-3.47	104.675	1891.125	-3.04
130.650	1867.962	-3.15	118.300	1879.506	-3.87	104.600	1891.193	-3.48
130.450	1868.125	-2.93	118.075	1879.720	-3.77	104.500	1891.284	-3.65
130.350	1868.228	-3.19	117.850	1879.935	-3.43	104.275	1891.489	-3.78
130.250	1868.330	-3.59	117.650	1880.125	-2.91	104.150	1891.602	-3.97
130.050	1868.535	-3.79	117.475	1880.309	-3.12	104.025	1891.716	-3.78
129.975	1868.612	-3.79	117.275	1880.520	-3.62	103.825	1891.898	-3.71
129.875	1868.715	-3.89	117.200	1880.599	-3.82	103.575	1892.125	-2.87
129.675	1868.920	-3.48	117.100	1880.704	-3.67	103.350	1892.270	-2.89
129.475	1869.125	-2.85	116.875	1880.941	-3.44	103.250	1892.335	-3.20
129.400	1869.192	-2.90	116.700	1881.125	-3.15	103.125	1892.415	-3.36
129.300	1869.281	-3.24	116.475	1881.345	-3.66	102.875	1892.577	-3.78
129.100	1869.458	-3.68	116.400	1881.418	-3.94	102.625	1892.738	-3.84
129.000	1869.547	-4.05	116.275	1881.540	-3.79	102.425	1892.867	-3.46
128.925	1869.614	-3.97	116.075	1881.735	-3.49	102.225	1892.996	-3.05
128.725	1869.792	-3.67	115.875	1881.930	-3.01	102.025	1893.125	-3.01
128.550	1869.947	-3.23	115.675	1882.125	-2.93	101.925	1893.236	-3.46
128.350	1870.125	-3.07	115.475	1882.383	-3.98	101.825	1893.347	-3.73
128.100	1870.358	-3.39	115.275	1882.641	-3.47	101.725	1893.458	-3.70
128.025	1870.427	-3.81	115.100	1882.867	-3.16	101.625	1893.569	-3.63
127.925	1870.520	-3.99	114.900	1883.125	-2.66	101.375	1893.847	-3.36
127.700	1870.730	-3.63	114.700	1883.325	-2.95	101.125	1894.125	-2.83
127.500	1870.916	-3.35	114.625	1883.400	-3.23	101.025	1894.205	-2.88
127.275	1871.125	-2.93	114.525	1883.500	-3.11	100.900	1894.305	-3.12
127.200	1871.193	-3.08	114.325	1883.700	-3.69	100.650	1894.505	-3.69
127.100	1871.284	-3.29	114.100	1883.925	-3.32	100.550	1894.585	-3.70
126.925	1871.443	-3.55	113.900	1884.125	-2.84	100.450	1894.665	-3.70
126.825	1871.534	-3.74	113.700	1884.285	-3.13	100.250	1894.825	-3.71
126.725	1871.625	-3.67	113.475	1884.465	-3.20	100.075	1894.965	-3.08
126.550	1871.784	-3.54	113.400	1884.525	-3.41	99.875	1895.125	-2.94
126.375	1871.943	-3.25	113.300	1884.605	-3.63	99.775	1895.225	-3.03
126.175	1872.125	-3.11	113.075	1884.785	-3.30	99.675	1895.325	-3.18
126.075	1872.214	-3.12	112.850	1884.965	-3.23	99.475	1895.525	-3.95
125.975	1872.303	-3.41	112.650	1885.125	-2.89	99.375	1895.625	-3.73
125.775	1872.481	-3.52	112.450	1885.311	-3.37	99.300	1895.700	-3.63
125.675	1872.569	-3.72	112.250	1885.497	-3.80	99.100	1895.900	-3.39
125.575	1872.658	-3.89	112.125	1885.613	-3.80	98.875	1896.125	-3.00
125.375	1872.836	-3.66	112.025	1885.706	-3.71	98.775	1896.205	-3.03
125.150	1873.036	-3.12	111.800	1885.916	-3.52	98.675	1896.285	-3.26

Coral core RUS-95 (*Porites* sp.) - Stable isotope data

Core depth [cm]	Age [years]	$\delta^{18}O$ [‰ PDB]	Core depth [cm]	Age [years]	$\delta^{18}O$ [‰ PDB]	Core depth [cm]	Age [years]	$\delta^{18}O$ [‰ PDB]
98.450	1896.465	-3.76	85.350	1909.989	-3.25	74.525	1924.125	-3.07
98.350	1896.545	-4.16	85.275	1910.125	-2.94	74.275	1924.403	-3.38
98.250	1896.625	-4.01	85.150	1910.304	-2.95	74.175	1924.514	-3.84
98.000	1896.825	-3.83	85.050	1910.446	-3.41	74.075	1924.625	-3.93
97.800	1896.985	-3.23	84.925	1910.625	-3.90	73.850	1924.875	-3.40
97.625	1897.125	-2.97	84.800	1910.804	-3.61	73.625	1925.125	-3.18
97.425	1897.320	-3.23	84.675	1910.982	-3.40	73.400	1925.345	-3.44
97.225	1897.515	-3.93	84.575	1911.125	-2.95	73.200	1925.540	-3.90
97.025	1897.710	-3.91	84.475	1911.325	-3.24	73.125	1925.613	-3.66
96.800	1897.930	-3.22	84.375	1911.525	-3.96	73.025	1925.710	-3.79
96.600	1898.125	-2.96	84.275	1911.725	-3.64	72.825	1925.905	-3.50
96.500	1898.218	-3.01	84.150	1911.975	-3.14	72.600	1926.125	-2.89
96.400	1898.311	-3.37	84.075	1912.125	-3.00	72.400	1926.315	-3.42
96.175	1898.520	-3.71	83.975	1912.273	-3.43	72.225	1926.482	-3.73
96.075	1898.613	-3.61	83.775	1912.569	-3.90	72.000	1926.696	-3.65
95.925	1898.753	-3.77	83.675	1912.718	-3.63	71.825	1926.863	-3.74
95.725	1898.939	-3.21	83.575	1912.866	-3.60	71.625	1927.054	-2.91
95.525	1899.125	-2.89	83.475	1913.014	-3.17	71.550	1927.125	-2.82
95.350	1899.344	-3.46	83.400	1913.125	-2.71	71.450	1927.208	-3.05
95.175	1899.563	-3.79	83.325	1913.268	-3.37	71.225	1927.396	-3.55
94.950	1899.844	-3.60	83.200	1913.506	-3.66	71.125	1927.479	-3.67
94.725	1900.125	-2.88	83.075	1913.744	-3.74	71.025	1927.563	-3.51
94.525	1900.307	-3.07	82.875	1914.125	-3.00	70.800	1927.750	-3.67
94.425	1900.398	-3.16	82.775	1914.263	-3.01	70.625	1927.896	-3.55
94.325	1900.489	-3.60	82.675	1914.401	-3.15	70.425	1928.063	-3.13
94.150	1900.648	-3.87	82.600	1914.504	-3.51	70.350	1928.125	-2.82
93.925	1900.852	-3.41	82.475	1914.677	-3.58	70.250	1928.212	-2.94
93.725	1901.034	-3.15	82.375	1914.815	-3.58	70.025	1928.408	-3.79
93.625	1901.125	-2.90	82.275	1914.953	-3.13	69.925	1928.495	-3.73
93.500	1901.250	-3.28	82.150	1915.125	-2.89	69.825	1928.582	-3.93
93.300	1901.450	-3.87	82.050	1915.243	-3.13	69.600	1928.777	-3.69
93.075	1901.675	-3.70	81.875	1915.449	-3.39	69.400	1928.951	-3.60
92.875	1901.875	-3.54	81.775	1915.566	-3.91	69.200	1929.125	-2.99
92.625	1902.125	-3.13	81.675	1915.684	-4.05	68.975	1929.301	-3.01
92.400	1902.375	-3.61	81.475	1915.919	-3.91	68.750	1929.478	-3.71
92.325	1902.458	-3.93	81.400	1916.007	-3.45	68.675	1929.537	-3.88
92.225	1902.569	-3.74	81.300	1916.125	-3.22	68.550	1929.635	-3.79
91.975	1902.847	-3.34	81.050	1916.428	-3.72	68.325	1929.811	-3.40
91.725	1903.125	-3.22	80.950	1916.549	-3.76	68.125	1929.968	-3.05
91.525	1903.375	-3.61	80.850	1916.670	-3.78	67.925	1930.125	-3.04
91.425	1903.500	-3.71	80.675	1916.883	-3.43	67.850	1930.195	-3.22
91.325	1903.625	-3.57	80.475	1917.125	-3.30	67.775	1930.265	-3.40
91.125	1903.875	-3.22	80.250	1917.375	-3.48	67.575	1930.451	-3.89
90.925	1904.125	-3.08	80.000	1917.653	-3.99	67.350	1930.660	-3.52
90.675	1904.321	-3.27	79.775	1917.903	-3.58	67.125	1930.869	-3.41
90.475	1904.478	-3.62	79.650	1918.042	-3.26	66.850	1931.125	-3.11
90.400	1904.537	-3.72	79.575	1918.125	-2.87	66.625	1931.375	-3.91
90.300	1904.615	-3.69	79.350	1918.298	-3.29	66.400	1931.625	-3.82
90.050	1904.811	-3.57	79.150	1918.452	-3.52	66.175	1931.875	-3.21
89.850	1904.968	-3.06	78.875	1918.663	-3.79	65.950	1932.125	-2.82
89.650	1905.125	-2.98	78.625	1918.856	-3.48	65.875	1932.202	-2.98
89.450	1905.320	-3.56	78.375	1919.048	-3.42	65.775	1932.304	-3.27
89.350	1905.418	-3.74	78.275	1919.125	-3.42	65.550	1932.535	-4.09
89.250	1905.515	-3.91	78.175	1919.307	-3.97	65.475	1932.612	-3.94
89.050	1905.710	-3.76	77.950	1919.716	-3.78	65.375	1932.715	-3.88
88.850	1905.905	-3.53	77.725	1920.125	-3.28	65.175	1932.920	-3.29
88.625	1906.125	-2.90	77.475	1920.482	-3.29	64.975	1933.125	-2.95
88.525	1906.223	-3.28	77.300	1920.732	-3.93	64.875	1933.236	-3.58
88.450	1906.296	-3.52	77.225	1920.839	-3.69	64.750	1933.375	-3.68
88.225	1906.515	-3.66	77.025	1921.125	-2.94	64.675	1933.458	-3.95
88.025	1906.710	-3.58	76.950	1921.245	-3.26	64.525	1933.625	-3.76
87.775	1906.954	-3.35	76.850	1921.405	-3.53	64.300	1933.875	-3.41
87.600	1907.125	-2.88	76.600	1921.805	-3.65	64.075	1934.125	-3.05
87.525	1907.202	-3.07	76.400	1922.125	-3.28	63.825	1934.388	-3.67
87.450	1907.279	-3.26	76.175	1922.398	-3.46	63.700	1934.520	-4.02
87.250	1907.484	-3.65	76.075	1922.519	-3.57	63.575	1934.651	-3.74
87.000	1907.740	-3.59	75.975	1922.640	-3.93	63.350	1934.888	-3.39
86.750	1907.997	-3.11	75.750	1922.913	-3.76	63.125	1935.125	-3.30
86.625	1908.125	-2.98	75.650	1923.034	-3.42	62.900	1935.446	-3.83
86.525	1908.250	-3.57	75.575	1923.125	-3.20	62.800	1935.589	-3.90
86.300	1908.531	-3.94	75.350	1923.339	-3.60	62.675	1935.768	-3.82
86.075	1908.813	-3.35	75.250	1923.435	-3.81	62.425	1936.125	-3.19
85.825	1909.125	-2.83	75.150	1923.530	-3.87	62.225	1936.325	-3.42
85.700	1909.352	-3.59	74.950	1923.720	-3.78	62.025	1936.525	-3.85
85.600	1909.534	-3.83	74.725	1923.935	-3.55	61.925	1936.625	-4.10
85.475	1909.761	-3.68	74.625	1924.030	-3.11	61.825	1936.725	-3.72

Coral core RUS-95 (*Porites* sp.) - Stable isotope data

Core depth [cm]	Age [years]	$\delta^{18}O$ [‰ PDB]	Core depth [cm]	Age [years]	$\delta^{18}O$ [‰ PDB]	Core depth [cm]	Age [years]	$\delta^{18}O$ [‰ PDB]
61.625	1936.925	-3.47	48.150	1949.125	-2.74	34.925	1961.792	-3.63
61.425	1937.125	-3.05	47.950	1949.383	-3.62	34.725	1961.949	-3.11
61.325	1937.246	-3.41	47.775	1949.609	-3.52	34.500	1962.125	-2.87
61.225	1937.367	-3.58	47.575	1949.867	-3.06	34.300	1962.276	-3.20
61.125	1937.489	-3.81	47.375	1950.125	-3.01	34.200	1962.351	-3.40
61.000	1937.640	-3.79	47.300	1950.195	-3.35	34.100	1962.427	-3.56
60.800	1937.883	-3.38	47.200	1950.288	-3.09	33.875	1962.597	-4.01
60.600	1938.125	-3.12	46.950	1950.520	-3.89	33.800	1962.653	-3.96
60.375	1938.339	-3.39	46.700	1950.753	-3.76	33.725	1962.710	-4.01
60.175	1938.530	-3.94	46.500	1950.939	-3.34	33.550	1962.842	-3.72
60.025	1938.673	-3.69	46.300	1951.125	-3.01	33.350	1962.993	-3.38
59.775	1938.911	-3.38	46.125	1951.344	-3.45	33.175	1963.125	-3.16
59.550	1939.125	-2.89	46.000	1951.500	-3.61	32.975	1963.299	-3.47
59.325	1939.382	-3.67	45.925	1951.594	-3.75	32.900	1963.364	-3.53
59.100	1939.639	-4.19	45.700	1951.875	-3.44	32.800	1963.451	-3.56
58.900	1939.868	-3.85	45.500	1952.125	-2.85	32.600	1963.625	-4.06
58.675	1940.125	-3.37	45.300	1952.315	-3.36	32.425	1963.777	-3.96
58.450	1940.345	-3.40	45.075	1952.530	-3.75	32.225	1963.951	-3.76
58.350	1940.442	-3.63	45.000	1952.601	-3.93	32.025	1964.125	-3.15
58.250	1940.540	-3.79	44.875	1952.720	-3.82	31.825	1964.276	-3.17
58.050	1940.735	-3.79	44.675	1952.911	-3.56	31.725	1964.351	-3.20
57.850	1940.930	-3.31	44.450	1953.125	-3.02	31.600	1964.446	-3.50
57.650	1941.125	-3.20	44.250	1953.320	-3.49	31.400	1964.597	-3.96
57.575	1941.213	-3.74	44.050	1953.515	-3.62	31.175	1964.767	-3.67
57.450	1941.360	-3.91	43.925	1953.637	-3.88	30.925	1964.955	-3.07
57.200	1941.654	-3.86	43.825	1953.735	-3.61	30.700	1965.125	-2.98
57.000	1941.890	-3.10	43.625	1953.930	-3.59	30.600	1965.216	-3.48
56.800	1942.125	-2.99	43.425	1954.125	-2.95	30.500	1965.307	-3.66
56.600	1942.341	-3.43	43.250	1954.284	-3.35	30.275	1965.511	-3.92
56.400	1942.557	-3.75	43.050	1954.466	-3.63	30.175	1965.602	-3.78
56.300	1942.666	-4.04	42.975	1954.534	-3.88	30.075	1965.693	-3.80
56.225	1942.747	-3.70	42.900	1954.602	-3.94	29.850	1965.898	-3.26
56.050	1942.936	-3.53	42.725	1954.761	-3.57	29.600	1966.125	-3.15
55.875	1943.125	-2.92	42.525	1954.943	-3.18	29.400	1966.360	-3.59
55.675	1943.288	-3.09	42.325	1955.125	-3.14	29.200	1966.596	-3.83
55.575	1943.370	-3.25	42.225	1955.233	-3.40	29.000	1966.831	-3.86
55.475	1943.452	-3.37	42.100	1955.368	-3.37	28.750	1967.125	-3.09
55.275	1943.615	-3.64	41.875	1955.611	-3.79	28.550	1967.311	-3.11
55.175	1943.696	-3.53	41.775	1955.720	-3.68	28.475	1967.381	-3.32
55.100	1943.758	-3.95	41.650	1955.855	-3.64	28.375	1967.474	-3.43
54.875	1943.941	-3.44	41.400	1956.125	-2.87	28.275	1967.567	-3.99
54.650	1944.125	-2.84	41.225	1956.292	-3.00	28.150	1967.683	-3.61
54.450	1944.261	-3.19	41.025	1956.482	-3.71	27.900	1967.916	-3.40
54.250	1944.396	-3.53	40.925	1956.577	-4.02	27.675	1968.125	-2.88
54.050	1944.532	-3.96	40.825	1956.673	-4.13	27.500	1968.288	-3.18
53.825	1944.684	-3.63	40.575	1956.911	-3.29	27.300	1968.474	-3.61
53.600	1944.837	-3.61	40.350	1957.125	-2.85	27.100	1968.660	-3.89
53.400	1944.972	-3.03	40.150	1957.311	-3.48	27.000	1968.753	-3.89
53.175	1945.125	-3.00	39.925	1957.520	-3.90	26.900	1968.846	-3.84
52.975	1945.295	-3.57	39.700	1957.730	-3.88	26.675	1969.055	-3.31
52.775	1945.465	-3.74	39.500	1957.916	-3.38	26.600	1969.125	-3.08
52.675	1945.551	-3.74	39.275	1958.125	-3.37	26.475	1969.229	-3.19
52.575	1945.636	-3.59	39.050	1958.334	-3.76	26.300	1969.375	-3.57
52.375	1945.806	-3.42	38.850	1958.520	-3.84	26.125	1969.521	-3.91
52.175	1945.976	-2.94	38.750	1958.613	-3.75	26.000	1969.625	-3.95
52.000	1946.125	-2.90	38.650	1958.706	-3.66	25.900	1969.708	-3.91
51.800	1946.292	-3.43	38.425	1958.916	-3.54	25.700	1969.875	-3.77
51.600	1946.458	-3.57	38.200	1959.125	-2.92	25.475	1970.063	-3.44
51.500	1946.542	-3.94	38.000	1959.303	-3.44	25.400	1970.125	-3.12
51.400	1946.625	-3.86	37.800	1959.481	-3.94	25.325	1970.195	-3.13
51.175	1946.813	-3.74	37.700	1959.569	-3.78	25.100	1970.404	-3.58
51.000	1946.958	-3.46	37.575	1959.681	-3.45	24.925	1970.567	-3.88
50.800	1947.125	-3.02	37.375	1959.858	-3.28	24.825	1970.660	-3.71
50.600	1947.268	-3.14	37.150	1960.058	-3.08	24.725	1970.753	-3.70
50.425	1947.393	-3.56	37.075	1960.125	-3.01	24.525	1970.939	-3.23
50.200	1947.554	-3.72	36.975	1960.202	-3.09	24.325	1971.125	-3.22
50.125	1947.607	-3.75	36.700	1960.413	-3.38	24.225	1971.254	-3.64
50.025	1947.679	-3.63	36.525	1960.548	-3.66	24.125	1971.383	-3.67
49.800	1947.839	-3.58	36.325	1960.702	-3.67	23.925	1971.641	-3.90
49.600	1947.982	-3.15	36.150	1960.837	-3.80	23.850	1971.738	-3.82
49.400	1948.125	-2.84	35.950	1960.990	-3.45	23.750	1971.867	-3.52
49.200	1948.285	-3.44	35.775	1961.125	-3.08	23.550	1972.125	-2.90
48.975	1948.465	-3.91	35.575	1961.282	-3.11	23.475	1972.225	-3.12
48.725	1948.665	-3.49	35.475	1961.360	-3.36	23.375	1972.358	-3.48
48.550	1948.805	-3.40	35.400	1961.419	-3.44	23.175	1972.625	-3.71
48.350	1948.965	-2.81	35.175	1961.596	-4.10	23.075	1972.758	-3.82

Coral core RUS-95 (*Porites* sp.) - Stable isotope data

Core depth [cm]	Age [years]	$\delta^{18}O$ [‰ PDB]	Core depth [cm]	Age [years]	$\delta^{18}O$ [‰ PDB]	Core depth [cm]	Age [years]	$\delta^{18}O$ [‰ PDB]
23.000	1972.858	-3.98	10.650	1985.434	-3.76	1.175	1994.686	-4.11
22.800	1973.125	-3.02	10.425	1985.598	-4.11	1.075	1994.784	-3.88
22.650	1973.255	-3.13	10.325	1985.670	-4.05	0.975	1994.881	-3.90
22.550	1973.342	-3.25	10.200	1985.761	-3.76	0.875	1994.979	-3.14
22.450	1973.429	-3.47	9.925	1985.961	-3.33	0.800	1995.052	-3.11
22.250	1973.603	-3.79	9.700	1986.125	-3.20	0.725	1995.125	-2.89
22.050	1973.777	-3.65	9.450	1986.419	-3.79	0.625	1995.225	-3.00
21.850	1973.951	-3.51	9.250	1986.654	-3.92	0.550	1995.300	-3.15
21.650	1974.125	-3.05	9.050	1986.890	-3.89	0.450	1995.400	-3.79
21.475	1974.314	-3.36	8.850	1987.125	-3.20	0.225	1995.625	-4.20
21.250	1974.557	-4.27	8.625	1987.301	-3.23	0.125		-3.67
21.050	1974.774	-3.63	8.525	1987.380	-3.30	0.000		-3.57
20.975	1974.855	-3.88	8.425	1987.458	-3.61			
20.900	1974.936	-3.77	8.200	1987.635	-3.82			
20.725	1975.125	-2.93	8.100	1987.713	-3.73			
20.525	1975.315	-3.57	8.000	1987.792	-3.64			
20.275	1975.554	-3.82	7.775	1987.968	-3.27			
20.200	1975.625	-3.93	7.575	1988.125	-3.21			
20.100	1975.720	-3.67	7.500	1988.213	-3.44			
19.875	1975.935	-3.26	7.400	1988.331	-3.75			
19.675	1976.125	-2.95	7.150	1988.625	-4.06			
19.600	1976.208	-3.51	6.975	1988.831	-3.70			
19.500	1976.319	-3.72	6.725	1989.125	-2.93			
19.275	1976.569	-3.78	6.625	1989.239	-3.27			
19.175	1976.681	-3.61	6.500	1989.382	-3.50			
19.050	1976.819	-3.74	6.300	1989.611	-3.95			
18.850	1977.042	-3.07	6.125	1989.811	-3.63			
18.775	1977.125	-3.02	6.050	1989.896	-3.28			
18.675	1977.228	-3.26	5.950	1990.011	-3.09			
18.450	1977.458	-3.75	5.850	1990.125	-2.82			
18.350	1977.561	-3.99	5.725	1990.272	-3.22			
18.225	1977.689	-3.85	5.625	1990.390	-3.47			
18.000	1977.920	-3.31	5.550	1990.478	-3.82			
17.800	1978.125	-2.96	5.450	1990.596	-3.85			
17.600	1978.360	-3.56	5.350	1990.713	-3.64			
17.500	1978.478	-3.84	5.225	1990.860	-3.66			
17.400	1978.596	-3.85	5.125	1990.978	-3.33			
17.175	1978.860	-3.76	5.000	1991.125	-3.04			
16.950	1979.125	-3.13	4.900	1991.223	-3.30			
16.750	1979.285	-3.17	4.750	1991.369	-3.43			
16.550	1979.445	-3.73	4.650	1991.466	-3.76			
16.325	1979.625	-4.04	4.525	1991.588	-3.68			
16.225	1979.705	-4.05	4.450	1991.662	-3.88			
16.100	1979.805	-4.00	4.375	1991.735	-3.71			
15.925	1979.945	-3.35	4.225	1991.881	-3.48			
15.700	1980.125	-3.24	4.075	1992.027	-3.04			
15.475	1980.398	-3.75	3.975	1992.125	-2.69			
15.400	1980.489	-3.99	3.875	1992.225	-3.10			
15.275	1980.640	-3.87	3.775	1992.325	-3.36			
15.075	1980.883	-3.56	3.700	1992.400	-3.95			
14.875	1981.125	-3.27	3.600	1992.500	-3.95			
14.625	1981.403	-3.98	3.500	1992.600	-3.76			
14.475	1981.569	-4.08	3.375	1992.725	-3.70			
14.375	1981.681	-3.68	3.275	1992.825	-3.44			
14.175	1981.903	-3.27	3.150	1992.950	-3.03			
13.975	1982.125	-3.03	3.050	1993.050	-2.88			
13.750	1982.485	-4.05	2.975	1993.125	-2.57			
13.550	1982.805	-3.79	2.850	1993.227	-3.52			
13.350	1983.125	-2.80	2.750	1993.309	-3.63			
13.175	1983.268	-3.09	2.675	1993.370	-3.62			
13.075	1983.349	-3.52	2.575	1993.452	-3.95			
12.975	1983.431	-3.53	2.450	1993.554	-3.98			
12.750	1983.615	-3.75	2.350	1993.635	-3.77			
12.625	1983.717	-3.75	2.275	1993.696	-3.82			
12.525	1983.798	-3.55	2.150	1993.798	-3.63			
12.325	1983.962	-3.21	2.075	1993.860	-3.37			
12.125	1984.125	-3.20	1.975	1993.941	-3.44			
11.925	1984.315	-3.39	1.900	1994.003	-3.11			
11.700	1984.530	-3.74	1.825	1994.064	-2.99			
11.500	1984.720	-3.88	1.750	1994.125	-2.98			
11.425	1984.792	-4.00	1.675	1994.198	-3.19			
11.325	1984.887	-3.89	1.575	1994.296	-3.54			
11.075	1985.125	-3.20	1.475	1994.393	-3.65			
10.875	1985.270	-3.36	1.400	1994.466	-3.68			
10.750	1985.361	-3.43	1.300	1994.564	-3.88			

Coral core RUS-95 (*Porites* sp.) - Annual coral growth rate

Year	Growth rate [cm/year]	Year	Growth rate [cm/year]	Year	Growth rate [cm/year]	Year	Growth rate [cm/year]
1751	1.000	1826	0.600	1901	1.000	1976	0.900
1752	0.700	1827	1.025	1902	0.900	1977	0.975
1753	1.025	1828	1.000	1903	0.800	1978	0.850
1754	0.825	1829	1.500	1904	1.275	1979	1.250
1755	0.650	1830	1.100	1905	1.025	1980	0.825
1756	1.150	1831	0.925	1906	1.025	1981	0.900
1757	0.875	1832	1.125	1907	0.975	1982	0.625
1758	0.925	1833	0.750	1908	0.800	1983	1.225
1759	0.875	1834	1.200	1909	0.550	1984	1.050
1760	0.775	1835	1.175	1910	0.700	1985	1.375
1761	0.650	1836	1.350	1911	0.500	1986	0.850
1762	0.775	1837	1.175	1912	0.675	1987	1.275
1763	0.450	1838	0.875	1913	0.525	1988	0.850
1764	0.550	1839	1.000	1914	0.725	1989	0.875
1765	0.825	1840	0.800	1915	0.850	1990	0.850
1766	0.850	1841	1.050	1916	0.825	1991	1.025
1767	0.875	1842	0.725	1917	0.900	1992	1.000
1768	0.650	1843	0.925	1918	1.300	1993	1.225
1769	0.750	1844	1.000	1919	0.550	1994	1.025
1770	0.625	1845	0.700	1920	0.700		
1771	0.600	1846	0.800	1921	0.625		
1772	1.000	1847	1.025	1922	0.825		
1773	1.200	1848	0.700	1923	1.050		
1774	1.000	1849	0.875	1924	0.900		
1775	0.950	1850	0.675	1925	1.025		
1776	0.925	1851	0.750	1926	1.050		
1777	1.050	1852	0.625	1927	1.200		
1778	0.650	1853	1.175	1928	1.150		
1779	0.875	1854	1.125	1929	1.275		
1780	0.950	1855	0.925	1930	1.075		
1781	1.300	1856	0.950	1931	0.900		
1782	0.875	1857	0.875	1932	0.975		
1783	1.275	1858	0.600	1933	0.900		
1784	1.200	1859	1.250	1934	0.950		
1785	1.200	1860	1.025	1935	0.700		
1786	1.400	1861	1.025	1936	1.000		
1787	1.025	1862	1.000	1937	0.825		
1788	1.125	1863	1.850	1938	1.050		
1789	1.250	1864	1.675	1939	0.875		
1790	1.075	1865	0.825	1940	1.025		
1791	1.375	1866	1.225	1941	0.850		
1792	1.150	1867	1.225	1942	0.925		
1793	0.975	1868	0.975	1943	1.225		
1794	0.875	1869	1.125	1944	1.475		
1795	1.200	1870	1.075	1945	1.175		
1796	0.975	1871	1.100	1946	1.200		
1797	1.125	1872	1.125	1947	1.400		
1798	0.775	1873	1.125	1948	1.250		
1799	0.550	1874	1.250	1949	0.775		
1800	1.100	1875	0.725	1950	1.075		
1801	0.900	1876	1.425	1951	0.800		
1802	0.775	1877	0.850	1952	1.050		
1803	1.200	1878	0.975	1953	1.025		
1804	0.800	1879	1.050	1954	1.100		
1805	0.975	1880	0.950	1955	0.925		
1806	0.750	1881	1.025	1956	1.050		
1807	0.925	1882	0.775	1957	1.075		
1808	0.750	1883	1.000	1958	1.075		
1809	1.175	1884	1.250	1959	1.125		
1810	1.025	1885	1.075	1960	1.300		
1811	0.700	1886	1.350	1961	1.275		
1812	0.825	1887	1.875	1962	1.325		
1813	0.775	1888	1.275	1963	1.150		
1814	0.725	1889	1.125	1964	1.325		
1815	1.075	1890	1.275	1965	1.100		
1816	0.800	1891	1.100	1966	0.850		
1817	0.875	1892	1.550	1967	1.075		
1818	1.050	1893	0.900	1968	1.075		
1819	0.725	1894	1.250	1969	1.200		
1820	0.825	1895	1.000	1970	1.075		
1821	0.850	1896	1.250	1971	0.775		
1822	0.650	1897	1.025	1972	0.750		
1823	0.925	1898	1.075	1973	1.150		
1824	0.600	1899	0.800	1974	0.925		
1825	0.700	1900	1.100	1975	1.050		

In dieser Reihe bereits erschienen:

Nr. 1 **Wefer, G., E. Suess und Fahrtteilnehmer**
Bericht über die POLARSTERN-Fahrt ANT IV/2, Rio de Janeiro - Punta Arenas, 6.11. - 1.12.1985.
60 Seiten, Bremen, 1986.

Nr. 2 **Hoffmann, G.**
Holozänstratigraphie und Küstenlinienverlagerung an der andalusischen Mittelmeerküste.
173 Seiten, Bremen, 1988. (vergriffen)

Nr. 3 **Wefer, G. und Fahrtteilnehmer**
Bericht über die METEOR-Fahrt M 6/6, Libreville - Las Palmas, 18.2. - 23.3.1988.
97 Seiten, Bremen, 1988.

Nr. 4 **Wefer, G., G.F. Lutze, T.J. Müller, O. Pfannkuche, W. Schenke, G. Siedler, W. Zenk**
Kurzbericht über die METEOR-Expedition Nr. 6, Hamburg - Hamburg, 28.10.1987 - 19.5.1988.
29 Seiten, Bremen, 1988. (vergriffen)

Nr. 5 **Fischer, G.**
Stabile Kohlenstoff-Isotope in partikulärer organischer Substanz aus dem Südpolarmeer (Atlantischer Sektor). 161 Seiten, Bremen, 1989.

Nr. 6 **Berger, W.H. und G. Wefer**
Partikelfluß und Kohlenstoffkreislauf im Ozean.
Bericht und Kurzfassungen über den Workshop vom 3.-4. Juli 1989 in Bremen.
57 Seiten, Bremen, 1989.

Nr. 7 **Wefer, G. und Fahrtteilnehmer**
Bericht über die METEOR - Fahrt M 9/4, Dakar - Santa Cruz, 19.2. - 16.3.1989.
103 Seiten, Bremen, 1989.

Nr. 8 **Kölling, M.**
Modellierung geochemischer Prozesse im Sickerwasser und Grundwasser.
135 Seiten, Bremen, 1990.

Nr. 9 **Heinze, P.-M.**
Das Auftriebsgeschehen vor Peru im Spätquartär. 204 Seiten, Bremen, 1990. (vergriffen)

Nr. 10 **Willems, H., G. Wefer, M. Rinski, B. Donner, H.-J. Bellmann, L. Eißmann, A. Müller, B.W. Flemming, H.-C. Höfle, J. Merkt, H. Streif, G. Hertweck, H. Kuntze, J. Schwaar, W. Schäfer, M.-G. Schulz, F. Grube, B. Menke**
Beiträge zur Geologie und Paläontologie Norddeutschlands: Exkursionsführer.
202 Seiten, Bremen, 1990.

Nr. 11 **Wefer, G. und Fahrtteilnehmer**
Bericht über die METEOR-Fahrt M 12/1, Kapstadt - Funchal, 13.3.1990 - 14.4.1990.
66 Seiten, Bremen, 1990.

Nr. 12 **Dahmke, A., H.D. Schulz, A. Kölling, F. Kracht, A. Lücke**
Schwermetallspuren und geochemische Gleichgewichte zwischen Porenlösung und Sediment im Wesermündungsgebiet. BMFT-Projekt MFU 0562, Abschlußbericht. 121 Seiten, Bremen, 1991.

Nr. 13 **Rostek, F.**
Physikalische Strukturen von Tiefseesedimenten des Südatlantiks und ihre Erfassung in Echolotregistrierungen. 209 Seiten, Bremen, 1991.

Nr. 14 **Baumann, M.**
Die Ablagerung von Tschernobyl-Radiocäsium in der Norwegischen See und in der Nordsee.
133 Seiten, Bremen, 1991. (vergriffen)

Nr. 15 **Kölling, A.**
Frühdiagenetische Prozesse und Stoff-Flüsse in marinen und ästuarinen Sedimenten.
140 Seiten, Bremen, 1991.

Nr. 16 **SFB 261 (Hrsg.)**
1. Kolloquium des Sonderforschungsbereichs 261 der Universität Bremen (14.Juni 1991):
Der Südatlantik im Spätquartär: Rekonstruktion von Stoffhaushalt und Stromsystemen.
Kurzfassungen der Vorträge und Poster. 66 Seiten, Bremen, 1991.

Nr. 17 **Pätzold, J., T. Bickert, L. Brück, C. Gaedicke, K. Heidland, G. Meinecke, S. Mulitza**
Bericht und erste Ergebnisse über die METEOR-Fahrt M 15/2, Rio de Janeiro - Vitoria,
18.1. - 7.2.1991. 46 Seiten, Bremen, 1993.

Nr. 18 **Wefer, G. und Fahrtteilnehmer**
Bericht und erste Ergebnisse über die METEOR-Fahrt M 16/1, Pointe Noire - Recife,
27.3. - 25.4.1991. 120 Seiten, Bremen, 1991.

Nr. 19 **Schulz, H.D. und Fahrtteilnehmer**
Bericht und erste Ergebnisse über die METEOR-Fahrt M 16/2, Recife - Belem, 28.4. - 20.5.1991.
149 Seiten, Bremen, 1991.